MODELING, METHODOLOGY AND APPLICATIONS FOR RESOURCE MANAGEMENT IN ENERGY HARVESTING SYSTEMS

Neda Edalat

NATIONAL UNIVERSITY OF SINGAPORE

2015

MODELING, METHODOLOGY AND APPLICATIONS FOR RESOURCE MANAGEMENT IN ENERGY HARVESTING SYSTEMS

Neda Edalat

(*M.Eng, NUS*)

A THESIS SUBMITTED FOR THE DEGREE OF

DOCTOR OF PHILOSOPHY

DEPARTMENT OF ELECTRICAL AND COMPUTER ENGINEERING

NATIONAL UNIVERSITY OF SINGAPORE

2015

Statement of Originality

I hereby certify that the content of this thesis is the result of work done by me and has not been submitted for a higher degree to any other University or Institution.

19 - July - 2015 ..... Neda

Date Neda Edalat

This thesis is dedicated to

my beloved parents and husband,

Mohammad Hassan Edalat, Mona Tehranchi and Ehsan Keikha

Acknowledgments

There are many people whom I wish to thank for the help and support they have given me throughout my PhD studies. Foremost, I would like to express my sincere gratitude to my supervisor Professor Mehul Motani. I thank him for his invaluable guidance, insights and suggestions that helped me throughout this work. Professor Motani supported me in all ways an advisor can support a student. Moreover, he gave me sufficient freedom and patience to work on research problems of interest to me. Besides my main advisor, I would like to thank Professor Jean Walrand for his great advice and support during my stay at UC Berkeley. I learned thinking in simple examples from him and it was always very comfortable to work with him. I also want to thank Dr. Longbo Huang and Professor Sajal K. Das for their useful guidance and suggestions in the couple of my works.

Last but not the least, I would like to thank my parents, my sister and my in-laws for always being there when I needed them most, and for supporting me through all these years. I would especially like to thank my beloved husband Ehsan, who with his unwavering support, patience, and love has helped me to achieve this goal.

Contents

Summary

Energy harvesting technologies have become a commercial reality, with many deployed embedded devices being powered from the natural resources in their environment. This deployment opens the exciting new possibility to build the self-powered and self-sustainable systems. Unlike conventional power sources, the output power of renewable sources is stochastic in nature, as they strongly depend on environmental changes. This makes the control of the systems that operates with such energy sources challenging. In this dissertation, we aim to develop the analytical foundations for the design of control policies for systems that completely or partially operate with renewable energy sources. We pursue our investigation for two key applications and in four main parts.

In the first part, we consider systems that utilize renewable energy and are equipped with energy storage to adjust for the variability in the available energy and energy usage. The problem under study is how to best use the stored energy to maximize the long-term utility. One approach is to formulate this problem as a Markov decision process in which the state of the system is the amount of stored energy, together with the state of the environment. Unless the battery is small, the size of the state space of this Markov decision problem is very large, which makes the problem difficult to solve. The key idea is to replace the Markov decision problem formulation by a simple optimization problem provided by large deviation theory.

In the second part, we consider the sensor node system that is equipped with renewable energy sources, which are capable of recharging their batteries and supporting data collection and transmission indefinitely. Energy and data management of these types of systems is challenging primarily due to the variability of renewable energy sources and transmission channels. The goal for this part is to jointly control the energy usage and data sampling rate to maximize the long-term performance of the system subject to the constraints imposed by the available energy and data. The design of this control is based on estimates of the large deviations of the energy stored in the battery and of the queued data.

In the third part, we study the task allocation problem for solar powered wireless sensor networks. The goals are to minimize the makespan and maximize the fairness in energy-driven task mapping (i.e., energy-balancing), while satisfying the task precedence constraints and energy harvesting causality constraints. The problem is accurately formulated as a mixed integer linear programming problem. The proposed

framework for this problem has a hybrid framework of static and dynamic adaptation stages.

Finally, we consider smart grid systems in which energy from renewable and non-renewable sources is used to satisfy the variable demand. One may use energy storage devices to absorb the fluctuation of both renewable energy and demands. This work explores a comprehensive methodology to study the effect of integrating renewable sources and energy storages in reducing the cost of smart grids operation and control of such systems.

List of Tables

List of Figures

Chapter 1

Introduction

Harvesting energy from the environment is a desirable and increasingly important capability in several emerging applications of embedded systems such as wireless sensor networks (WSNs) [1], Internet of things (IoT) [2], smart grids [3], biomedical implants [4], etc. While energy harvesting has the potential to enable near-perpetual system operation, designing an efficient energy harvesting system that actually realizes this potential requires an in-depth understanding of several complex challenges. These challenges arise due to the interaction of numerous factors such as the characteristics of the harvesting sources, capacity of the batteries used (if any), power supply requirements and power management features of the embedded system, application behavior, etc. In this thesis, these challenges in the design of control policies for systems that completely or partially operate with renewable energy sources are studied.

In this section, first a brief introduction is provided to these notions. It is then followed by the motivation and main contributions of this thesis.

1.1 Energy Harvesting Systems

Energy harvesting is the process of scavenging ambient energy from sources in the surrounding environment and converting it into the electrical energy. Energy harvesting allows low-power embedded devices to be powered from naturally occurring environmental energy (e.g., light, wind, vibration, or temperature difference). A typical energy harvesting system has three components, the energy source, the harvesting architecture and the load. Energy source refers to the ambient source of energy to be harvested. Harvesting architecture consists of mechanisms to harness and convert the input ambient energy to electrical energy. Load refers to the activity that consumes energy and acts as a sink for the harvested energy [5].

A vital component of any energy harvesting architecture is the energy source. It dictates the amount and rate of energy available for use. Energy sources have different characteristics along the axes of controllability, predictability and magnitude [6]. A controllable energy source can provide the harvestable energy whenever it is required and energy availability need not be predicted before harvesting. With non-controllable energy sources, energy must be simply harvested whenever available. In this case, if the energy source is predictable, then a prediction model which forecasts its availability can be used to indicate the time of the next recharge cycle. In this thesis, we mainly use the non-controllable renewable energy sources.

1.2 Wireless Sensor Networks with Renewable Energy Sources

One of the systems that increasingly incorporate the energy harvesting techniques is a wireless sensor networks (WSN). This is because, a major limitation of sensor nodes is the finite battery capacity. Nodes will operate for a finite duration, only as long as the battery lasts. Finite nodes lifetime implies a finite lifetime of the applications or additional cost and complexity to regularly change batteries. However, there are emerging WSNs' applications where sensors are required to operate for much longer durations (like years or even decades) after they are deployed. Examples include in-situ environmental/habitat monitoring and structural health monitoring of critical infrastructures and buildings, where batteries are hard (or impossible) to replace/recharge. Nodes may also opt to use low-power hardware like a low-power processor and radio, at the cost of lesser computation ability and lower transmission ranges. An alternative practical technique that has been applied to address the problem of a finite node lifetime is the use of energy harvesting systems. Known implementations of energy harvesting sensor nodes include Fleck [7], Enviromote [8], Trio [9], Everlast [10], Twin-Star node [11] and Solar Biscuit [12].

1.2.1 Power Management in WSNs with Renewable Energy Sources

Renewable energy sources can be attached to sensor nodes to provide energy replenishment for prolonging the lifetime of sensor networks. The power management for such networks seems to be challenging. This is because, the environmental energy availability is often highly variable and non deterministic. Moreover, for networks with replenishment, conservative energy expenditure may lead to miss-recharging opportunities due to battery capacity limitations, while aggressive usage of energy may result in reduced coverage or connectivity for certain time periods. Thus, new power management schemes need to be designed to balance these seemingly contradictory goals, in order to maximize the sensor network performance. In Chapters 4 and 5, we study the power management and control algorithms for the task allocation problem as well as the joint data collection and power allocation problem for energy harvesting wireless sensor networks.

1.3 Smart Grids and Renewables

A smart grid is a modernized electrical grid that uses information and communications technology to gather and act on information. The information is about the behaviors of suppliers and consumers, in an automated fashion to improve the efficiency, reliability, economics, and sustainability of the production and distribution of electricity [13]. Smart grid technology is the key for an efficient use of renewable

energy resources. The ever increasing price of petroleum products and the reduction in the cost of renewable energy power systems, bring opportunities for penetration of renewable energy systems into the smart grid. Another resurgence of interest in the use of renewable energy is driven by the need to reduce the high environmental impact of fossil-based energy systems. Harvesting energy on a large scale is undoubtedly one of the main challenges of our time. Future energy sustainability depends heavily on how the renewable energy problem is addressed in the next few decades. However, to achieve commercialization and widespread use, an efficient energy management strategy of system needs to be addressed. Part of this thesis presents the study of integrating renewable energy and energy storage devices in smart grid systems.

1.3.1 Power Management in Smart Grids with Renewables

Although in most power generating systems, the main source of energy (the fuel) can be manipulated, this is not true for renewable sources such as solar and wind energies. The main problems with these energy sources are the cost and availability: wind and solar power are not always available where and when needed. Unlike conventional power sources, the output of these renewable sources cannot be controlled. Daily and seasonal effects and limited predictability result in intermittent generation. Smart grids promise to facilitate the integration of renewable energy and will provide other benefits as well.

Energy management in smart grid systems can be seen as a large-scale optimization problem: Given current and (possibly uncertain) future information on pricing,

consumption preferences, distributed generation prospects, and other factors, how should devices and systems be used optimally? Part of this thesis focuses on energy management systems at the customer premises that are able to control consumption, on site generation and storage. Specifically, it explores a methodology to study the effect of integrating energy storage devices and renewable sources in the operation of smart grid as well as the energy management and control of such systems.

1.4 Energy Storage Systems

While batteries have conventionally been used to power embedded systems, they have a finite capacity and must be replaced or recharged when depleted. For this reason, energy harvesting is an attractive power source as it potentially offers a perpetual source of energy, provided there is sufficient and appropriate energy in the deployment environment. Many energy harvesting systems need energy storage because they need to continue operation even when there is no energy to harvest (e.g., at night for a solar-powered system). Chapters 3 and 4 of this thesis explore the methodology that shows the effect of the energy storage capacity on the optimum performance of energy harvesting sensor networks. This part of the thesis has established that key aspects of the use of energy storage can be captured by a simplified probabilistic approach, which requires only limited input data.

In smart grid systems, the energy from renewable and non-renewable sources is used to satisfy the variable demand. One may use energy storage devices to absorb the fluctuation of both renewable energy and demand as two stochastic sources in

smart grid systems. Variable electricity prices are another uncertain features in the operation of smart grids. Again, energy storage can be a solution to moderate this uncertainty and to control the electricity cost. This happens by storing the energy in storage during off-peak periods with cheap energy sources and later use it for high-peak demand. Hence, we allow users to exploit the price variations without having to shift their demand to the low-cost periods with dynamic pricing [85]- [88]. Chapter 6 of this thesis explores the methodology for integrating renewable energy sources and energy storage devices in smart grid systems.

1.5 Motivation of This Thesis

Harvesting energy from the environment is a desirable and increasingly important capability in several emerging applications. Energy harvesting sources have the potential to enable near-perpetual operation of the system that partially or fully operates with such sources. An example of systems that successfully adopts these sources is wireless sensor networks. This is because, energy is the most precious and limited resource in these networks. To ensure sustainable operations designing energy efficient protocols is essential. For example, in sustainable sensor networks, ambient energy (e.g., solar or wind) is normally not sufficient to sustain continuous active operation of sensor nodes in the long run [14], [15]. It has been shown in [16] that even on a sunny day, the total energy harvested at an energy harvesting sensor node (e.g., Twin-Star node [11]) can only allow the node to work at %100 duty cycle for 6.37 hours. The limited available energy is the main factor that prohibits a node from fully

utilizing its hardware resources (such as computing and sensing). Also, for networks with replenishment, conservative energy expenditure may lead to missed recharging opportunities due to battery capacity limitations, while aggressive usage of energy may result in reduced coverage or connectivity for certain time periods. Thus, new resource management schemes need to be designed to balance these seemingly contradictory goals, in order to maximize the performance of sensor networks. Hence, part of the research accomplished for this thesis concentrates on resource management protocols for wireless sensor networks that operate with such sources.

One of the key application scenarios for sensor networks is task allocation, in which a central entity allocates tasks to a set of geographically distributed sensor nodes to accomplish an overall objective. In wireless sensor networks, energy-aware task allocation algorithms deal with energy availability of batteries, which are monotonically decreasing. However, in energy harvesting wireless sensor networks, due to the fluctuating energy sources, the energy availability follows an uncertain outline. For these nodes a new paradigm of task allocation is needed, which takes into account that nodes currently having little or no energy left might have enough in the future to carry out new tasks. In part of this thesis, we study the task allocation algorithms to investigate how to dynamically schedule tasks to match the time-varying renewable energy.

Unlike conventional power sources, the output power of renewable sources is stochastic in nature, as they strongly depend on environmental changes. Many energy harvesting systems need energy storage because they need to continue operation even when there is no energy to harvest or to adjust for the variability in the energy

availability and usage. Then, the important question is how to best use the stored energy to maximize the long-term utility. For instance, in the case of a wireless sensor node, the average power used must be less than the average power of the source. However, unless the battery is very large, the variability may cause the battery to go empty even when that condition is met. In such a situation, one suspects that the energy use should take into account the instantaneous amount of energy stored in the battery. One approach is to formulate this problem as a Markov decision process in which the state of the system is the amount of stored energy, together with the state of the environment. Unless the battery is small, the size of the state space of this Markov decision problem is very large, which makes the problem difficult to solve. In this research, we study a scalable methodology and simple control policy that results in the near optimum results.

Besides renewable sources, the broadcast nature of the wireless medium and random channel variations in wireless systems are another uncertain features. Consider a wireless sensor node equipped with a solar cell, a battery that stores the energy, and a data queue. The sensor node samples data and transmits it opportunistically depends on the communication channel status and available energy and data. A complex control system would determine when to sample additional data and when to transmit on the basis of the backlog in the data queue, the energy stored in the battery, and the state of the environment, such as the weather and the quality of the channel. However, one hopes that a simpler system that does not include the data backlog and the stored energy in its decisions might perform almost as well, provided that the battery and data queue capacities are not very small. In this research, we

explore how to jointly control the energy usage and data sampling rate to maximize the long-term performance of the system subject to the constraints imposed by the available energy and data.

Smart grid is another system that is the key for an efficient use of renewable energy resources. The ever increasing price of petroleum products and the reduction in the cost of renewable energy power systems, bring opportunities for penetration of renewable energy systems into the smart grid. Renewable energy, variable demands and electricity prices in the operation of smart grid are the most uncertain features. One may use the energy storage to absorb these fluctuations and alleviate the cost and uncertainties. Then, the challenging questions are what is the best battery size and how to store, buy and use energy so that the overall long-term cost is minimized. In part of this thesis, we study a comprehensive methodology to explore the effect of integrating renewable sources and energy storages in reducing the cost of smart grids operation and control of such systems.

1.6 Thesis Contributions

In this thesis, several challenges in the design of control policies for systems that completely or partially operate with renewable energy sources are studied. We mainly focus on the control design methodologies for wireless sensor networks and smart grids with renewable sources. Our proposed approaches are efficient and simple in comparison to those in literature. The contributions of each part of this research are explained in detail as follows.

1.6.1 Control of Systems That Store Renewable Energy

Chapter 3 of this thesis is concerned with systems that utilize renewable energy and are equipped with a battery to adjust for the variability in the available energy and its usage. The problem under study is how to best use the stored energy to maximize the long-term utility. One approach is to formulate this problem as a Markov decision process in which the state of the system is the amount of stored energy, together with the state of the environment. The core idea of our proposed approach is to convert the complex Markov decision problem to a simple optimization problem where its constraint is based on large deviation theory. The main advantage of our approach in comparison to literature is that the control policy for the energy usage rate does not involve the instantaneous amount of energy stored in the nodes, when the size of the battery is moderate or large. The state of the system is modeled as a finite Markov chain. Hence, we study the large deviation of Markov chain through few possible approximation approaches; 1) a direct method based on Chernoff's inequality and the

first step equations of a Markov chain; 2) a method based on the analysis of the occupation measure and the contraction principle; 3) a Gaussian approximation method. We evaluate these approaches for random walk process and two-state Markov chain. We demonstrate the use of the approach for two simple problems: a wireless sensor node equipped with a solar panel and a self-sufficient building. The methodology applies to much more complex situations. The benefit is that the resulting control law is simple, as it does not depend on the instantaneous charge of the battery.

1.6.2 A Methodology for Designing the Control of Energy Harvesting Sensor Nodes

In Chapter 4 of this thesis, we study the joint energy and data management problem for energy harvesting wireless sensor networks. We consider a wireless sensor node equipped with a solar cell, a battery that stores the energy, and a data queue. The sensor node samples data and transmits it opportunistically depends on the communication channel status and available energy and data. The goal is to jointly control the energy usage and data sampling rate to maximize the long-term performance of the system subject to the constraints imposed by the available energy and data. We propose a novel approach for designing the control policy for such systems. This approach takes into account the size of the energy and data buffers and produces a policy that performs satisfactorily for *medium* value of those sizes. Despite the literature, the control policy for the energy usage and data sampling rate do not involve the instantaneous amount of energy stored in the nodes and data backlog which sig-

nificantly simplifies the implementation. A key feature of the approach is to estimate the outage probability for the energy storage and the overflow probability for the data buffer and to design the policy to keep these probabilities acceptably small. We evaluate the proposed method on representative examples. Another contribution of this work is to adapt the notion of *effective bandwidth* (see e.g., [71, 72]) to variable sources and variable loads, as a summary of their statistical characteristics. The novelty of our analysis is that we consider queues where the arrivals and departures are both variable. The result of this part is that one can define the *effective power* of a variable renewable source and the *effective consumption rate* of a variable load in a way that the battery is almost never empty if and only if the former is larger than the latter.

1.6.3 Task Allocation for Energy Harvesting Wireless Sensor Networks

In Chapter 5 of this thesis, we present novel task allocation algorithms for energy harvesting wireless sensor networks. In contrast to traditional computing oriented task allocation methods that focus on reducing computational energy consumption and meeting the tasks' deadlines, we present an adaptive task allocation method, which dynamically schedules and assigns tasks based on the tasks' energy consumption and the time-varying environmental energy. The solution objectives are to minimize the scheduling length of the task graph and maximize the fairness in energy-driven task mapping, while satisfying energy harvesting causality constraints and the task prece-

dence constraints. The fairness in task mapping means tasks with longer task lengths are assigned to the nodes with higher energy levels. The result of this task allocation is balanced energy levels among all the nodes in the network while the schedule length is minimized. This work is presented in Chapter 5. The main contributions of this work are summarized as follows:

- We propose a novel task allocation algorithm for energy harvesting wireless sensor networks that operates in two phases: task scheduling of the directed acyclic graph (DAG) and task mapping to the solar-powered sensor nodes. To the best of our knowledge, this is the first work on energy harvesting aware task allocation at the network level to multiple solar-powered sensor nodes.

- The problem is formulated in an optimization framework as a mixed integer linear program (MILP). The proposed framework for our scheme operates in two stages consisting of the static and dynamic adaptation specialized for energy harvesting systems.

- An appropriate energy prediction model and algorithm are incorporated to increase the accuracy of our task allocation scheme.

- A genetic algorithm based multi-objective task allocation strategy is implemented for the comparison purpose.

- The performance of our proposed algorithms in terms of the scheduling length and fairness in the energy-driven task mapping objectives is evaluated through the simulation.

1.6.4 Toward Integration of Renewable Sources and Energy Storage Devices into Smart Grids

Chapter 6 of this thesis explores a comprehensive methodology to study the effect of integrating renewable sources and energy storage devices in reducing the cost of smart grids operation and control of such systems. We explicitly address dimensioning of the energy storage and solar panel as well as control for grid-connected households. The main objective is to minimize the long-term average cost while the variable demand is completely served. The cost contains the operating and capital costs. The problem is a complex Markov decision problem. The simple parametric policies are provided by using measurement-driven simulations. The outcome of these simulations is a choice of policy parameters and size of the battery and solar panel. One may use this outcome for making the investment decisions. Finally, we analyze how well parametric policies perform by comparing them to the solution of a Markov decision problem using dynamic programing.

1.7 Thesis Outline

The outline of this thesis is presented in this chapter. The comprehensive related works and mathematical preliminaries of the research conducted toward this thesis are introduced in Chapter 2. Chapter 3 presents a methodology for designing the control policy of systems that utilize the renewable energy and are equipped with energy storage to adjust for the variability in the available energy and energy usage.

Chapter 4 explores the methodology for the sensor node systems that equipped with renewable energy sources to jointly control the energy usage and data sampling rate. Chapter 5 explains the task allocation algorithms designed for wireless sensor networks equipped with solar panel. This chapter provides the model and a hybrid framework for this problem and the proposed energy aware solutions. Chapter 6 presents the proposed methodology to study the effect of integrating renewable energy sources and energy storage devices on designing the control policy for operation of smart grid systems. Chapter 7 concludes this thesis by summarizing the results and major achievements. Recommendations for future work are also discussed in this chapter.

Chapter 2

Background

This chapter includes the background study for this thesis. It conducts an excessive review of the previous studies and mathematical preliminaries involved in this thesis.

2.1 Related Work

This chapter presents the literature review of our research in different categories.

2.1.1 Power and Rate Control for Systems That Store Renewable Energy

Resource management techniques for energy harvesting systems with uncertain resource availability pose a new set of challenges. These techniques lead to utility maximization considering the energy constraint. For energy harvesting wireless sensor networks EH-WSNs where the resources of interest are energy and data, the transmission rate and data sampling rate maximization satisfying the energy constraint

are two important problems. These problems have been addressed in [21]- [31]. The work in [21] solved the transmission completion minimization problem for energy harvesting communication systems. They adaptively change the transmission rate according to the traffic load and battery charge. The authors in [22] proposed a solution for rate maximization for transmission over multiple fading channels, assuming that the future values of the available power and channel states are known. Under the same assumptions, [23] showed that the transmission time minimization problem and the transmission data maximization problem are the dual of each other and their solutions are identical for the same parameters. That problem was extended to the multiple access channel in [24] and the broadcast channel in [25]. The authors in [26] addressed the routing and power allocation problems as a standard convex optimization problem with energy constraints; they consider a finite horizon formulation and then relax it to derive an online algorithm. The authors in [27] designed a solution for fair and high throughput data extraction from all nodes guaranteeing fairness while maximizing the sampling rate and throughput. [28] proposed a joint data queue and battery buffer control algorithm, thus the long-term average sensing rate maximization subject to stability of data queue and desired data loss ratio could be achieved. They considered a static channel model and offline knowledge about the energy input. A policy with decoupled admission control and power allocation decisions is developed in [29] that achieves asymptotic optimality for sufficiently large battery capacity to maximum transmission power ratio (explicit bounds are provided). The authors in [30] obtained the energy management policies that are throughput optimal and minimize the mean delay in the queue. The information-theoretic approach [31]

used a best effort to transmit scheme which does not depend on the current size of the energy queue. Because it is assumed that the battery size is large enough, the data is transmitted with a Gaussian codebook whose average power is less than the average recharge rate.

In this thesis, we propose a novel approach for designing the control policies. That approach takes into account the size of the energy and data buffers and produces a policy that performs satisfactorily for medium value of those sizes. Also, the policy does not depend on the instantaneous charge of the battery and backlog of the data queue and it has a low complexity. A main feature of the approach is to estimate the outage probability for the energy storage and the overflow probability for the data buffer and to design the policy to keep these probabilities acceptably small. Chapters 3 and 4 elaborate these ideas of designing the methodology and control policies for the energy buffer as well as the coupled energy and data buffers.

2.1.2 Task Allocation for Energy Harvesting Wireless Sensor Networks (EH-WSNs)

Many applications for energy harvesting sensor networks, such as structural health monitoring [32], disaster recovery [33] and health monitoring [34], require real-time reliable network protocols and efficient task scheduling. In such networks, it is important to dynamically schedule node and network tasks based on remaining energy and current energy intake, as well as predictions about future energy availability.

In task allocations for WSNs [37], [38], [39], [42], [43], given a directed acyclic

graph (DAG) and initial available resources, the set of tasks is assigned to sensor nodes before the task execution starts. However, the time-varying nature of EH-WSNs offers new considerations for designing resource management schemes.

The resource management of real-time energy harvesting embedded systems has been studied in the literature. In some works, such as [45], [46], [47], dynamic voltage scaling policies are used to reduce the energy consumption, but they result in a longer schedule length in case of allocation of the task graph to the set of processors. In [48] and [49] authors constructed the Lazy Scheduling Algorithms (LSA) which are energy-clairvoyant, i.e., generated energy in the future is known. Lazy scheduling algorithms can be categorized as non-work conserving scheduling disciplines where a lazy scheduler may be idle, although waiting tasks are ready to be processed. Moreover, there is an assumption that tasks are independent from each other and preemptive. More precisely, the currently active task may be preempted at any time and have its execution resumed later, at no additional cost. Also, since LSA is only based on a "as late as possible" heuristic, it is more likely that the battery overflows from harvested energy which results in missed-recharging opportunities. Moreover, the above mentioned works mainly focused on the task allocation to a single processor with the energy harvesting capability, but not the allocation of a task graph with precedence constraints to multiple nodes.

The most closely related works are [40] and [41]. The works in [40] proposes a dynamic energy-oriented scheduling algorithm. By conducting decomposition, combination, concurrent execution and admission control their proposed method allocates tasks based on the dynamically changed available energy. The work in [41] presents a

distributed mission assignment scheme for wireless sensor nodes with the rechargeable battery.

Our approach differs from these works in two ways. First, the problem we address is energy harvesting-aware task allocation at the network level, i.e., how to assign nodes in the network to the tasks from task graph with precedence constraints. Such problem is quite different from the task allocation problem tackled by existing works, which instead focus on individual task scheduling at the node level. Second, they maximize the network profit within a given time horizon, rather than enabling the network to operate perennially.

Chapter 5 of this thesis presents task allocation algorithms to deal with these issues. These algorithms account for the energy harvesting characteristics of sensor nodes (i.e. uncertainty in energy availability) and make the best use of available energy. The solution objectives are to minimize the scheduling length of the task graph and maximize the fairness in energy-driven task mapping, while satisfying energy harvesting causality constraints and the task precedence constraints.

2.1.3 Integrating the Energy Storage and Renewable Energy with Smart Grids

Uncertainties associated with renewable sources, which are intermittent and essentially variable, create a challenge for their integration into the current grids [84]. Energy storage has a significant effect on penetration of uncertain renewable energy generations in smart grids. Variable demands and prices are another uncertain fea-

tures in the operation of smart grids. Again, energy storage can be a solution to moderate this uncertainty and to control the electricity cost. Storage allows users to exploit the price variations without having to shift their demand to the low-cost periods with dynamic pricing [85]- [88].

Researchers have studied approaches for storage management and control in order to optimize several features in smart grid systems. They have explored using energy storage for minimizing energy imbalance (the differences between demand and local energy). The authors in [90] proposed an approach to reduce reserve energy requirement in power system dispatch. They formulate the power imbalance problem for each timescale as an infinite horizon stochastic control problem and show that a greedy policy minimizes the average magnitude of the residual power imbalance. Their analysis applies to the case in which the utility company owns and operates the storage. They use the prediction for multi time scale of renewable generation. The optimal power flow problem with energy storage is formulated in [91] assuming deterministic load with the objective of minimizing the total quadratic generation cost. [92] addresses algorithms for minimizing the long-term energy cost in the presence of large storages, using online dynamic control approach. They assume that the prices and demands follow a fixed but unknown distribution. Moreover, they assume there are no renewable sources and the battery is used only for the purpose of arbitrage. Similarly, in [93] the authors consider the problem of energy storage from the point of view of the grid operator, and propose a threshold policy that is shown to be asymptotically optimal for the large size of the storage unit. In [94] algorithm leverages a prediction model they develop, which forecasts future demand using statistical

machine learning techniques given to know the next-day prices. There are some other relevant works such as [95] for storage with demand response and [96] for operating storage co-located with end-user demands which is a similar approach used in data centers.

Controlling the residential energy storage has been proposed in [97] - [99]. The authors analyzed the benefits of buying energy when it is cheap and selling it later to the grid for higher price, assuming that the prices and statistics are known in a finite horizon. They formulated the deterministic optimization problem and solved it by linear programing methods.

The above-mentioned algorithms are mainly designed for large battery capacity and do not take into account the cost of battery and solar panel. Chapter 6 of this thesis explores a methodology to study the effect of integrating energy storages in the operation of smart grids and control of such systems. To the best of our knowledge, this is the first work that uses a comprehensive methodology to determine the optimum battery and solar panel sizes as well as the policy for dispatching energy from the grid so that the overall cost minimized. In this work, we consider the deterministic and stochastic approaches to calculate the optimum policy.

2.2 Mathematical Preliminaries

In this section, a brief explanation on some of the mathematical and theoretical concepts used in this thesis are provided.

2.2.1 Stochastic Dynamic Programing

In this thesis, we utilize the dynamic programing for solving the Markovian decision problem in Chapters 3 , 4 and 6. The results from dynamic programing can be used as a baseline to evaluate the performance of our proposed approaches. So, in this section, we provide a brief intuition to this technique.

The term dynamic programming was originally used in the 1940s by Richard Bellman to describe the process of solving problems where one needs to find the best decisions one after another [77]. Dynamic programming is both a mathematical optimization method and a computer programming method. In both contexts, it refers to simplifying a complicated problem by breaking it down into simpler subproblems in a recursive manner. If subproblems can be nested recursively inside larger problems, so that dynamic programming methods are applicable, then there is a relation between the value of the larger problem and the values of the subproblems [19]. This is done by defining a sequence of value functions $V_1,\ V_2, ..., V_n$ with an argument $\mathcal{X}$ representing the state of the system at time from 1 to n. The definition of $V_n(\mathcal{X})$ is the value obtained in state $\mathcal{X}$ at the last time n. The values V_i at earlier times $i = n-1,\ n-2,\ ...,\ 2,\ 1$ can be found by working backwards, using a recursive relationship called the Bellman's equation [18]. When the horizon is infinite, this problem (conditional on the initial state) is the same at each point since we always have an infinite number of periods left to go, hence the environment is stationary. It follows that the value function $V(\mathcal{X})$ will be time invariant as well.

Formally, a stochastic dynamic program has the same components as a determin-

istic one; the only differences is the state transition equations. When events in the future are uncertain, the state does not evolve deterministically; instead, states and actions today lead to a distribution over possible states in the future. In the infinite horizon case, one can write the Bellman's equation with discount factor $0 < \zeta < 1$ as:

$$
\begin{aligned}
V(x) &= \min_{\mathcal{U}} \mathbb{E}(\sum_{n=0}^{\infty} \zeta^n . \mathrm{g}(\mathcal{X}_n, \mathcal{U}_n)) \qquad (2.1)\\
&= \min_{\mathcal{U}} \{\mathrm{g}(\mathcal{X}_0, \mathcal{U}_0) + \mathbb{E}(\sum_{n=1}^{\infty} \zeta^n . \mathrm{g}(\mathcal{X}_n, \mathcal{U}_n)) \\
&\quad |\mathcal{X}_0 = x, \mathcal{U}_0 = u\} \\
&= \min_{\mathcal{U}} \{\mathrm{g}(\mathcal{X}_0, \mathcal{U}_0) + \zeta . \mathbb{E}(\sum_{n=0}^{\infty} \zeta^n . \mathrm{g}(\mathcal{X}_{n+1}, \mathcal{U}_{n+1})) \\
&\quad |\mathcal{X}_0 = x, \mathcal{U}_0 = u\} \\
&= \min_{\mathcal{U}} \{\mathrm{g}(\mathcal{X}_0, \mathcal{U}_0) + \zeta . \mathbb{E}(V(\mathcal{X}_{n+1}) | \mathcal{X}_0 = x, \mathcal{U}_0 = u\} \\
&= \min_{\mathcal{U}} \{\mathrm{g}(x, u) + \zeta . \sum_{x'} P(x', x; u) . V(x')\} \qquad (2.2)
\end{aligned}
$$

If one optimizes the long-term average cost, it is often meaningful to utilize the average cost dynamic programming Bellman's equation [20]. Staring from state x, it is defined by

$$V(x) = \liminf_{N \to \infty} \frac{1}{N} \mathbb{E}(\sum_{n=0}^{\infty} \mathrm{g}(\mathcal{X}_n, \mathcal{U}_n)) \qquad (2.3)$$

The optimum cost $V^*(x)$ has common value for all initial states,

$$V^*(x) = \lambda^* \quad \forall x \in \mathcal{X}. \qquad (2.4)$$

λ^* together with the differential cost vector $\mathcal{H} = (\mathcal{H}(1), \mathcal{H}(2), ...)$ satisfies Bellman's equation:

$$\lambda^* + \mathcal{H}(x) = \min_{\mathcal{U}}[\mathrm{g}(x,u) + \sum_{x'} P(x', x; u).\mathcal{H}(x')] \tag{2.5}$$

In this expression, λ^* is the optimum cost, $\mathcal{H}(x)$ is the differential cost starting from state x and $\mathrm{g}(x,u)$ is the cost of taking action u in state x.

The *value iteration* for average cost dynamic programing works as follows: one chooses the value of $\mathcal{H}^0(x) = 0$ for all states $x \in \mathcal{X}$. For each time step $k = 1, ..., K$, the Bellman's equation $Th^k(x) := \min_{u \in \mathcal{U}}[\mathrm{g}(x,u) + \sum_{x'} P(x, x'; u)\mathcal{H}^k(x')]$ is updated for all states. We choose an arbitrary reference state x_0 which is constant for all time steps. Then, we set $\lambda^k = Th^k(x_0)$ and update the differential cost function as $\mathcal{H}^{k+1}(x) = Th^k(x) - \lambda^k$. The value of λ^k for the last step is the optimum average cost.

2.2.2 Large Deviations

The theory of large deviation is used in Chapters 3 and 4 of this thesis. Hence, in this section a brief introduction to this theory and some other relevant ones are provided.

Large deviations refers to a collection of techniques for estimating properties of rare events such as their frequency and most likely manner of occurrence [69]. In probability theory, the theory of large deviations concerns the asymptotic behavior of remote tails of sequences of probability distributions. Some basic ideas of the theory can be traced back to Laplace and Cramer, but a clear and unified formal

definition was only introduced in 1966, in a paper by Varadhan [66]. Some other references on large deviations include Bahadur (1971) [67], Varadhan (1984) [66], Deuschel and Stroock (1989) [70], and Dembo and Zeitouni (1998) [69]. One of well-known applications that adopted the theory of large deviations is for the analysis of Asynchronous Transfer Mode (ATM) networks [71] and [72]. ATM is a packet switching standard that aimed to limit the rate of cell losses due to buffer overflow to negligible values, comparable to losses caused by transmission errors.

Large deviations turns probability problems into deterministic optimization problems. Loosely speaking, to calculate the probability of a rare event, one assigns a cost to each sample path that would cause the event to occur. Then, one finds the cheapest path in that set of sample paths. The probability is then estimated by

$$P(\text{event}) \approx e^{-n.\text{cost}} \tag{2.6}$$

where n is an asymptotic parameter that often represents the size of the system under consideration or represents a length of time over which one observes a system. This equivalence between probability and cost gives a point of view for thinking about rare events that is perhaps the most useful thing to come out of large deviations. In order to find the probability of a rare event, one simply has to find the cheapest way the event can happen.

Large deviation of i.i.d. random variable

Consider a collection $\{X_n,\ n \geq 1\}$ of independent and identically distributed random variables with common distribution $F(.)$ and with finite mean value m. Define partial sum S_n

$$S_n = \sum_{k=1}^{n} X_k.$$

From the theory of large number we have,

$$\frac{S_n}{n} \to m \text{ as } n \to \infty \text{ with probability 1.}$$

Hence, the probability that $\frac{S_n}{n}$ is away from m goes to 0 as n increases. It can be shown that this convergence to 0 occurs exponentially fast in n. More precisely, for $a \geq m$,

$$\lim_{n\to\infty} \frac{1}{n} \log P(S_n \geq na) = -\Lambda^*(a). \tag{2.7}$$

where

$$\Lambda^*(a) = \sup_{\theta}[\theta a - \Lambda(\theta)] \text{ with } \Lambda(\theta) = \log E(e^{\theta X_1}).$$

For this result to be valid, one needs $\Lambda(\theta)$ to be differentiable and finite in a neighborhood of 0. Algebra shows that $\Lambda^*(m) = 0$.

Roughly, this result states that

$$P(S_n \approx na) \approx e^{-\Lambda^*(a)}. \tag{2.8}$$

This is called *Cramer's Theorem*. This shows that it is unlikely that $\frac{S_n}{n}$ is away from m, and it is exponentially unlikely in n. The value of $\Lambda^*(a)$ which in the large deviation principle called *rate function*, indicates how difficult is for $\frac{S_n}{n}$ to be close to a. If $\Lambda^*(a)$ is large, then it is very difficult for $\frac{S_n}{n}$ to be close to a. The precise proof of Cramer Theorem is provided in Chapter 7.4 [64].

Large Deviation of a Queue

The objective is to evaluate the loss rate at a queue. That is, the queue has a finite buffer capacity B and one wants to estimate the fraction of arrivals that occurs when the queue is full. For many arrival processes, this fraction is comparable to the fraction of times that the queue with an infinite buffer capacity has a buffer occupancy that exceeds B. Hence, one estimates $P(W > B)$, the invariant probability that the buffer occupancy exceeds B. Consider the following discrete-time queuing system. For, $n \geq 1$, X_n customers arrives at the queue at time n and up to c customers in the queue are served at that time. For $\delta > 0$, the probability that starting empty, the queue occupancy reaches a large value B before becoming empty again as follows:

$$P(W > B) \approx exp\{-\delta B\}. \tag{2.9}$$

where the decay rate $\delta = \min_{a>c} \frac{\Lambda^*(a)}{a-c}$ and $\Lambda^*(a) = \sup_\theta[\theta a - \Lambda(\theta)]$ with $\Lambda(\theta) = \log E(e^{\theta X_1})$.

The above argument shows that the probability that the buffer occupancy reaches a large value B in a busy cycle decays exponentially in B. The detailed explanation is provided in Theorem 7.4.2 [64].

Effective Bandwidth: A natural question is to ask what the value of c should be for the decay rate to be equal to specific value, say γ. That is, we want to find the smallest value of c such that

$$\min_{a>c} \frac{\Lambda^*(a)}{a-c} = \gamma$$

We denote that value of c by $\alpha(\gamma)$, and we call it *effective bandwidth* of the arrival stream. The interpretation is that the effective bandwidth $\alpha(\gamma)$ is the rate at which the stream must be served so that the buffer occupancy decays as an exponential with rate γ.

Large deviation of Markov processes

This relationship for i.i.d. sequences can be extended to the Markovian context. For simplicity, let us assume that we have a finite state space X and transition probabilities $\pi(x, y)$ of a Markov chain on X. Let us suppose that $\pi(x, y) > 0$ for all $x,\ y$. If $V(.) : X \to R$ is a function of X, then

$$E_x[exp[V(X_1) + V(X_2) + ... + V(X_n)]]$$

can be explicitly evaluated as

$$\sum_y \pi_V^n(x,y),$$

where $\pi_V(x,y) = \pi(x,y)e^{V(y)}$ and π_V^n is the nth power of π_V. Since π_V is a matrix with positive entries,

$$\frac{1}{n}\log\sum_y \pi_V^n(x,y) \to \log\lambda_\pi(V),$$

where λ_π is the principal eigenvalue of π_V. That approximation is used to study the large deviation of sum of $V(X_n)$ process. One has Chernoff's inequality [17] for $\theta > 0$ to drive the following inequality:

$$P(V(X_1)+V(X_2)+...+V(X_n)\geq nc) \leq E(exp\{\theta(V(X_1)+V(X_2)+...+V(X_n)-nc)\})$$

$$\approx exp\{-n(\theta c - \log\lambda_{\pi,\theta}(V))\}.$$

The detailed proof is provided in [65].

Chapter 3

Control of Systems that Store Renewable Energy

3.1 Introduction

By increasing the use of renewable energy sources, the energy usage control of the systems that operates with such sources are the great of interest. Unlike conventional power sources, the output power of renewable sources cannot be controlled as there are daily and seasonal fluctuations and inaccurate energy prediction. This makes the control of the systems that operates with such sources challenging [63].

This chapter is concerned with systems that utilize renewable energy and are equipped with a battery to adjust for the variability in available power and energy usage. Examples include wireless sensor nodes and buildings.

The problem under study is how to best use the stored energy to maximize the long-term utility. For instance, in the case of a wireless sensor node, the average

power used must be less than the average power of the source. However, unless the battery is very large, the variability may cause the battery to go empty even when that condition is met. In such a situation, one suspects that the energy use should take into account the instantaneous amount of energy stored in the battery. One approach is to formulate this problem as a Markov decision in which the state of the system is the amount of stored energy, together with the state of the environment. Unless the battery is small, the size of the state space of this Markov decision problem is very large, which makes the problem difficult to solve. Moreover, this formulation results in a complex control strategy that depends on the stored energy. However, intuition suggests that if the battery is moderate in size, then using energy at an average rate slightly less than the average rate of the source should guarantee that the battery rarely goes empty. This chapter explains how to make that intuition precise using the theory of large deviations. The large deviation analysis leads to the constraint for energy usage. The novelty of the analysis is that the source and usage are both variable, in contrast with the theory of effective bandwidth [71] and [72]. Indeed, the usage affects the large deviations of the battery discharge, so that the large deviations appear as constraints for the optimization problem. One contribution of this work is a formulation that enables the analysis of the large deviations of the battery in a numerically tractable way that can be included in the optimization problem. We compare this approach to the large deviations analysis based on the occupation measure of a Markov chain. We also examine the case when the variability of the energy source and that of the load are independent.

It would be tempting to use a Gaussian approximation [76] to study the large

deviations. However, simple examples show that this approximation is very poor.

3.1.1 Contributions of this chapter

In this chapter, we show that by considering the storage capacity of the system, one can design efficient and simple algorithms. The main advantage of our approach in comparison to literatures is that the control policy for the energy usage rate does not involve the instantaneous amount of energy stored in the nodes, when the size of the battery is moderate or large. The core idea is to convert the complex Markov decision problem to a simple optimization problem where its constraint is based on large deviation theory. Please refer to section 2.2.2 for introduction on this theory.

In this work, the state of the system is modeled as a finite Markov chain. There are a few possible approaches to study the large deviations of a Markov chain. One method is based on the occupation measure of Markov chains [74]. The basic idea of this approach is that the most likely way for a Markov chain to have an empirical distribution that differs from the invariant distribution is for it to behave as if it had different transition probabilities consistent with the observed empirical distribution. This is the essence of the contraction mapping theorem [68].

Another approach, that we call the direct method, is to start with Chernoff's inequality and calculate the relevant moment generating functions using the first step equations of a Markov chain.

Yet another approach is to consider a Gaussian approximation for the changes of the Markov chain over a number of steps [75], [76]. However, we explain that

this method yields poor estimates of the likelihood that the battery becomes empty for realistic system parameters, which should not be surprising since large deviations typically depend strongly on the higher moments of the distributions.

This chapter is structured as follows. We introduce the system model and problem formulation in Section 3.2. This is followed by Section 3.3 which is approximating the control policy by replacing the constraint based on large deviation techniques. In Section 3.4, the large deviation techniques are applied in three ways: direct method which is based on the Chernoff's inequality, a method based on occupation measure and a Gaussian approximation method. Section 3.5 explains the evaluation of the approach for random walk and 2-state Markov chain, respectively. In Section 3.6, we present the same problem for the case when the variability of the energy source and that of the load are independent. In order to clarify the proposed approach, Section 3.7 provides several examples. Section 3.8 concludes and summarizes this chapter.

3.2 Model

A discrete time model of the system is as follows. At time $n \geq 0$, the battery, with capacity B, has accumulated an amount $X_n \in \{0, 1, \ldots, B\}$ of energy, the environment state such as weather condition is Y_n, a Markov chain on some finite state space $\mathcal{Y}$ with a transition probability matrix P, and one uses a control action $U_n \in \mathcal{U}$ where $\mathcal{U}$ is a finite set. The net amount of battery discharge at time n is a function of Y_n and U_n denoted as $g(Y_n, U_n)$. Hence, $E[g(Y_n, U_n)]$ can take positive as well as negative values. A negative value means that the battery tends to recharge

more than drain. Also, $r(Y_n, U_n)$ represents the reward of taking action U_n in state Y_n. The action u is possible at time n only if $g(Y_n, u) \leq X_n$. The objective is to choose the control actions to maximize the long term average value of $r(Y_n, U_n)$. That is, the problem is as follows:

$$\begin{aligned} \text{Maximize} \quad & E(r(Y_n, U_n)) \\ \text{over} \quad & U_n \\ \text{s.t.} \quad & g(Y_n, U_n) \leq X_n \\ \text{and} \quad & X_{n+1} = [X_n - g(Y_n, U_n)]_0^B. \end{aligned}$$

Note that in the above problem formulation U_n is the function of state of the system and energy level of the battery. In the last expression, we use the notation

$$[x]_0^B = \max\{0, \min\{x, B\}\}.$$

Since (X_n, Y_n) is a Markov chain controlled by U_n, this is a Markov decision problem. It can be solved by Dynamic Programming. The size of the state space of this problem is $(B + 1) \times |\mathcal{Y}|$ and it can be very large unless the battery capacity B is not relatively small. More importantly, the resulting control strategy is complex as it depends on the instantaneous amount of stored energy.

For the purpose of simplifying the solution of the problem and also for deriving some insight into the solution, we examine approximation methods that we explore in the next section.

3.3 Approximations

If the battery is not too small, the fact that it goes empty is a large deviation under a suitable operating regime. This suggests that one can replace the constraint $g(Y_n, U_n) \leq X_n$ by a constraint on the probability that the battery goes empty. Moreover, this constraint can be guaranteed by using a control strategy that depends only on Y_n and is designed so that the statistics of U_n make it very unlikely to deplete the battery faster than it charges for a duration long enough to empty it. This approach has the benefit of resulting in a much simpler control scheme that does not have to depend on the state of charge of the battery. Moreover, the calculation of the control strategy is also much simpler.

Specifically, we consider the problem

$$\begin{aligned} \text{Maximize} \quad & E(r(Y_n, U_n)) \\ \text{over} \quad & q \\ \text{s.t.} \quad & P[U_n = u | Y_n = y] = q(y, u) \\ \text{and} \quad & P(X_n = 0) \leq \beta \\ \text{and} \quad & X_{n+1} = [X_n - g(Y_n, U_n)]_0^B. \end{aligned}$$

In this formulation, β is a small probability. Also, q defines a stationary control strategy that depends only on Y_n, not on X_n. Thus, we have relaxed the tight constraint $g(Y_n, U_n) \leq X_n$ by replacing it by the constraint $P(X_n = 0) \leq \beta$. We will enforce this constraint by considering the large deviations of the process X_n.

Specifically, if $E(g(Y_m, U_m)) < 0$, which is a necessary requirement for the battery to have a small probability of being empty, one can expect the probability, under the stationary distribution, to be on the order of

$$K \exp\{-B\psi(q)\}$$

where K is a constant and $\psi(q)$ depends on the control policy q. That is, the constraint $P(X_n = 0) \leq \beta$ can be replaced by

$$\psi(q) \geq \frac{\delta}{B} \tag{3.1}$$

where δ is chosen so that $K \exp\{-\delta\} = \beta$.

To determine $\psi(q)$, one argues as follows. The battery becomes empty after $n = B/c$ steps if it discharges at an average rate c for these n steps for some $c > 0$. Thus, one is led to study the probability of such a discharge rate, i.e., the probability

$$P(Z_1 + \cdots + Z_n \geq nc)$$

where

$$Z_m = g(Y_m, U_m).$$

We will show that, when $E(Z_n) < 0$, this probability is approximately equal to

$$\exp\{-n\phi(c, q)\}.$$

Accordingly, with $n = B/c$, we see that this probability is of the order of

$$\exp -B\frac{\phi(c,q)}{c}.$$

Since every $c > 0$ is a possible discharge rate that would empty the battery in B/c steps, the probability that the battery empties is the sum over all $c > 0$ of these probabilities. If B is not too small, this sum is well approximated by the term that corresponds to the smallest exponential rate of decay as a function of B. That is, the probability is well approximated by

$$\exp\{-B\psi(q)\}$$

where

$$\psi(q) := \inf_{c>0} \frac{\phi(c,q)}{c}.$$

To analyze the probabilities, we note that for a given q the random variables (Y_n, U_n) form a Markov chain. Thus, Z_n is a function of a Markov chain. Now, the main concern is how to calculate the value of $\phi(.,.)$ and $\psi(.)$. This is explained in next section.

Before proceeding, we review some results about Markov chains.

3.4 Large Deviations

To develop our estimates, we need to study the large deviations of the process $Z_1 + \cdots + Z_n$ driven by the Markov chain Y_n. To do this, we consider three methods: a direct method, an analysis of the occupation measure of a Markov chain, and a Gaussian approximation. We explain that the direct method is numerically simple and yields good estimates. We use the occupation measure to derive properties of the large deviations. We show that the Gaussian approximation is not satisfactory for our problems.

Direct Method

The direct method is based on Chernoff's inequality and on the first step analysis of a Markov chain.

For $y \in \mathcal{Y}$, $\theta > 0$ and $n \geq 1$, let

$$s_n(y) := E[\exp\{\theta(Z_1 + \cdots + Z_n)\}|Y_1 = y], \forall y \in \mathcal{Y}.$$

Note that (see Appendix A)

$$s_{n+1}(y) = E[\exp\{\theta Z_1\}|Y_1 = y] \sum_{y'} P(y, y')s_n(y'), \forall y \in \mathcal{Y}.$$

Let $\mathbf{s}_n$ be the column vector with components $\{s_n(y), y \in \mathcal{Y}\}$. Then

$$\mathbf{s}_{n+1} = G_\theta \mathbf{s}_n, n \geq 1$$

where

$$G_\theta(y, y') = h_\theta(y)P(y, y')$$

with

$$h_\theta(y) = E[\exp\{\theta Z_1\}|Y_1 = y] = \sum_u q(y, u)\exp\{\theta g(y, u)\}.$$

Consequently,

$$\mathbf{s}_n = G_\theta^n \mathbf{s}_0$$

where $\mathbf{s}_0 = [1, 1, \ldots, 1]'$. Also, from conditional expectation we have,

$$E[\exp\{\theta(Z_1 + \cdots + Z_n)\}] = \pi\mathbf{s}_n = \pi G_\theta^n \mathbf{s}_0 \tag{3.2}$$

where π is the distribution of Y_1.

Let $\lambda(\theta)$ be the largest eigenvalue of G_θ. We can approximate the mean value above by

$$E[\exp\{\theta(Z_1 + \cdots + Z_n)\}] \approx K\lambda(\theta)^n, n \gg 1$$

where K is a constant. To see this approximation, note that if the eigenvalues of G_θ are distinct, then one can use the eigendecomposition of matrix G_θ

$$G_\theta = VDV^{-1}$$

where D is the diagonal matrix of eigenvalues. Then,

$$G_\theta^n = VD^nV^{-1}$$

and the approximation follows. If the eigenvalues are not distinct, one replaces D by the block Jordan matrix and the same approximation results.

We use that approximation to study the large deviations of Z_n. One has Chernoff's inequality for $\theta > 0$:

$$P(Z_1 + \cdots + Z_n \geq nc) \leq E(\exp\{\theta(Z_1 + \cdots + Z_n - nc)\})$$

$$\approx K\lambda(\theta)^n \exp\{-n\theta c\} = K \exp\{-n(\theta c - \log(\lambda(\theta)))\}.$$

Since this inequality holds for all $\theta > 0$, one can minimize the right-hand side over $\theta > 0$ and find

$$P(Z_1 + \cdots + Z_n \geq nc) \leq K \exp\{-n\phi(c, q)\}$$

where

$$\phi(c, q) = \sup_{\theta > 0}\{\theta c - \log(\lambda(\theta))\}.$$

As we explained earlier, $\psi(q) = \inf_{c>0} \phi(c, q)/c$, so that

$$\psi(q) = \inf_{c>0} \frac{\phi(c, q)}{c} = \inf_{c>0} \frac{1}{c} \sup_{\theta > 0}\{\theta c - \log(\lambda(\theta))\}. \tag{3.3}$$

The value of c that minimizes $\frac{\phi(c,q)}{c}$ is the average draining rate which results in the battery to go empty rarely. Moreover, $\psi(q)$ is a strictly decreasing function in terms of our control policy q. Hence, the value of q such that $\psi(q)$ is equal to $\frac{\delta}{B}$ from constraint (3.1) is the optimum control policy.

Occupation Measure

For the purpose of deriving properties of the large deviations, we consider an estimate based on the occupation measure of the Markov chain $V_n = (Y_n, U_n)$. We use the occupation measure to obtain an expression for the probability that a Markov chain with a given transition matrix behaves as if it had another transition rate matrix over a long period of time.

Consider a Markov chain V_n with transition matrix P_0. For another transition matrix P_1 and a sequence $\mathbf{v} = (v_0, \ldots, v_n)$, let

$$L(\mathbf{v}) = \frac{\pi_0(v_0)P_0(v_0, v_1)\ldots P_0(v_{n-1}, v_n)}{\pi_1(v_0)P_1(v_0, v_1)\ldots P_1(v_{n-1}, v_n)}$$

where π_1 is invariant under P_1 and π_0 is invariant under P_0. Note that

$$\log(L(\mathbf{v})) = \log\left(\frac{\pi_0(v_0)}{\pi_1(v_0)}\right) + \sum_{v,v'} N_n(v, v') \log\left(\frac{P_0(v, v')}{P_1(v, v')}\right) \tag{3.4}$$

where $N_n(v, v')$ is the number of transitions from v to v' in $\mathbf{v}$. Thus, $L(\mathbf{v})$ is the ratio of the likelihood of $\mathbf{v}$ under P_0 divided by its likelihood under P_1. Note that under P_1, one has

$$N_n(v, v') \approx n\pi_1(v)P_1(v, v').$$

Consequently, for the random sequence $V^n = \{V_1 \ldots, V_n\}$, if we get an exponential from both sides of (3.4), under P_1 we have,

$$L(V^n) \approx \exp\{-nH(P_1)\} \tag{3.5}$$

where

$$H(P_1) = -\sum_{v,v'} \pi_1(v) P_1(v,v') \log\left(\frac{P_0(v,v')}{P_1(v,v')}\right).$$

Consider a set A of sequences $\mathbf{v}$ that are typical under P_1. These sequences satisfy the law of large numbers for the Markov chain so that (3.5) holds and, moreover,

$$P_1(A) \approx 1. \tag{3.6}$$

We claim that

$$P_0(A) = E_1(1_A(V^n)L(V^n)) \approx \exp\{-nH(P_1)\}. \tag{3.7}$$

To see the first equality, note that for any function $f(V^n)$ one has

$$\begin{aligned} E_0(f(V^n)) &= \sum_{\mathbf{v}} P_0(\mathbf{v}) f(\mathbf{v}) = \sum_{\mathbf{v}} P_1(\mathbf{v}) \frac{P_0(\mathbf{v})}{P_1(\mathbf{v})} f(\mathbf{v}) \\ &= \sum_{\mathbf{v}} P_1(\mathbf{v}) L(\mathbf{v}) f(\mathbf{v}) = E_1(f(V^n)L(V^n)). \end{aligned}$$

To get the approximation in (3.7), we use (3.5) and (3.6).

This calculation shows that the likelihood that the Markov chain V_n with transition matrix P_0 behaves as if its transition matrix were P_1 for n steps is exponentially small in n and given by the expression (3.7).

The next step is to estimate the likelihood $\kappa(\pi_1, n)$ that the empirical distribution of $\{V_1, \ldots, V_n\}$ is π_1. One can use the contraction principle (see e.g., [69] and [65]) to argue that this likelihood is the maximum over P_1 of the probability that the Markov chain behaves as if its transition matrix were P_1, where the maximum is over all P_1

with empirical distribution π_1. Hence, one finds that

$$\kappa(\pi_1, n) = \max_{P_1 : \pi_1 P_1 = \pi_1} \exp\{-nH(P_1)\} \approx \exp\{-nR(\pi_1)\}$$

where

$$R(\pi_1) := \inf_{P_1 : \pi_1 P_1 = \pi_1} H(P_1)$$

with $H(P_1)$ as given above.

Now, consider the likelihood that the empirical average value of $\{Z_1, \ldots, Z_n\}$ is $c > 0$, where

$$Z_m = g(V_m), m = 0, 1, \ldots, n.$$

One argues that this likelihood is the maximum of the probabilities that V_n has an empirical distribution π_1, where the maximum is over all π_1 such that

$$\sum_v \pi_1(v) g(v) = c.$$

Thus, this probability is estimated as $\exp\{-n\phi(c, q)\}$ where

$$\phi(c, q) = \min_{\pi_1 : \sum_v \pi_1(v) g(v) = c} R(\pi_1). \tag{3.8}$$

Finally, one argues that the likelihood that the battery discharges is of the order of

$$\exp\{-B\psi(q)\}$$

where

$$\psi(q) = \min_{c>0} \frac{\psi(c,q)}{c}. \tag{3.9}$$

Gaussian Approximation

The Gaussian approximation considers that

$$Z_1 + \cdots + Z_n \approx \mathcal{N}(n\alpha, n\sigma^2),$$

where $\alpha = E(Z_n)$ is as before and $n\sigma^2 \approx \text{var}(Z_1 + \cdots + Z_n)$.

As we will see below, this approximation is not satisfactory.

3.5 Evaluation

We have explained three methods for estimating the likelihood that the battery gets discharged: a direct method, a method based on the occupation measure of the Markov chain, and a Gaussian approximation. In the following subsections, we evaluate these methods for a random walk and two-state Markov chain.

3.5.1 Evaluation for Random Walk

Let Z_n be i.i.d. with $P(Z_n = 1) = a$ and $P(Z_n = -1) = 1 - a =: b$. We assume that $E(Z_n) = a - b = 2a - 1 < 0$, so that the battery tends to charge more than it discharges. We consider the Markov chain W_n defined by

$$W_{n+1} = (W_n + Z_n)^+, n \geq 0.$$

This is a random walk reflected at 0 that models the discharge process of the battery. The state X_n of charge of the battery can be seen to be essentially $B - W_n$, so that if W_n reaches the value B, the battery gets discharged.

Direct Method

The reflected random walk W_n is a simple Markov chain on $\{0, 1, \ldots\}$ with

$$P(k, k+1) = a \text{ and } P(k+1, k) = b, \forall k \geq 0.$$

Also, $P(0, 0) = b$. We can analyze explicitly this Markov chain without having to resort to Chernoff's bound. If $a < b$, the invariant distribution of X_n is π where

$$\pi(k) = (1 - \rho)\rho^k, k \geq 0 \text{ with } \rho := \frac{a}{b}.$$

In particular,

$$P(W_n \geq B) = \sum_{k=B}^{\infty} \pi(k) = \rho^B =: p_Q(B). \tag{3.10}$$

Occupation Measure

Using (3.7), we find that the likelihood that the increments Z_n behave as if $P(Z_n = 1) = a'$ instead of a over n steps is approximately

$$\phi(a') := \exp\{-nH(a')\}$$

where

$$H(a') = -a' \log(\frac{a}{a'}) - (1-a') \log(\frac{1-a}{1-a'}).$$

Thus, according to (3.8),

$$\phi(c) := \min\{H(a') | E_{a'}(Z_n) = a' - (1-a') \geq c\} = H(\frac{1+c}{2}).$$

Hence, by (3.9),

$$\psi_O := \inf_{c>0} \frac{\phi(c)}{c} = \log(\frac{1-a}{a}).$$

Finally, we get the estimate for the probability that the battery gets empty as

$$\exp\{-B\psi_O\} = (\frac{a}{1-a})^B,$$

which agrees with (3.10).

Gaussian Approximation

A Gaussian approximation for this process would work as follows. We argue that for $n \gg 1$,

$$\frac{Z_1 + \cdots + Z_n - n\alpha}{\sqrt{n}} \approx \mathcal{N}(0, \sigma^2)$$

where

$$\sigma^2 = \text{var}(Z_n) = E(Z_n^2) - (E(Z_n))^2 = 1 - \alpha^2.$$

Recall that if W is $\mathcal{N}(0,1)$, then

$$P(W > x) \leq \frac{1}{x\sqrt{2\pi}} \exp\{-\frac{x^2}{2}\}, \forall x > 0.$$

Moreover, this upper bound on the error function is asymptotically tight. Thus, if $V = Z_1 + \cdots + Z_n - n\alpha$, one uses the (poor) approximation $V =_D \sqrt{n\sigma^2}W$, so that

$$\begin{aligned} P(V > na) &= P(W > \frac{na}{\sqrt{n\sigma^2}}) = P(W > \sqrt{n}\frac{a}{\sigma}) \\ &\leq \frac{\sigma}{a\sqrt{n}} \exp\{-n\frac{a^2}{2\sigma^2}\}. \end{aligned}$$

Note that this approximation is a bad application of the Central Limit Theorem. Using this approximation, we get

$$P(Z_1 + \cdots + Z_n > n(\alpha + a)) \approx \frac{\sigma}{a\sqrt{n}} \exp\{-n\frac{a^2}{2\sigma^2}\}.$$

This leads to the probability of the battery going empty being of the order of

$$\exp\{-B\psi\}$$

where

$$\psi = \inf_{a:a+\alpha>0} \frac{1}{a+\alpha}\frac{a^2}{2\sigma^2} = -\frac{2\alpha}{\sigma^2},$$

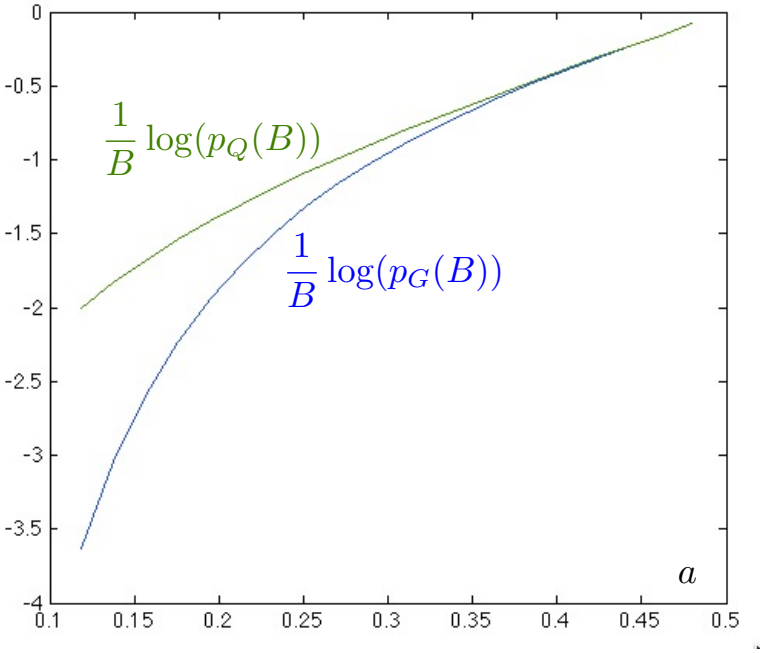

Figure 3.1: Comparison of (3.10) and (3.11). The Gaussian approximation underestimates the probability of large deviations.

which gives the following estimate for the probability that the battery goes empty:

$$\exp\{B\frac{2\alpha}{\sigma^2}\} = \exp\{B\frac{2\alpha}{1-\alpha^2}\} =: p_G(B). \tag{3.11}$$

Thus, the correct expression is given by (3.10) and the Gaussian approximation is given (3.11). Note that

$$\frac{1}{B}\log(p_Q(B)) = \log(\frac{a}{1-a})$$

and

$$\frac{1}{B}\log(p_G(B)) = \frac{2\alpha}{\sigma^2} = \frac{2a-1}{2a(1-a)}.$$

Figure 3.1 compares these expressions as functions of a. We note that the Gaussian

approximation is not very good. This is to be expected since one knows that the Central Limit Theorem provides good estimates of the probability

$$P(Z_1 + \cdots + Z_n > \alpha n + \delta\sqrt{n}),$$

but not of

$$P(Z_1 + \cdots + Z_n > \alpha n + (c - \alpha)n).$$

3.5.2 Evaluation for 2-state Markov Chain

Next, we compare and validate the estimates obtained by the direct method and from the occupation measure in the case of a $\{-1, 1\}$-Markov chain Z_n with $P(-1, 1) = a$ and $P(1, -1) = b$. The goal is to estimate the probability that the process

$$Z_1 + \cdots + Z_n$$

reaches some large value B. This probability, say $p(B)$ is of the order of $\exp\{-B\psi\}$. We will derive three estimates for ψ: ψ_D, ψ_O and ψ_G using the three methods.

Direct Method for two-state Markov Chain

We find

$$G_\theta = \begin{bmatrix} e^{-\theta}(1-a) & e^{-\theta}a \\ e^{\theta}b & e^{\theta}(1-b) \end{bmatrix}.$$

We can then evaluate the largest eigenvalue $\lambda(\theta)$ of G_θ and calculate ψ_D using (3.3).

Occupation Measure

We use (3.7), (3.8) and (3.9) for the two-state Markov chain and we find that the probability of the battery going empty is

$$\exp\{-B\psi_O\}$$

where

$$\psi_O = \inf_{c>0}(\min_{\{P_1:E_1(Z_n)=c\}} H(a',b'))$$

with

$$H(a',b') = -\frac{a'}{a'+b'}[(1-a')\log(\frac{1-a}{1-a'}) + a'\log(\frac{a}{a'})] \\ -\frac{b'}{a'+b'}[(1-b')\log(\frac{1-b}{1-b'}) + b'\log(\frac{b}{b'})].$$

Occupation Measure vs. Simulations

We compare $p(B)$ measured from simulations to the estimates given by the occupation measure approach.

Figure 3.2 shows representative results measured by simulating the battery status and for each value a, it runs as many times as the number of loss events (when the battery goes empty) reaches a constant value (say 100). Then, the loss rate is calculated as the number of loss event (say 100) over the number of steps the simulation runs (before reaching to 100 loss events). The estimate is based on the large deviation of the occupation measure as explained above.

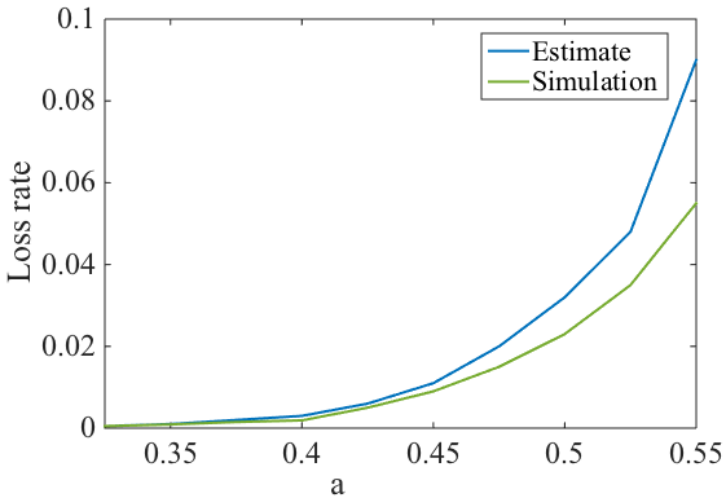

Figure 3.2: Comparison of actual loss rate and estimate. Here, $b = 0.5$ and $B = 30$.

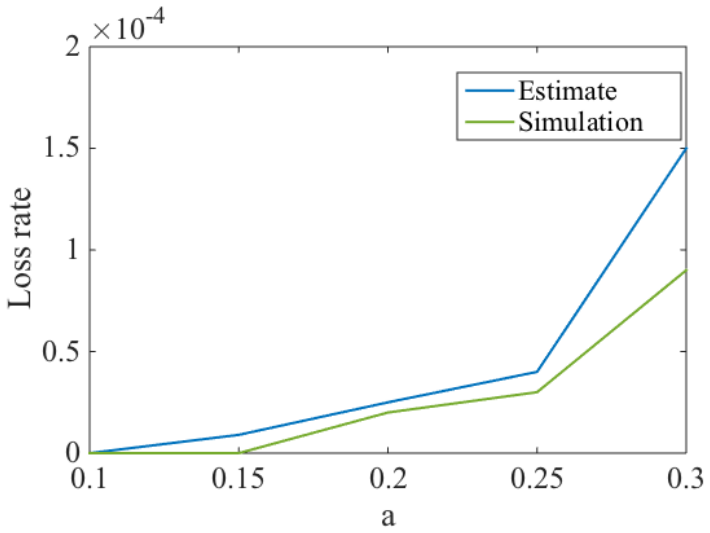

Figure 3.3: Comparison of actual loss rate and estimate for smaller values of a. Here, $b = 0.5$ and $B = 30$.

Figure 3.3 shows more results for smaller values of a.

Gaussian Approximation

For this Markov chain, one finds that (see Appendix B)

$$\sigma^2 := cd\frac{2-a-b}{a+b} \text{ with } c = \frac{a}{a+b}, d = 1-c.$$

This gives the estimate

$$\exp\{B\frac{2\alpha}{\sigma^2}\} = \exp\{-B\frac{2(b-a)(a+b)^2}{ab(2-a-b)}\}.$$

Comparison

Figure 3.4 compares the values of ψ for the probability

$$\exp\{-B\psi\}$$

that the battery becomes empty derived using the three methods. The values are shown for $b = 0.5$ and as a function of $a < b$. As in the case of the random walk, we find that the Gaussian approximation yields poor estimates, which should not be surprising.

3.6 Independent Source and Load

In this section we consider the case where $Y_n = (Y_n^1, Y_n^2)$ and

$$g(Y_n, U_n) = -a(Y_n^1) + b(Y_n^2, U_n).$$

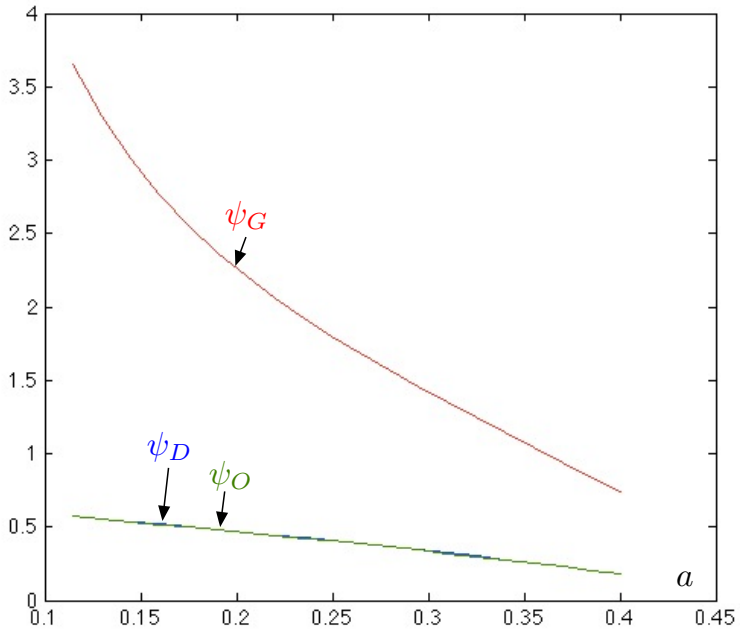

Figure 3.4: Comparison of estimates with occupation measure, direct method and Gaussian approximation. As before, $b = 0.5$ and $B = 30$.

Here, the Markov chains Y_n^1 and Y_n^2 are independent.

For instance, Y_n^1 models the weather that affects the charging rate $a(Y_n^1)$ of the battery and Y_n^2 models the quality of a transmission channel, which affects the reward of transmitting with a given power. We assume that the control policy is defined by q_0 where

$$P[U_n = u | Y_n^1 = y_1, Y_n^2 = y_2] = q_0(y_2, u).$$

The empirical average value of $g(Y_n, U_n)$ differs from its expected value if Y_n^1, Y_n^2 and U_n given Y_n^2 make large deviations. The likelihood of a large deviation where Y_n^1 behaves as if its transition matrix were P^1 instead of P_0^1, Y_n^2 as if its transition matrix were P^2 instead of P_0^2 and U_n given Y_n^2 behaves as it its condition distribution were

q instead of q_0 is exponentially small with exponent

$$H(P^1) + H(P^2) + K[q|\pi_2]$$

where

$$\begin{aligned}
H(P^1) &= -\sum_{y_1, y_1'} \pi_1(y_1) P^1(y_1, y_1') \log\left(\frac{P_0^1(y_1, y_1')}{P^1(y_1, y_1')}\right) \\
H(P^2) &= -\sum_{y_2, y_2'} \pi_2(y_2) P^2(y_2, y_2') \log\left(\frac{P_0^2(y_2, y_2')}{P^2(y_2, y_2')}\right) \\
K[q|\pi_2] &= -\sum_{y_2, u} \pi_2(y_2) q(y_2, u) \log\left(\frac{q_0(y_2, u)}{q(y_2, u)}\right).
\end{aligned}$$

In these expressions, π_1 is invariant for P^1 and π_2 is invariant for P^2. Thus, the empirical rate of $a(Y_n^1)$ is some value a and the empirical rate of $g(Y_n^2, U_n)$ is some value b with an exponentially small probability with an exponent

$$\phi_1(a) + \phi_2(b).$$

The empirical drain rate of the battery is then $b - a$.

Claim 3.1. *The likelihood that a battery of size B drains is exponentially small in B with an exponent*

$$\inf_{b>a} \frac{\phi_1(a) + \phi_2(b)}{b - a}.$$

Proof. Assume that there is some value of c such that, for all $a > c$ and $b < c$,

$$\frac{\phi_1(a)}{a-c} \geq \gamma \text{ and } \frac{\phi_2(b)}{c-b} \geq \gamma.$$

Then

$$\phi_1(a) \geq \gamma(a-c) \text{ and } \phi_2(b) \geq \gamma(c-b),$$

so that

$$\frac{\phi_1(a)+\phi_2(b)}{a-b} \geq \gamma.$$

The interpretation of this result is as follows. Assume that there is some constant rate c such that if the battery drains at rate c, its likelihood of getting empty has an exponent γ and also that if the battery recharges at rate c, then the likelihood that the load makes it go empty also has an exponent γ. Then, the combined system with variable charging and discharging rate has rate at least γ. □

A converse of that result is as follows.

Claim 3.2. *Assume that the combined system has an exponent γ. Then there is some rate c such that each of the two decoupled systems has an exponent γ.*

Proof. To see this, let a^* and b^* be the minimizers of

$$\frac{\phi_1(a)+\phi_2(b)}{b-a}$$

and let γ be the minimum value. The first order conditions are

$$\phi_1'(a^*) = -\phi_2'(b^*) = \gamma.$$

Now, choose c so that

$$\frac{\phi_1(a^*)}{c - a^*} = \gamma.$$

Then we see that

$$\phi_1'(a^*)(c - a^*) = \phi_1(a^*),$$

so that a^* minimizes

$$\frac{\phi_1(a)}{a - c}$$

and the minimum is γ. Similarly, b^* minimizes

$$\frac{\psi_2(b)}{c - b}$$

and the minimum is also γ, which proves the claim. □

3.7 Examples

To clarify the analysis, we consider a few simple examples.

No Control

In our first example, $Y_n \in \{0, 1\}$ with $P(0, 1) = a_0, P(1, 0) = b_0, g(0) = -1, g(1) = 1$.

We also assume that $U_n = Y_n$, so that there is no randomization of the control.

Finally, assume that $a_0 < b_0$, so that

$$E(g(U_n)) = E(g(Y_n)) = \frac{a_0 - b_0}{a_0 + b_0} < 0.$$

Using the occupation method approach, we note that a transition matrix $P(0,1) = a$ and $P'(1,0) = b$ is such that $E(Y_n) = c$ if

$$b = a\frac{1-c}{1+c}.$$

Substituting this value of b in $H(P)$ and minimizing over a, we find

$$\phi(c) = \min_a H(P).$$

We then minimize $\phi(c)/c$ over c. The results is ψ and the likelihood that the battery goes empty is

$$\exp\{-\psi B\}.$$

Numerical examples give the values of ψ, in terms of a and b, shown in Table 3.1.

a_0	b_0	ψ_O	ψ_D
0.1	0.15	0.057	0.067
0.2	0.3	0.134	0.155
0.3	0.45	0.241	0.282
0.4	0.6	0.406	0.472
0.2	0.4	0.288	0.288
0.3	0.6	0.560	0.561
0.4	0.8	1.099	1.101

Table 3.1: Values of ψ when $U_n = Y_n$ obtained using the occupation measure (ψ_O) and the direct method (ψ_D)

This table shows that the battery is less likely to get empty (ψ is larger) when b_0 increases or a_0 decreases. Moreover, that is also the case if a_0 and b_0 increase, for a given value of a_0/b_0. Thus, for a given value of $E(g(Y_n))$, the battery is less likely to get empty if Y_n changes faster instead of staying equal to 1 for longer periods of time. This results confirm our intuition.

Using the direct method, we consider the matrix

$$G_\theta(y, y') = e^{\theta y} P(y, y')$$

and define $\lambda(\theta)$ to be its largest eigenvalue. Then

$$\psi_D = \min_{c>0} \frac{1}{c} \sup_{\theta>0} [\theta c - \log(\lambda(\theta))].$$

Control

We now consider the same situation as in the previous example, except that

$$P[U_n = 1|Y_n = 1] = \gamma_0 \text{ and } P[U_n = 1|Y_n = 0] = 0.$$

As a concrete example, say that $a_0 = 0.2$ and $b_0 = 0.3$. We saw that $\psi = 0.134$ if $U_n = Y_n$. This corresponds to a probability of a battery of size 20 going empty that is of the order of

$$\exp\{-20 \times 0.134\} = \exp\{-2.5\} = 0.07,$$

which is not acceptable. Thus, it makes sense to choose the value $U_n = 1$ only a fraction γ_0 of the time that $Y_n = 1$.

A large deviation of $g(U_n)$ occurs when its empirical mean value c is different from its expected value

$$\begin{aligned} E(g(U_n)) &= \gamma_0 P(Y_n = 1) - (1 - \gamma_0) P(Y_n = 1) - P(Y_n = 0) \\ &= \frac{2a_0\gamma_0}{a_0 + b_0} - 1. \end{aligned}$$

This can occur as a combination of two events: Y_n can be equal to 1 a fraction of time $\pi(1)$ that differs from $a_0/(a_0 + b_0)$ and the fraction of time that $U_n = 1$ when $Y_n = 1$ can be γ instead of γ_0.

Using the occupation method approach, the resulting empirical mean value of $g(U_n)$ is then

$$\frac{2a\gamma}{a + b} - 1$$

with a probability that is of the order of

$$\exp\{-nH(P) - nK[\gamma|P]\}$$

where $H(P)$ is as before and

$$K[\gamma|P] = -\pi(1)\gamma \log\left(\frac{\gamma_0}{\gamma}\right) - \pi(1)(1 - \gamma) \log\left(\frac{1 - \gamma_0}{1 - \gamma}\right)$$

Using the direct method, one calculates ψ_D from (3.3). Table 3.2 shows some numer-

ical results that again confirm the intuition.

a_0	b_0	γ_0	ψ_O	ψ_D
0.1	0.15	0.9	0.096	0.101
0.1	0.15	0.8	0.152	0.155
0.1	0.15	0.6	0.360	0.361
0.2	0.3	0.9	0.215	0.225
0.2	0.3	0.6	0.608	0.607

Table 3.2: Values of ψ when $P[U_n = 1|Y_n = 1] = \gamma_0$

Optimization

The setup is the same as in the previous example. However, in this example we want to choose γ_0 to maximize

$$E(r(Y_n, U_n))$$

subject to

$$P(W_n = 0) \approx \beta.$$

Assume that $r(0, u) = r(y, 0) = 0$ and $r(1, 1) = 1$. Thus, we want to maximize γ_0 such that $\psi \geq \beta/B$. The goal is to have a probability of the battery going empty of the order of $\exp\{-\beta\}$.

Say that $\beta = 4.6$, so that $\exp\{-\beta\} = 1\%$. Then, we find the results shown in Table 3.3 for $a = 0.1$ and $b = 0.15$. (We used the direct method.)

Not surprisingly, if the battery is smaller, one has to be more cautious in using it.

B	γ_0
50	0.92
40	0.87
30	0.80
20	0.70
10	0.54

Table 3.3: Values of γ_0 for optimization problem

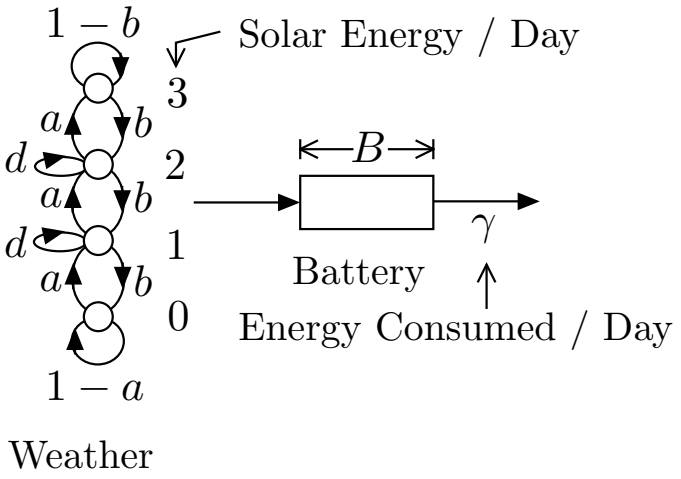

Figure 3.5: A wireless sensor node equipped with a solar cell.

Wireless Sensor Node

Figure 3.5 illustrates the power flow in a wireless sensor node. The node is equipped with a solar cell that generates a variable amount of power, depending on the state of the weather. Here, for the purpose of illustration, we think of the time unit being one day. The system is designed to transmit an amount of energy equal to γ per day. The problem is to determine the maximum value of γ such that the probability that the battery goes empty is about 1%.

We use the direct method, with the model that

$$P[U_n = 1|Y_n = y] = \gamma \text{ and } P[U_n = 0|Y_n = y] = 1 - \gamma.$$

Let $Y_n \in \{0, 1, 2, 3\}$ be the Markov chain that represents the weather. In the figure, $d := 1 - a - b$. The increment in the battery discharge is then

$$Z_n = V_n - Y_n,$$

where the V_n are i.i.d. Bernoulli with mean γ and are independent of the weather.

Using the direct method, we let

$$s_n(y) = E[\exp\{\theta(Z_1 + \cdots + Z_n)\}|Y_1 = y]$$

and we find that

$$\mathbf{s}_{n+1} = G_\theta \mathbf{s}_n$$

where

$$G_\theta(y, y') = h(y)P(y, y')$$

with

$$h(y) = E(\exp\{\theta(V_1 - y)\}) = [\gamma e^\theta + (1 - \gamma)]e^{-y\theta}.$$

We calculate the largest eigenvalue of G_θ then proceed as before, by using (3.3). Figure 3.6 shows the exponential rate of decay $\psi(\gamma)$ as a function of γ for relatively sunny and cloudy weathers.

From these curves, one can determine the maximum value of the usage of the sensor node described by γ as a function of the target error probability and of the battery size.

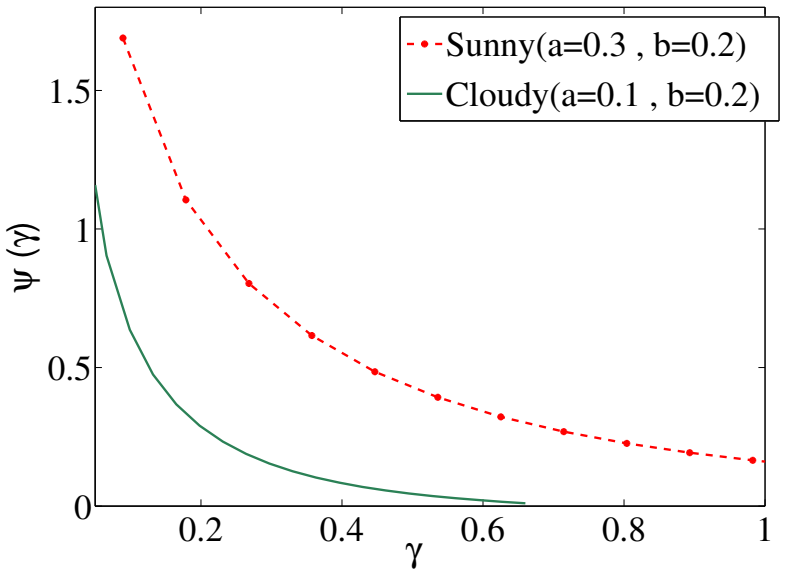

Figure 3.6: Exponential rate of decay as a function of γ in cloudy and sunny environments.

To verify the effectiveness of our proposed approach, we compare them to more complex policies derived using stochastic dynamic programming. Bellman's equation for the long-term average reward are as follows (see e,g. [77]):

$$v^* + \mathcal{H}(x) = \max_{u \in \mathcal{U}} [\mathrm{r}(x,u) + \sum_{x'} P(x,x';u)\mathcal{H}(x')]. \tag{3.12}$$

In this expression, v^* is the optimum reward, $\mathcal{H}(x)$ is the differential reward starting from state x and $\mathrm{r}(x,u)$ is the reward of taking action u in state x.

Figure 3.7 shows the comparison between direct method and dynamic programing for $a = 0.1,\ b = 0.15$. It can be shown in this figure that by increasing battery sizes, the average energy drain rate increases and our proposed direct method is relatively near to the result from dynamic programing. It also shows that they converge for larger battery sizes. This is quite promising as we claim our approach results in the

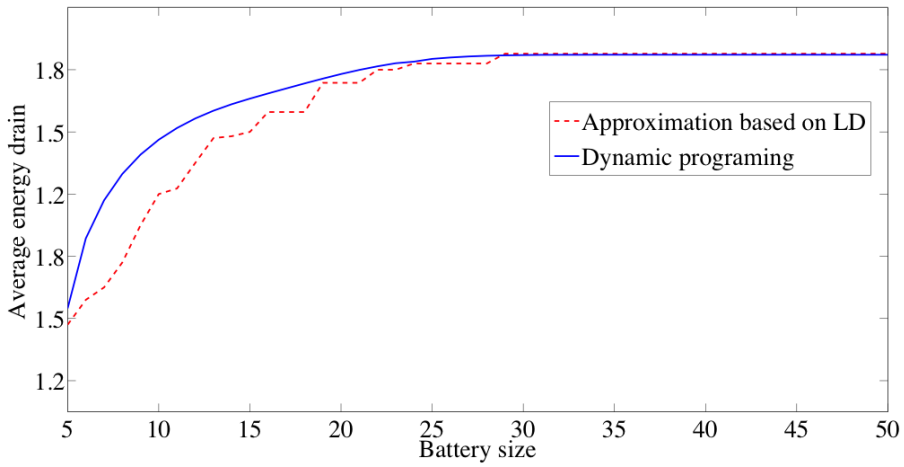

Figure 3.7: Comparison between dynamic programing and direct method over battery sizes for WSNs.

optimum solution for medium and large battery sizes. For smaller battery sizes, since the state space is relatively small, dynamic programing is less complex and can be a viable solution approach.

Building with Solar Panels and Variable Load

Figure 3.8 sketches the power flow of a building with a solar cell, a battery, and a variable load. The control parameter γ is the probability of using a higher rate instead of a lower one, given the level of activity in the building and $\bar{\gamma} = 1 - \gamma$. The problem is to determine the largest possible value of γ so that the probability that the battery gets depleted is acceptably small. As before, we compute $\psi(\gamma)$. The one-day depletion of the battery is

$$Z(n) = U(n) - Y_1(n).$$

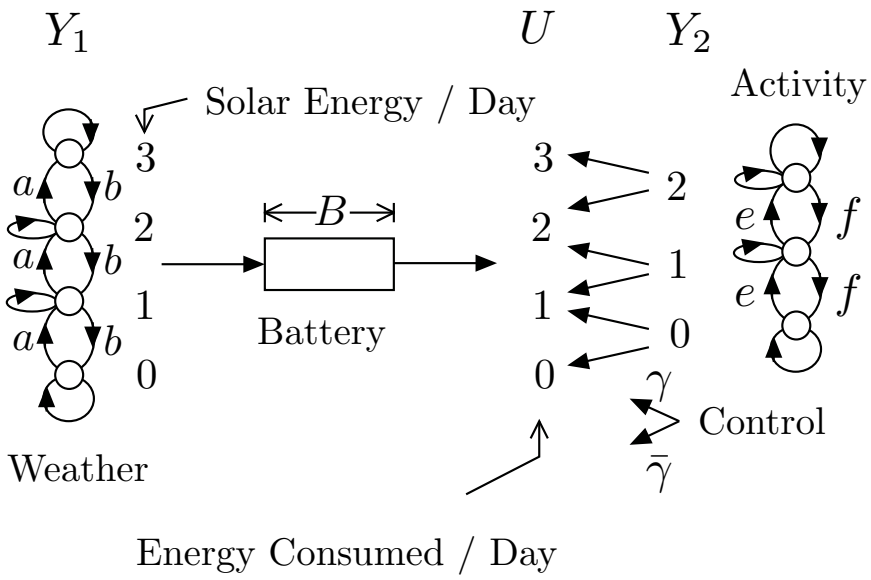

Figure 3.8: A self-sufficient building with a control parameter γ.

As before, we find

$$\mathbf{s}_{n+1} = G_\theta \mathbf{s}_n$$

where

$$G_\theta(y, y') = h(y)P(y, y'),$$

where

$$h(y) = E[\exp\{\theta(U(1) - y_1)\}|Y_2(1) = y_2]$$

$$= e^{\theta(y_2 - y_1)}[\gamma e^\theta + 1 - \gamma].$$

Figure 3.9 shows the numerical results.

Figure 3.10 shows the comparison between dynamic programing and direct method over battery sizes for $a = 0.1,\ b = 0.15,\ e = 0.15,\ b = 0.1$. By increasing battery

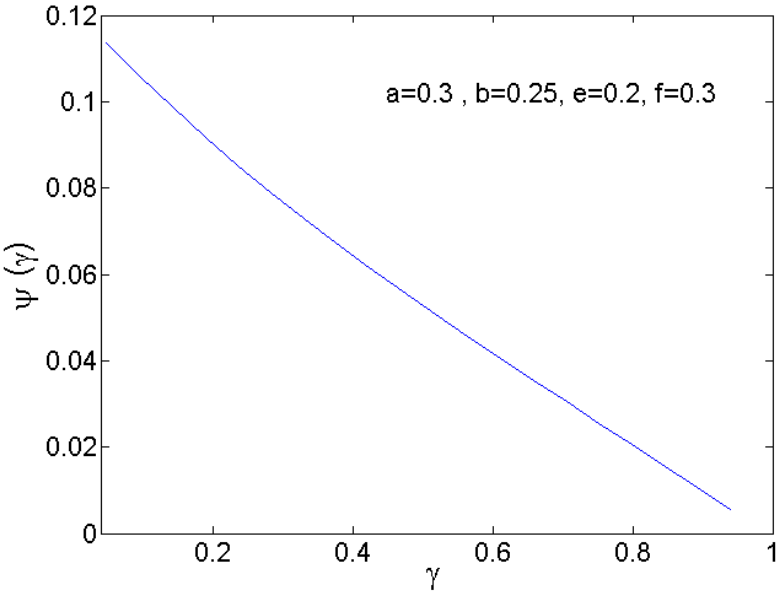

Figure 3.9: The numerical result for the building model.

sizes, the average energy drain rate increases. For medium and large battery sizes our proposed direct method is relatively near to the result from dynamic programing.

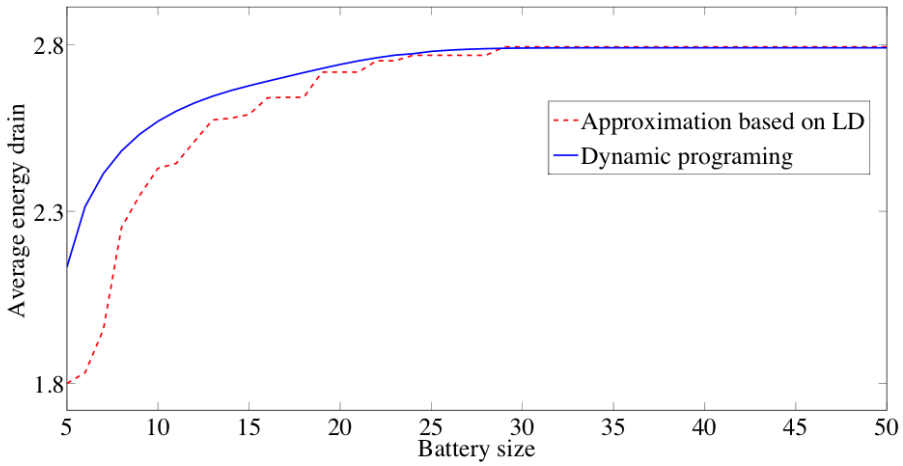

Figure 3.10: Comparison between dynamic programing and direct method over battery sizes for control of the self-sufficient building.

3.8 Conclusions

This work studies the control of systems that store renewable energy. The problem is to maximize the long-term utility of the energy by controlling how it is used. The methodology for designing the control policy depends on the size of the battery. When the battery size is moderate, the control is based on the large deviations of the battery charge. The benefit is that the resulting control law is simple, as it does not depend on the instantaneous charge of the battery. This work illustrates these methods with a number of examples.

Chapter 4

A Methodology for Designing the Control of Energy Harvesting Sensor Nodes

4.1 Introduction

Ambient energy harvesting is a solution to mitigate the typical finite energy supply of sensor nodes in wireless sensor networks (WSNs). Energy from renewable energy sources can recharge the sensor nodes' battery and extend the network's lifetime. However, designing the control of such systems that use renewable sources of energy presents new challenges because of the variability of these sources [63]. The energy usage should be carefully controlled in order to maximize system performance.

Consider a wireless sensor node equipped with a solar cell, a battery that stores the energy, and a data queue. The sensor node samples data and transmits it oppor-

tunistically depends on communication channel status and available energy and data. A complex control system would determine when to sample additional data and when to transmit on the basis of the backlog in the data queue, the energy stored in the battery, and the state of the environment, such as the weather and the quality of the channel. However, one hopes that a simpler system that does not include the data backlog and the stored energy in its decisions might perform almost as well, provided that the battery and data queue capacities are not very small.

4.1.1 Contributions of This Chapter

This chapter proposes a novel approach for designing the control policy for such systems. This approach takes into account the size of the energy and data buffers and produces a policy that performs satisfactorily for *medium* value of those sizes. Unlike existing literature, the policy does not depend on the instantaneous charge of the battery and backlog of the data queue and it has a low complexity. A main feature of the approach is to estimate the outage probability for the energy storage and the overflow probability for the data buffer and to design the policy to keep these probabilities acceptably small.

This methodology developed in this chapter uses results from the theory of large deviations. This theory offers a collection of techniques to estimate the properties of rare events, such as their frequency and most likely manner of occurrence.

The main idea of this chapter is to use a stochastic model of the system and estimate the likelihood that the data queue gets full or that the battery goes empty

by studying the large deviations of functions of appropriate Markov chains. These functions are parametrized by design choices for the control policy. The result is an optimization problem where the constraints are on the exponents of the large deviation probabilities. The main advantage of this approach is that the control policy for the energy usage and data sampling rate do not involve the instantaneous amount of energy stored in the nodes and data backlog which significantly simplifies the implementation. We evaluate the proposed method on representative examples.

This chapter is structured as follows. We introduce the system model and problem formulation in Sections 4.2 and 4.3. In Section 4.4, we approximate the control policy by replacing the constraints on probabilities by constraints on large deviation exponents. Section 4.5 explains the large deviation properties and introduces the notions of effective power of a variable source and effective consumption rate of a variable load. Section 4.6 provides numerical results for different examples. Section 4.7 concludes and summarizes this chapter.

4.2 Model

The system model for a sensor node is sketched in Figure 4.1. A discrete time model of the system is as follows. At time $n \geq 0$, the battery, with capacity B, has accumulated an amount $X_n \in \{0, 1, \ldots, B\}$ of energy. The finite data buffer at time n has $W_n \in \{0, 1, \ldots, D\}$ amount of data, where D is the capacity of data buffer. A battery stores energy it gets from a variable source and the node uses that energy to sample and transmit data. The more data the node transmits, the better. However, the node

cannot transmit when it runs out of energy. In this model, there are three independent Markov chains Y_n^1, Y_n^2 and Y_n^3, with respective transition matrices P_1, P_2, and P_3, that model the state of the sensed environment, the communication channel, and the renewable source, respectively. The amount A_n of data that the node samples is a function of Y_n^1 and of a control variable S_n. For instance, the sensor may sample the environment at a slow rate under normal conditions and more frequently when triggered by a proximity sensor or some other detection of an unusual condition. The

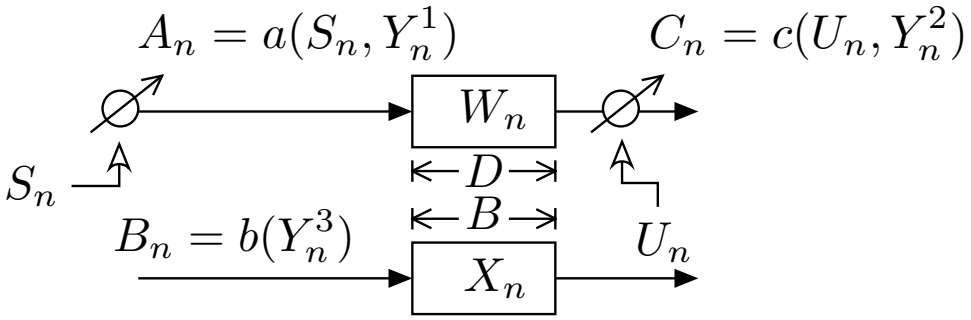

Figure 4.1: The sensor node.

sampling is controlled by the variable $S_n \in \mathcal{S}$, where $\mathcal{S}$ is a finite set, to adjust its rate to a value compatible with the ability of the node to transmit the data it samples. Moreover, $U_n \in \mathcal{U}$ is the amount of energy the node uses to transmit at time n where $\mathcal{U}$ is a finite set. The amount C_n of data that the node transmits depends on the state Y_n^2 of the communication channel and on the amount U_n of energy that the node uses to transmit under a given physical layer modulation and coding strategy. This model considers that the energy required to sample the environment is negligible compared to the energy required to transmit data. Finally, the amount B_n of energy that the renewable source produces at time n is a function of a Markov chain Y_n^3.

This model is representative of the type of system that the methodology in this work can address. Many variations are possible. For instance, the energy that sampling requires might be non-negligible. Moreover, one might be able to move the solar cell by spending some energy. Our goal is to illustrate the methodology on a fairly simple, but non-trivial, example that captures the essence of the method but avoids complicating the setup.

4.3 Formulation

The objective is to maximize the average rate at which the node gets to sample *and* transmit data. Note that these average rates must be equal if the system is stable. The node cannot sample when its data buffer is full and it cannot transmit when it runs out of energy.

One could formulate this objective as a Markov decision problem. The result would be control decisions of the form

$$S_n = \gamma_1(Y_n^1, Y_n^2, Y_n^3, X_n, W_n) \text{ and } U_n = \gamma_2(Y_n^1, Y_n^2, Y_n^3, X_n, W_n).$$

The possible actions S_n and U_n at each time are constrained to avoid the battery

underflows and data buffer overflows. That is, the problem is as follows:

$$
\begin{aligned}
\text{Maximize} \quad & \lim_{N\to\infty} \frac{1}{N} \sum_{n=0}^{N} E(a(S_n, Y_n^1)) \\
\text{over} \quad & \gamma_1, \gamma_2 \\
\text{s.t.} \quad & X_{n+1} = \min\{X_n + b(Y_n^3) - U_n, B\}, \\
& W_{n+1} = W_n + a(S_n, Y_n^1) - c(U_n, Y_n^2), \\
& U_n \leq X_n + b(Y_n^3), \\
& c(U_n, Y_n^2) \leq W_n + a(S_n, Y_n^1), \\
& a(S_n, Y_n^1) \leq D - W_n + c(U_n, Y_n^2).
\end{aligned}
$$

where $a(.)$ (as can be seen in Figure 4.1) is the data rate input to the data queue which is a function of the sensed environment and sampling decision. $b(.)$ is the energy input to the battery and $c(.)$ is the data transmission rate. The optimal policy is complicated to implement because it requires monitoring precisely the data backlog and the amount of energy stored in the battery. Finding the policy also requires solving a Markov decision problem with a large state space. For those reasons, we explore simpler policies.

4.4 Control Policy

Intuition suggests that if the battery capacity is not too small, then the fluctuations in the amount of renewable power B_n average out and make it unnecessary to react in real time to them. Thus, one expects that the transmission and sampling decisions

should not depend on the state Y_n^3. Similar considerations suggest that S_n should not depend on the fluctuations of the transmission channel Y_n^2 or the weather Y_n^3. Moreover, one expects that the decisions should not depend on the instantaneous values of X_n and W_n. Thus, a good policy should be one where the sampling decision S_n depends only on the state Y_n^1 of the sensed environment and the transmission decisions U_n depend only on the quality Y_n^2 of the communication channel. Clearly this simplification of the control policies results in a loss of performance, but the conjecture is that this loss is negligible when D and B are not too small.

Accordingly, we formulate the problem as follows. We choose control policies of the form

$$S_n = \gamma_1(Y_n^1) \text{ and } U_n = \gamma_2(Y_n^2).$$

That is, at the outset we limit the complexity of the control policies. The sampling rate depends on the state of the sensed environment and the transmission rates depend on the state of the channel. The intuitive justification for the structure of these policies is that the effectiveness of sampling is related instantaneously to the state Y_n^1 and that of transmission to Y_n^2. The constraints appear indirectly through the battery and data buffer, and are thus decoupled in time from the instantaneous states of the Markov chains.

More generally, we consider randomized policies specified as follows:

$$P[S_n = s|Y_n^1 = y^1] = \sigma(y^1, s) \text{ and } P[U_n = u|Y_n^2 = y^2] = \tau(y^2, u).$$

Thus, a policy is completely specified by the two stochastic matrices σ and τ. The randomization enlarges the set of strategies to make it possible to meet the performance constraints with equality.

Figure 4.2 shows the resulting system.

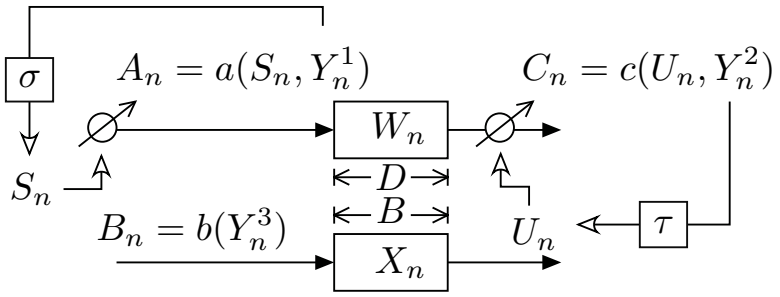

Figure 4.2: The sensor node with its control policies.

The goal of this work is to explore a methodology for designing good policies of the form indicated above.

A brute force approach would be to formulate the problem of optimizing σ and τ as a linear optimization problem of the following form :

$$\text{Maximize } E_{\sigma,\tau}(A) \tag{4.1}$$

$$\text{over } \sigma \text{ and } \tau$$

$$\text{s.t. } P_{\sigma,\tau}(X = 0) \leq \epsilon, P_{\sigma,\tau}(W = D) \leq \epsilon. \tag{4.2}$$

In this formulation, $P_{\sigma,\tau}(\cdot)$ and $E_{\sigma,\tau}(\cdot)$ correspond to the invariant distribution of $(Y_n^1, Y_n^2, Y_n^3, X_n, W_n)$ that results from the policy (σ, τ). This problem is linear in σ and τ because the expectation and the probability constraints are linear in the invariant distribution, and the latter solves linear equations in the transition probabilities

and these are linear in σ and τ. See Theorem 3.1 of [78] for a discussion of this formulation of average cost dynamic programming as a linear program.

Also, ϵ is a very small value. The justification for this formulation is that, since the control decisions S_n and U_n are not based on X_n nor W_n, one must make sure that the policies do not violate the physical constraints. This constraint is relaxed by specifying that the probability that they are violated is very small.

Instead of pursuing this large optimization problem, we use the structure of the problem to express the constraints in terms of large deviations of W_n and X_n. The central idea is that (see Appendix C)

$$P_{\sigma,\tau}(X = 0) \approx \exp\{-\alpha(\tau)B\} \text{ and } P_{\sigma,\tau}(W = D) \approx \exp\{-\beta(\sigma,\tau)D\}.$$

Here, α and β are the large deviations exponents for the random processes X_n and W_n, respectively. Also, the first expression means precisely that

$$\lim_{B\to\infty} \frac{1}{B} \log\{P_{\sigma,\tau}(X = 0)\} = -\alpha(\tau), \tag{4.3}$$

and similarly for the second approximation. Thus, the approximations are asymptotic in the relevant size and they ignore the factors of the exponentials. We use these approximations to obtain estimates of the small probabilities.

Using the approximations, we rewrite the problem as follows:

$$\text{Maximize } E_{\sigma,\tau}(A) \tag{4.4}$$

$$\text{over } \sigma \text{ and } \tau$$

$$\text{s.t. } \alpha(\tau) \geq -\log(\epsilon)/B \text{ and } \beta(\sigma,\tau) \geq -\log(\epsilon)/D. \tag{4.5}$$

In the next section, we explain the method for calculating $\alpha(\tau)$ and $\beta(\sigma,\tau)$. The problem is then solved by first choosing τ such that $\alpha(\tau) = -\log(\epsilon)/B$ and then choosing σ such that $\beta(\sigma,\tau) = -\log(\epsilon)/D$. This solution is justified by the fact that, in our problem, the data transmission rate is maximized by using the most energy possible, given the constraint on the probability that the battery is empty. Thus, one can first choose τ to meet that objective and then choose the value of σ to meet the constraint on the data buffer occupancy.

When D and W become large, the solutions of the formulations (4.1)-(4.2) and (4.4)-(4.5) become identical. The reason is that, in that case, the constraints (4.5) become $\alpha(\tau) \geq 0$ and $\beta(\sigma,\tau) \geq 0$, which are satisfied if $E(A_n) \leq E(C_n)$ and $E(B_n) \geq E(U_n)$, and these are the same as constraints (4.2).

4.5 Large Deviations for Markov chains

In this section, we explain a method for calculating the large deviation exponents α and β. The backlog in the data queue and the amount of energy stored in the battery are both modeled as the content of a queue whose arrivals and departures are

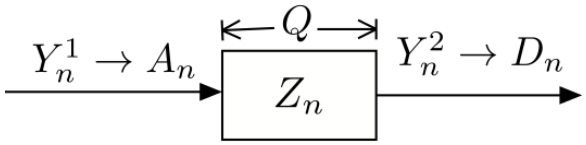

Figure 4.3: The queue with Markov-modulated arrivals and departures.

determined by the states of two independent Markov chains.

Accordingly, we need to study systems such as the one shown in Figure 4.3 where we have a buffer with the capacity Q and accumulated content of the buffer Z_n. In this system, there are two independent Markov chains Y_n^1 and Y_n^2 and random variables for arrival A_n and departure D_n such that

$$P[A_n = a|Y_n^1 = y^1, Y_n^2 = y^2] = p(y^1, a), P[D_n = d|Y_n^1 = y^1, Y_n^2 = y^2] = q(y^2, d).$$

One then defines the backlog Z_n in a queue with arrivals A_n and departures D_n as follows:

$$Z_{n+1} = [Z_n + A_n - D_n]_0^Q$$

where Q is the capacity of the queue. In the last expression, the notation is $[z]_0^Q = \max\{0, \min\{x, Q\}\}$.

One expects that if

$$E(A_n) > E(D_n),$$

then the stationary probability $P(Z_n = 0)$ that the queue is empty is very small when

Q is large. In fact, we explain in Appendix C that

$$\lim_{Q\to\infty} \frac{1}{Q} \log\{P(Z_n = 0)\} = -\psi(p, q) \tag{4.6}$$

for some $\psi(p, q) > 0$. Specifically,

$$\psi(p, q) = \inf_{d>a} \frac{\phi_A(a, p) + \phi_D(d, q)}{d - a}. \tag{4.7}$$

In this expression,

$$\phi_A(a, p) = \sup_{\theta<0}\{\theta a - \log(\lambda_A(\theta, p))\} \tag{4.8}$$

where $\lambda_A(\theta, p)$ is the largest eigenvalue of the matrix $G^A_{\theta,p}$ defined by

$$G^A_{\theta,p}(y^1, \tilde{y}^1) = [\sum_a e^{\theta a} p(y^1, a)] P_1(y^1, \tilde{y}^1).$$

where $P_1(y^1, \tilde{y}^1) = P_1[Y^1_n = \tilde{y}^1 | Y^1_{n-1} = y^1]$. Similarly,

$$\phi_D(d, q) = \sup_{\theta>0}[d\theta - \log(\lambda_D(\theta, q))] \tag{4.9}$$

where $\lambda_D(\theta)$ is the largest eigenvalue of the matrix $G^D_{\theta,q}$ defined by

$$G^D_{\theta,q}(y^2, \tilde{y}^2) = [\sum_d e^{\theta d} q(y^2, d)] P_2(y^2, \tilde{y}^2).$$

Using this method, we can calculate the decay rates $\alpha(\tau)$ and $\beta(\sigma, \tau)$ for the battery and the data buffer shown in Figure 4.2.

To calculate $\alpha(\tau)$, one notes that the battery system is identical to the system in Figure 4.3 since its arrivals B_n and departures U_n are functions of two independent Markov chains Y_n^3 and Y_n^2. Similarly, to calculate $\beta(\sigma, \tau)$, one observes that if one considers a queue with arrivals C_n and departures A_n, then its occupancy Z_n behaves like $D - W_n$, so that the probability that it is empty is the probability that $W_n = D$. Accordingly, $P(W_n = D) = P(Z_n = 0)$ can be calculated using the method of this section.

4.6 Effective Power and Effective Consumption Rate

In this section, we adapt the notion of *effective bandwidth* (see e.g., [71,72]) to variable sources and variable loads, as a summary of their statistical characteristics. The novelty of our analysis is that we consider queues where the arrivals and departures are both variable.

The result of this section is that one can define the *effective power* of a variable renewable source and the *effective consumption rate* of a variable load in a way that the battery is almost never empty if and only if the former is larger than the latter. The effective power and effective consumption rate depend on the battery capacity. If the capacity is infinite, the effective power and consumption rate are simply the mean values. For a finite capacity, the effective power is less than the average renewable power and the effective consumption rate is larger than the mean value of the load. In such a system, the battery is rarely empty if there is a sufficient gap between the average power and the average consumption rate, and the effective values determine

the required gap.

The results provided in this section correspond to the model shown in Figure 4.3 where the queue is the battery and A_n and D_n represent the energy arrival and consumption, respectively.

Definition 4.1. *Consider a random sequence A_n that is a function of a Markov chain, as in Figure 4.3. For a given $\delta > 0$, the* effective power *of the sequence A_n is the maximum value of c such that the sequence Z_n defined by*

$$Z_{n+1} = [Z_n + A_n - c]_0^Q, n \geq 0$$

has a stationary distribution $P(\cdot)$ such that

$$\lim_{Q\to\infty} \frac{1}{Q} \log\{P(Z_n = 0)\} \leq -\delta.$$

□

Thus, the effective power of the sequence A_n is the maximum constant departure rate $D_n = c$ from a queue with arrivals A_n in the model shown in Figure 4.3 so that the probability that the queue is empty decays exponentially fast in Q with rate at least δ.

Intuitively, if the effective power of a random source A_n is c, then the source equipped with a battery can deliver a constant power c. The effective power is a value that decreases from the mean value $E(A_n)$ to 0 as δ increases. Thus, if the battery size is Q and we want the probability that the battery is empty to be of the

order of $\epsilon \ll 1$, then we need $\exp\{-Q\delta\} \approx \epsilon$, so that $\delta \approx -\log(\epsilon)/Q$. The effective power for a given $\epsilon \ll 1$ then increases from 0 to $E(A_n)$ as the battery size increases. For instance, the effective power of a solar panel is its average power if it is equipped with a very large battery. If the battery is small, the effective power is considerably smaller.

Using the results of Appendix A, one can show that

$$\lim_{Q\to\infty} \frac{1}{Q} \log\{P(Z_n = 0)\} = -\inf_{a<c} \frac{\phi_A(a,p)}{c-a}. \tag{4.10}$$

Thus, the effective power is the maximum value of c such that

$$\inf_{a<c} \frac{\phi_A(a,p)}{c-a} \geq \delta. \tag{4.11}$$

Using the argument introduced in [71], one then has the following result.

Theorem 4.1. *The effective power of a sequence* $\{A_n, n \geq 1\}$ *is given by*

$$\frac{\phi_A(\delta,p)}{\delta}$$

where

$$\phi_A(\delta,p) = \sup_{\theta<0}\{\theta\delta - \log(\lambda_A(\theta,p))\}.$$

■

We also have the following definition.

Definition 4.2. *Consider a random sequence* D_n *that is a function of a Markov*

chain, as in Figure 4.3. For a given $\delta > 0$*, the* effective consumption rate *of the sequence* D_n *is the minimum value of* a *such that the sequence* Z_n *defined by*

$$Z_{n+1} = [Z_n + a - D_n]_0^Q, n \geq 0$$

has a stationary distribution $P(\cdot)$ *such that*

$$\lim_{Q\to\infty} \frac{1}{Q} \log\{P(Z_n = 0)\} \leq -\delta.$$

Thus, the effective consumption rate of the sequence D_n is the minimum constant power that one needs to provide the battery with output D_n so that it is empty only with a small probability. This value is an equivalent constant power, after being smoothed out by the battery. The effective consumption rate for a given small probability of the battery being empty decreases from the peak value of D_n to the average value $E(D_n)$ as the battery increases.

Using the results of Appendix A, one can show that

$$\lim_{Q\to\infty} \frac{1}{Q} \log\{P(Z_n = 0)\} = -\inf_{d>a} \frac{\phi_D(d, q)}{d - a}. \tag{4.12}$$

Thus, the effective power consumption is the smallest value of a such that

$$\inf_{d>a} \frac{\phi_D(d, q)}{d - a} \geq \delta. \tag{4.13}$$

Once again using the argument of [71], one has the following result.

Theorem 4.2. *The effective consumption rate of the sequence* $\{D_n, n \geq 1\}$ *is given by*

$$\frac{\phi_D(\delta, q)}{\delta}$$

where

$$\phi_D(\delta, q) = \sup_{\theta>0}\{\theta d - \log(\lambda_D(\theta, q))\}.$$

■

We then have the following intuitive result for the system model of Figure 4.3 where the queue is energy buffer. This result is a two-sided version of the corresponding result in [71] in that it applies to queues with random arrivals and departures.

Theorem 4.3. *For some* $\delta > 0$*, the stationary probability* $P(\cdot)$ *of the queue is such that*

$$\lim_{Q\to\infty} \frac{1}{Q} \log\{P(Z_n = 0)\} \leq -\delta \tag{4.14}$$

if and only if there is some c *such that the effective power of the arrivals* A_n *is at least* c *and the effective consumption rate of the departures* D_n *is less than* c*.*

Proof.

(a) Sufficiency. Assume that the effective power of A_n is larger than c. That implies, by (4.11), that

$$\frac{\phi_A(a, p)}{c - a} \geq \delta, \forall a < c,$$

so that

$$\phi_A(a, p) \geq (c - a)\delta, \forall a < c.$$

Similarly, assuming that the effective consumption rate of D_n is less than c, we get that

$$\phi_D(d,q) \geq (d-c)\delta, \forall d > c.$$

Consequently,

$$\phi_A(a,p) + \phi_D(d,q) \geq (d-a)\delta, \forall d > a.$$

Hence,

$$\frac{\phi_A(a,p) + \phi_D(d,q)}{d-a} \geq \delta, \forall d > a,$$

which implies, from (4.7), that (4.14) holds.

(b) Necessity. Assume that the queue has the indicated property. Let a^* and d^* be the minimizers of

$$\frac{\phi_A(a,p) + \phi_D(d,q)}{d-a}$$

with $a^* > d^*$ and let δ be the minimum value. The first order conditions are

$$\phi'_A(a^*,p) = -\phi'_D(d^*,q) = \delta.$$

Now, choose c so that

$$\frac{\phi_A(a^*,p)}{c-a^*} = \delta.$$

Then we see that

$$\phi'_A(a^*,p)(c-a^*) = \phi_A(a^*,p),$$

so that a^* minimizes

$$\frac{\phi_A(a,p)}{a-c}$$

and the minimum is δ. Similarly, d^* minimizes

$$\frac{\phi_D(d,q)}{c-d}$$

and the minimum is also δ, which proves the claim.

□

4.7 Numerical Results

In this section, we present numerical results for the system shown in Figure 4.4. In this example, the two-state Markov chains $Y_n^1,\ Y_n^2,\ Y_n^3 \in \{1,\ 2\}$ represent the sensed environment, communication channel and harvested energy per unit time, respectively.

We consider randomized policies specified as follows:

$$P[S_n = y|Y_n^1 = y] = \sigma,\ \ \forall\ y = 1, 2.$$

$$P[S_n = y-1|Y_n^1 = y] = 1-\sigma,\ \ \forall\ y = 1, 2.$$

Similarly,

$$P[U_n = y|Y_n^2 = y] = \tau,\ \ \forall\ y = 1, 2.$$

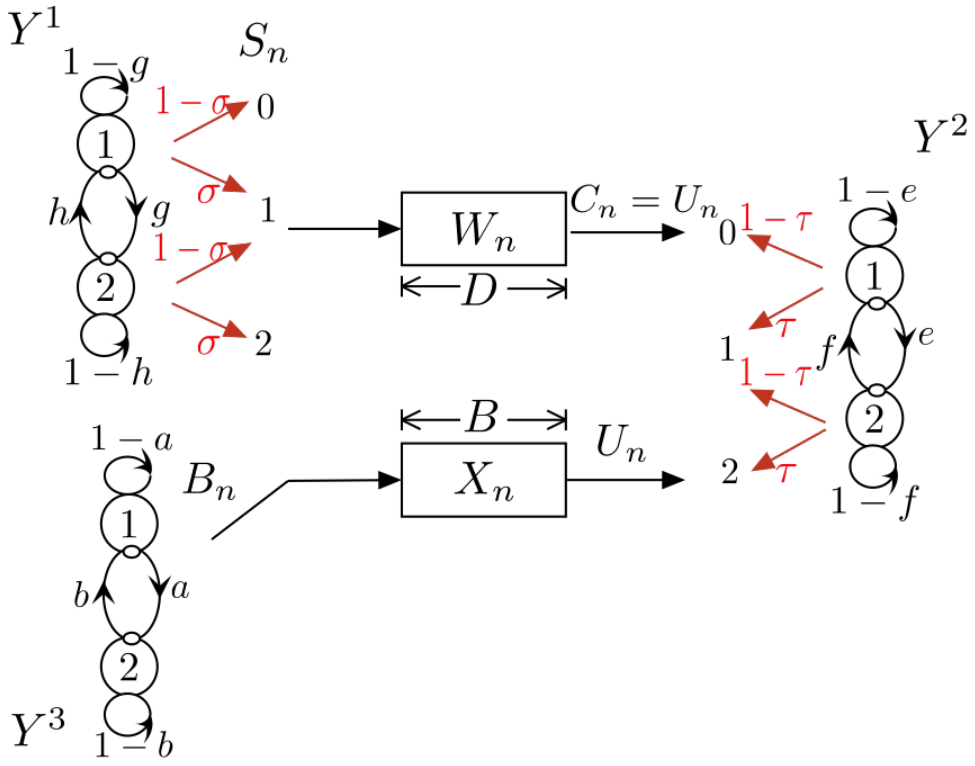

Figure 4.4: Model of the system with 2-state Markov chains Y^1, Y^2, Y^3.

$$P[U_n = y - 1 | Y_n^2 = y] = 1 - \tau, \quad \forall\, y = 1, 2.$$

We set $C_n = U_n$. To use the results of the previous section, we compute the largest eigenvalue of the matrix

$$G_\theta(y^2, y^3, y'^2, y'^3) = h(y^2, y^3) P(y^2, y^3, y'^2, y'^3),$$

where

$$\begin{aligned} h(y^2, y^3) &= E[\exp\{\theta(U_0 - B_0)\} | Y_0^2 = y^2, Y_0^3 = y^3] \\ &= e^{\theta(y^2 - y^3)}[\tau + (1-\tau)e^{-\theta}]. \end{aligned}$$

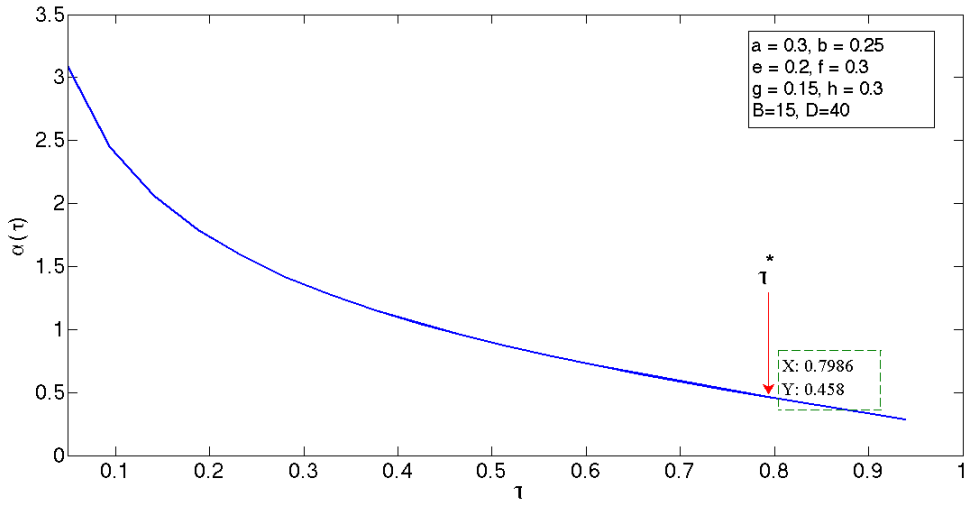

Figure 4.5: Exponential rate of decay as a function of τ with parameters from Fig. 4.4.

Figure 4.5 shows the exponential rate of decay $\alpha(\tau)$ as a function of τ. In order to calculate the τ^*, we need to find the lower bound for $\alpha(\tau)$ which is $-\log(\epsilon)/B$ from (4.4). We set the probability that battery goes empty (ϵ) to be 0.02 and B battery capacity to be 15 units. Hence, τ^* is determined as shown in Figure 4.5.

Considering τ^* and analyzing the data buffer, we can compute $\beta(\sigma, \tau^*)$. The value of $h(y^1, y^2)$ is calculated as follows

$$\begin{aligned} h(y^1, y^2) &= E[\exp\{\theta(S_0 - C_0)\} | Y_0^1 = y^1, Y_0^2 = y^2] \\ &= \tau^* e^{\theta(y^1 - y^2)}[\sigma + (1-\sigma)e^{-\theta}] + (1-\tau^*)e^{\theta(y^1-y^2)}[\sigma e^{\theta} + (1-\sigma)]. \end{aligned}$$

Figure 4.6 shows the exponential rate of decay $\beta(\sigma, \tau^*)$ as a function of σ. We can determine σ^* by finding the lower bound $-\log(\epsilon)/D$ where $\epsilon = 0.01$, $D = 40$. Then,

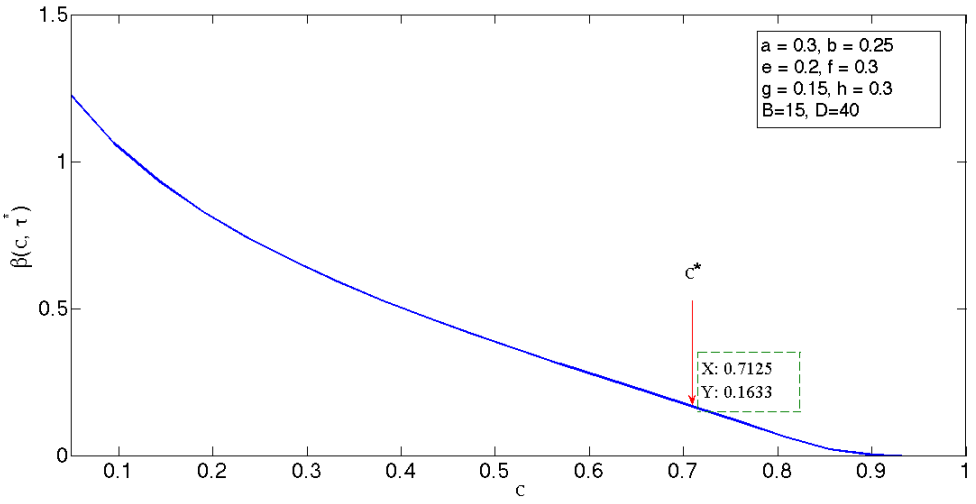

Figure 4.6: Exponential rate of decay as a function of σ with parameters from Fig. 4.4.

the average sampling rate can be calculated as follows

$$\pi(1)\sigma^* + \pi(2)(\sigma^* + 1).$$

Numerical examples are provided which shows that this method works for different system parameters. This is tabulated in Table 4.1, which shows that the values of a and b have an effect on both control policies τ^* and σ^*. Not surprisingly, increasing b or decreasing a causes the values of the control policy to decrease.

a	b	τ^*	σ^*	$\alpha(\tau^*)$	$\beta(\sigma^*, \tau^*)$
0.15	0.1	0.65	0.71	0.46	0.15
0.3	0.2	0.82	0.94	0.44	0.14
0.45	0.3	0.94	1	0.42	0.13
0.15	0.2	0.39	0.13	0.81	0.12
0.15	0.35	0.16	0.08	1.5	0.15

Table 4.1: Values of control policy obtained using the direct method, given $g = 0.15$, $h = 0.3$.

Table 4.2 shows the effect of varying g and h on the control policies. As can be

g	h	τ^*	σ^*	$\alpha(\tau^*)$	$\beta(\sigma^*, \tau^*)$
0.15	0.3	0.79	0.70	0.45	0.16
0.25	0.3	0.79	0.61	0.45	0.14
0.45	0.3	0.79	0.46	0.45	0.16
0.15	0.2	0.79	0.37	0.45	0.17
0.45	0.4	0.79	0.56	0.45	0.13

Table 4.2: Values of control policy obtained using the direct method, given $a = 0.3$, $b = 0.2$.

seen in Table 4.2, increasing g causes the policy for sampling rate σ to act more conservatively by decreasing σ. Not surprisingly, τ^* and $\alpha(\tau^*)$ are constant by changing the values of g and h.

4.7.1 Stochastic Dynamic Programming

To demonstrate the effectiveness of the solution approach, we compare it with the results obtained by stochastic dynamic programming. It solves the original problem introduced in Section 4.3. Bellman's equation for the long-term average reward are as follows (see e,g. [77]):

$$v^* + \mathcal{H}(x) = \max_{u \in \mathcal{U}} [\mathrm{r}(x, u) + \sum_{x'} P(x, x'; u)\mathcal{H}(x')]. \tag{4.15}$$

In this expression, v^* is the optimum reward, $\mathcal{H}(x)$ is the differential reward starting from state x and $\mathrm{r}(x, u)$ is the reward of taking action u in state x.

The value iteration for average reward dynamic programing works as follows: we choose the value of $\mathcal{H}^0(x) = 0$ for all states $x = 1, ..., n$. For each time step $k =$

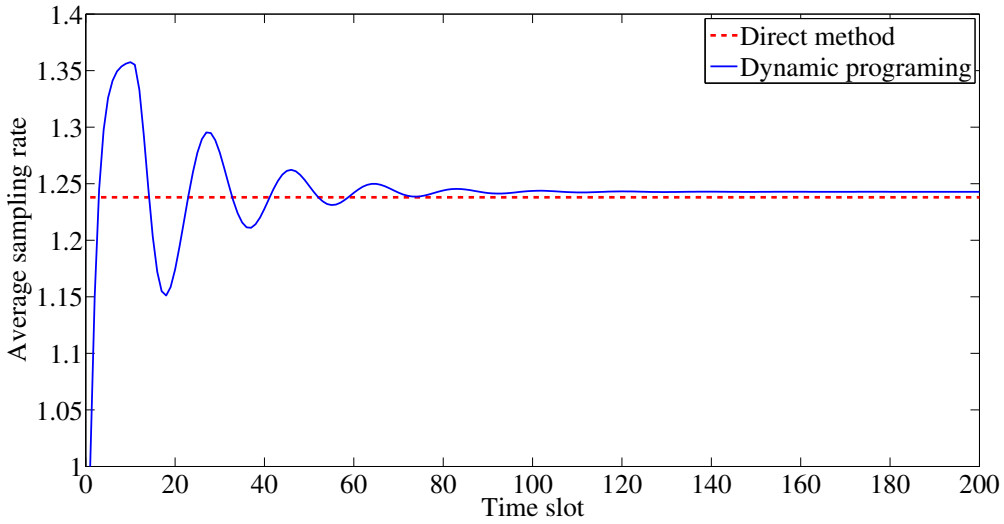

Figure 4.7: Comparison of dynamic programing and direct method with same settings.

$1, ..., K$, the Bellman's equation $Th^k(x) := \max_{u \in \mathcal{U}}[\mathrm{r}(x,u) + \sum_{x'} P(x,x';u)\mathcal{H}^k(x')]$ is updated for all states. We choose an arbitrary reference state x_0 which is constant for all time steps. Then, we set $v^k = Th^k(x_0)$ and update the differential reward function as $\mathcal{H}^{k+1}(x) = Th^k(x) - v^k$. The value of v^k for the last step is the optimum average reward. For our example shown in Figure 4.4, the system states are $(X_n, W_n, Y_n^1, Y_n^2, Y_n^3)$. We use the same setting applied for developing our approach. Figure 4.7 shows the optimal average reward that the algorithm calculates, as a function of the number of iterations. As can be seen, the algorithm converges to the essentially the same average value as determined from our control policy with same setting. This shows that our solution method results in essentially the optimal transmission rate achieved by dynamic programing. Note that in dynamic programing, we observe the state of the battery and the data buffer at the start of every time slot for making decisions.

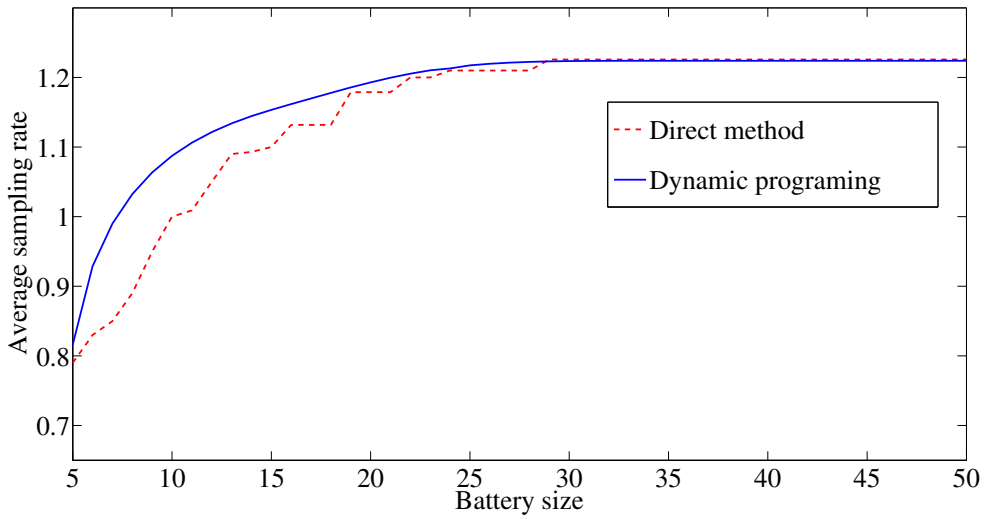

Figure 4.8: Comparison of sampling rate results from dynamic programing and direct method for different battery sizes.

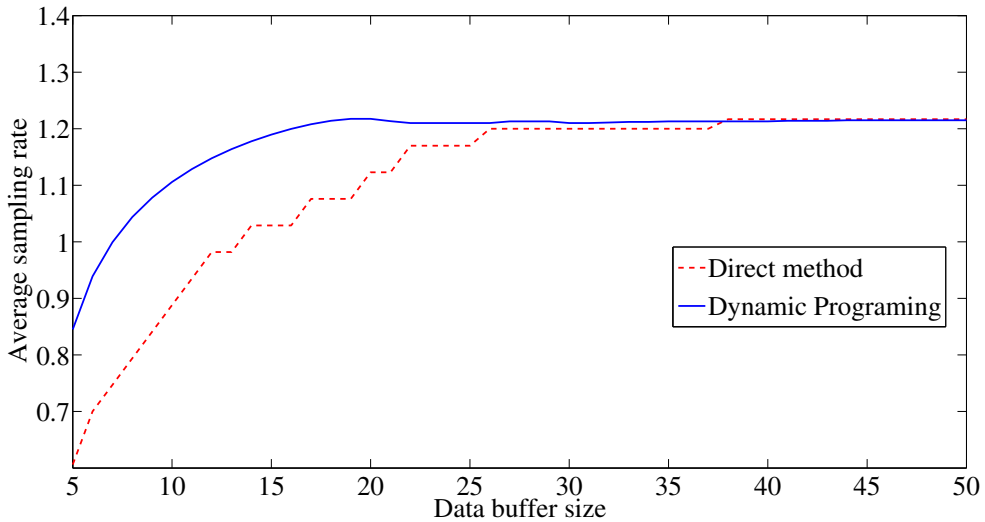

Figure 4.9: Comparison of sampling rate results from dynamic programing and direct method for different data buffer sizes.

Another set of simulation runs is conducted using different battery sizes. Figure 4.8 shows that by increasing battery sizes, the average sampling rate increases and our proposed direct method is relatively near to the result from dynamic programing. It also shows that they converge for larger battery sizes. This is quite promising as we claim our methodology results in optimum solution for medium and large battery sizes. For smaller battery sizes, since the state space is relatively small, dynamic programing is less complex and can be a viable solution approach. Similar results for different data buffer sizes are shown in Figure 4.9. By increasing the size of the buffer (data or energy), the dynamic programing alters to a linear programing with constraints related to average arrival and departure. For example, the constraint for energy queue is to drain the energy at the rate less than the average arrival rate. For our approach, given the constant ϵ, by increasing the size of the buffer, the large deviation exponent is approaching to zero. This point, for example in energy buffer, means that the drain rate should be less than the expected value of arrival rate (for more details see Theorem 3.1. in [68]). This is the reason that for the very large battery size, the result from both approaches converges. The key point of this result is the advantage of our approach for the medium battery size, which for our proposed approach is fairly near to the optimum result.

Figure 4.10 and 4.11 show representative results measured by simulating X_n and W_n for 10^6 steps for different value of battery sizes. The failure rate for the battery is calculated as the number of times that the battery goes empty over the number of steps (10^6 in the example here). The failure rate for the buffer is calculated as the number of times that the buffer becomes full over the number of steps. The results

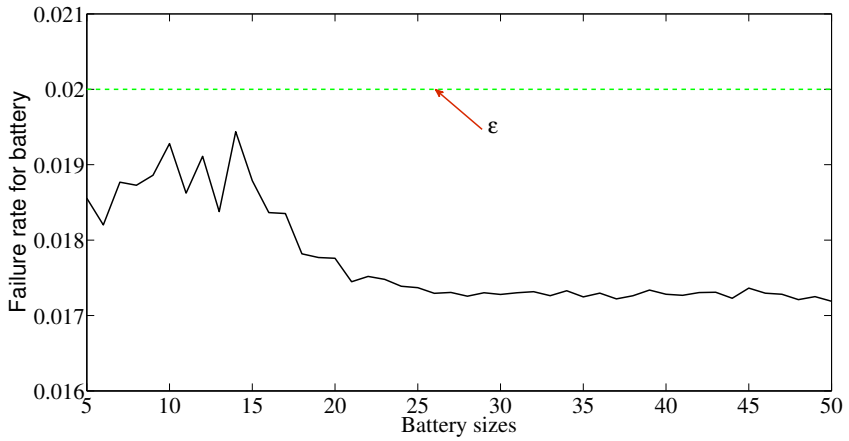

Figure 4.10: Failure rate for battery applying direct method, given ϵ for battery is 0.02.

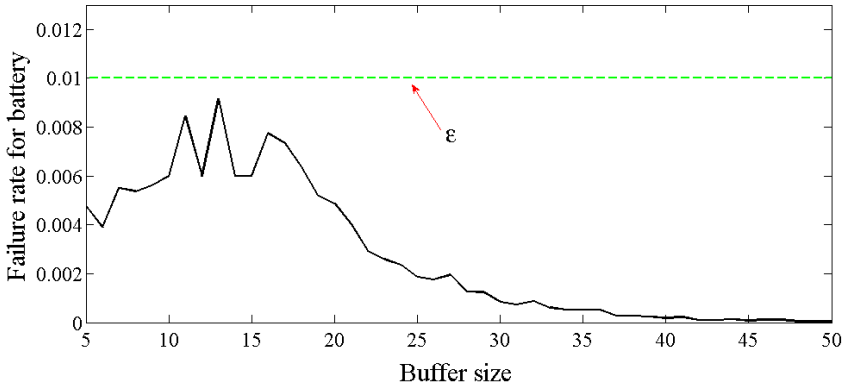

Figure 4.11: Failure rate for buffer applying direct method, given ϵ for data buffer is 0.01.

show that for different battery sizes, the constraints for the battery and data buffer are not violated, since they are always less than ϵ. This is because in our simulation for calculating σ^* and τ^*, $\alpha(\tau)$ and $\beta(\sigma, \tau)$ are bounded by $-\log(\epsilon)/B$ and $-\log(\epsilon)/D$ respectively.

4.8 Conclusions

This is a methodological work that presents a technique for state space dimension reduction for solving optimal control of systems with coupled data buffer and energy storage. The technique consists of relaxing the underflow constraint on the energy level in the battery and overflow constraint on the data backlogs in data buffer by replacing them with a bound on the probability of energy underflow and data overflow as derived via large deviation theory. The considered policies do not depend on the state of the battery and data buffer, but rather only of the state of the environment. We demonstrated the use of the approach for the control of a wireless sensor node equipped with a solar panel and compared the results with the solution of the Markov decision problem.

It should be noted that the analysis assumes a detailed knowledge of the statistics of the renewable source and the environment. The methodology suggests adaptive schemes that do not require such knowledge and the analysis of such schemes is left for further investigation.

Our approach assumes a knowledge of statistical models of the renewable energy, of the channel, and of the data collection. Hopefully, these models can be fitted

over time. Also, although the numerical complexity of the approach grows with the complexity of the model, the method may be practical even for fairly large models.

Chapter 5

Energy Harvesting Aware Task Allocation for Solar-Powered Sensor Networks

5.1 Introduction

A sensor network, which is a network of collaborating embedded devices with capabilities of sensing, computation and communication, is used to run specific applications (such as target tracking, event detection, etc). Energy is a most precious resource in running these applications [63]. Hence, nodes will operate for a finite duration which implies a finite lifetime of the applications of interest or additional cost to regularly change batteries. An alternative technique is the use of energy harvesting as a source of powering sensor nodes. This ensures sustainable operation of such systems. However, the harvested energy is usually not sufficient to allow the sensor nodes to

stay active all the time. Moreover, the time varying availability of environmental energy results in dynamic changes of the system's available energy. Therefore, the dynamic resource and task allocation for energy harvesting wireless sensor networks (EH-WSNs) are required, presenting a new set of problems in the area of networking and communication [6].

In wireless sensor networks (WSNs), energy-aware task allocation algorithms deal with energy availability of batteries, which typically have a monotonically decreasing energy profile. However, in EH-WSNs, due to the fluctuating energy sources, the energy availability profile is uncertain, making task allocation a challenging problem.

Generally, two design considerations for energy harvesting systems are maximizing performance and ensuring energy neutral operation. Energy neutral operation [1] means operating the network such that, at all times, the energy used is less than the harvested energy. Also, while ensuring energy neutral operation, 'what is the *best performance* level that can be achieved in a given harvesting environment?'.

In this chapter, we address the task allocation problem which allocates and schedules a set of tasks represented by a task graph to a set of geographically distributed sensor nodes to achieve an overall system objective. Such a scenario is depicted in Figure 5.1. We consider a scenario in which the sensor nodes are equipped with solar panels.

[1]Researchers use both terms 'energy causality' or 'energy neutrality' to mean the same thing.

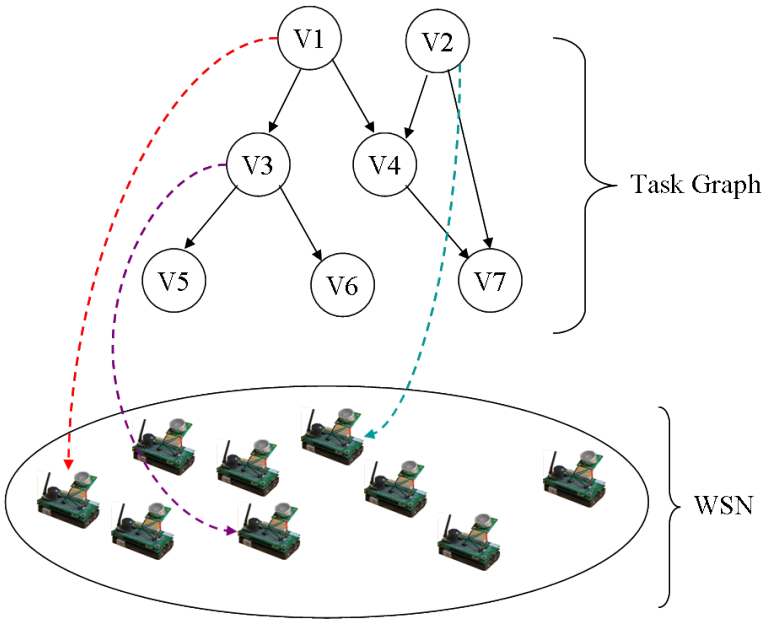

Figure 5.1: Task allocation problem.

5.1.1 Contributions of This Chapter

In this chapter, we propose the task allocation algorithms for EH-WSNs. These algorithms account for the energy harvesting characteristics of sensor nodes (i.e. uncertainty in energy availability) and make the best use of available energy. The solution objectives are to minimize the scheduling length of the task graph and maximize the fairness in energy-driven task mapping, while satisfying energy harvesting causality constraints and the task precedence constraints. The fairness in task mapping means tasks with longer task lengths are assigned to the nodes with higher energy levels. The proposed solution results in balanced energy levels among all the nodes in the network and minimum schedule length. The main contributions of this work are summarized as follows:

- We propose a novel task allocation algorithm for energy harvesting wireless sensor networks that operates in two phases: task scheduling of the directed

acyclic graph (DAG) and task mapping to the solar-powered sensor nodes. To the best of our knowledge, this is the first work on energy harvesting aware task allocation at the network level to multiple solar-powered sensor nodes.

- The problem is formulated in an optimization framework as a mixed integer linear program (MILP). The proposed framework for our scheme is operated in two stages consisting of the static and dynamic adaptation specialized for energy harvesting systems.

- An appropriate energy prediction model and algorithm are incorporated to increase the accuracy of our task allocation scheme.

- A genetic algorithm based multi-objective task allocation strategy is implemented for the comparison purpose.

- The performance of our proposed algorithms in terms of the scheduling length and fairness in the energy-driven task mapping objectives is evaluated through the simulation.

This chapter is structured as follows. In Section 5.2, we introduce the system overview and proposed framework for our task allocation scheme in EH-WSNs. In Section 5.3 the energy prediction model and algorithm are explained. This is followed by the problem formulation in the form of a mixed integer linear program in Section 5.4. In Sections 5.5 and 5.6, the energy harvesting aware task scheduling and mapping algorithms are described. The simulation results are discussed in Section 5.7. Section 5.8 provides a summary and conclusion.

5.2 System Overview

In this section, the model for the task allocation problem in EH-WSNs is explained. Figure 5.2 shows the overall structure of this model. The centralized manager collects some initial data from the energy harvesting source. It then runs the energy prediction algorithms. Given, the predicted energy and the task graph from WSNs' application, the task allocation algorithm can be run. The output of this algorithm is the set of actions for sensor nodes. The main objective is to minimize the scheduling length of the task graph and maximize the lifetime of the sensor nodes.

We consider a discrete time model. The network consists of multiple solar-powered sensor nodes denoted as $n \in \mathcal{N}$ where $\mathcal{N}$ is a set of all available sensor nodes. Tasks are units of execution that make up an application. The application for wireless sensor networks can be target tracking, event detection, etc. A single application may perform a variety of tasks such as sensing, computation, storage and communication. Applications are represented by a DAG, composed of all tasks $m \in \mathcal{M}$ where $\mathcal{M}$ is the set of tasks that must be completed for the application. L_m denotes the size of the task m which refers to the number of time slots required to accomplish that task ($L_m \in \mathbb{Z}^+$). Tasks must be sequentially executed to satisfy the precedence constraints. A task has one or more inputs and once all inputs are available, the task is triggered to execute.

The harvesting period is divided into equal-length time slots which are indexed as $t \in \mathcal{T}$ where $\mathcal{T} \in \mathbb{Z}^+$. We consider an energy storage device with capacity B and discharge efficiency $\eta_d < 1$. $\mathcal{H}_t^n$ is the amount of harvested energy in slot t in node n.

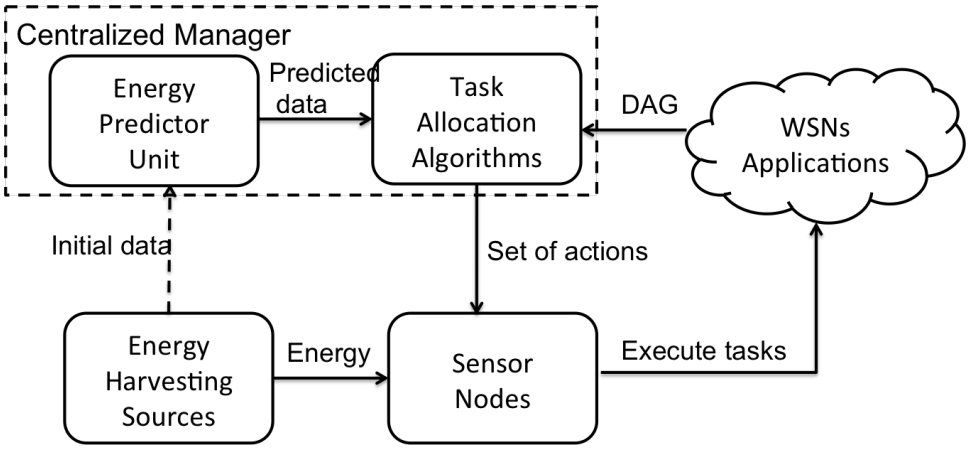

Figure 5.2: Structure of resource management for EH-WSNs.

The available energy at each node n and time slot t is denoted as $\mathcal{A}_t^n$ and calculated as

$$\mathcal{A}_{t+1}^n = [\mathcal{A}_t^n + \mathcal{H}_t^n - \eta_d.E_0.Y_t^{m,n}]_0^B,$$

where E_0 denotes the energy which is drained from the battery during each busy slot. E_0 is assumed to be constant for each node and task. $Y_t^{m,n}$ is a boolean function indicating whether node n is busy with task m in time slot t. The available energy is bounded by the capacity of battery B.

5.2.1 Framework of Task Allocation in EH-WSNs

In this part, the framework of our proposed task allocation scheme for EH-WSNs is described. It is a hybrid framework of static and dynamic stages.

The static stage is executed *offline* in the centralized manager which can be a node with the high computational capability such as Stargate [79]. In this stage, the centralized manager runs the prediction algorithm to extrapolate information about the harvested energy in the next harvesting period. It then allocates an energy budget

in terms of the harvesting rate for each time slot of the next period. The predicted information and the task graph are the inputs to our static allocation algorithm. The allocation outcomes and energy budget for each slots are then communicated to sensor nodes.

The dynamic stage is executed *online* in the sensor nodes. This stage may modify the real-time execution of the task allocations from the previous stage to adapt to unpredictable fluctuation in energy availability. At the beginning of each time slot, the corresponding energy budget is retrieved from the memory and is compared with the corresponding baseline error margin. If the energy budgets from the prediction do not match with actual harvested energy and the error margin is higher than the predefined threshold, then the dynamic adaptation method is executed. Adaptation allows the system to cope with variation in renewable energy source and maintain sustainable system. Moreover, energy harvesting statistics are sent to the centralized manager to update the data for the energy harvesting prediction of the next harvesting period.

5.3 Prediction Algorithm

In this section, the energy harvesting prediction method is described. An accurate prediction of the near-future harvested energy has a critical effect on decision making for task allocation procedure in energy harvesting systems. A time series [54] is a sequence of observations of a random variable such as energy harvesting rate. A time series analysis provides a proper tool for forecasting future events. There are

several methods for forecasting the near future of real data such as regression analysis, exponential smoothing, moving average and etc. [54]. Weather-Conditioned Moving Average (WCMA) is the common approach adopted for the weather prediction. It first introduced in [51] and then extended for cloud cover case and wind energy prediction in [52] and [53]. Our prediction model called Autoregressive Weather-Conditioned Moving Average (AR-WCMA) has its foundation on WCMA which is a low overhead solar energy prediction algorithm. The key idea of our prediction model is to apply an Autoregressive (AR) time series model at the beginning of each day, since the solar irradiance is a periodic phenomena. It has been proven in [55] that a simple linear regression model is an appropriate model for real-time and random data. Then, the model is further improved by utilizing the moving average of the information from past days.

For this prediction algorithm, a day is divided into T equal duration of time slots. The power sampling and prediction are performed once per slot. To predict the harvesting energy in the next slot, the algorithm uses the values of power measurement $\tilde{e}(j) \in \tilde{E}_T$ of the current day. It also utilizes the values of power measurement $\tilde{e}(i,j) \in \tilde{E}_{D\times T}$ of the last D days, $D \in \mathbb{Z}^+$. The unit of power measurements and accordingly the prediction values are irradiance (W/m^2). The matrix $\tilde{E}_{D\times T}$ and the vector $\tilde{E}_T$ are shown in Figure 5.3. Assume that t slots have elapsed on the current day shown shaded in Figure 5.3 and $\tilde{e}(t+1)$ is the estimation of the power value at the start of slot $t+1$.

The time-series analysis begins with some response measurements of the structure at a particular sensor location. Assuming the response to be stationary, an AR process

model is used to fit the discrete measurement data to a set of linear coefficients from past time history observations as follows:

$$\tilde{e}(t+1) = \sum_{i=1}^{k} b_i \tilde{e}(t+1-i) + r_k. \tag{5.1}$$

The response of the structure at sample index t, as denoted by $\tilde{e}(t)$, is a function of k previous observations of the system response, plus a residual constant term ,r_k. Weights of the previous observations $\tilde{e}(t+1-i)$ are denoted by the b_i coefficients which are calculated daily based on the available information of last D days.

The goal is to predict the power $\hat{e}(t+1)$ at the beginning of slot $t+1$ (marked with a '?' in Figure 5.3). In Figure 5.3, $\mu(t+1)$ represents average of power measured at beginning of all $t+1$ slots for last D days. The predicted power for the next slot considers the power measurement from the present information of last k slots $\tilde{e}(t+1)$ and the average power $\mu(t+1)$ of the same slot $(t+1)$ for past D days:

$$\hat{e}(t+1) = \alpha.\tilde{e}(t+1) + (1-\alpha).\mu_D(t+1)\Phi_K. \tag{5.2}$$

The prediction algorithm consists of two terms as shown in (5.2). The first term is the effect of the AR and the latter one is the conditioned average term. The AR term determines the effect of the current day to the predicted value, while the conditioned average term is the average of past D days on time slot $(t+1)$ which scaled by the conditioning factor Φ_K. The parameter α shows the trade-off between these two terms $(0 \leq \alpha \leq 1)$.

In (5.2), $\mu_D(j)$ is the average of power measured at beginning of slots j in the past D days:

$$\mu_D(j) = \frac{\sum_{i=1}^{D} e(i,j)}{D} \tag{5.3}$$

Φ_K is a conditioning factor for $\mu(t+1)$ and it is a function of previous K ($K \in \mathbb{Z}^+$) time slots before time slot $(t+1)$ of current day (can be seen in Figure 5.3).Φ_K shows how much brighter or cloudy the current day is compared to previous days. It is calculated using (5.4), which is a weighted average of ratio $\eta(K) \in H_k$, (shown in (5.5)), where each ratio $\eta(k)$ compares the current day measured power of one particular slot to the average of the past days. Since the slots earlier than t are assumed to be less correlated to the future slot $t+1$, the weights $\theta(k) \in \Theta$ calculated in (5.6) decrease from 1 to $1/K$ starting at the slot t.

$$\Phi_K = \frac{(\Theta_K)^T . H_K}{\sum_{k=1}^{K} \theta(k)} \tag{5.4}$$

$$\eta(k) = \frac{\tilde{e}(t-K+k)}{\mu_D(t-K+k)} \tag{5.5}$$

$$\theta(k) = k/K \tag{5.6}$$

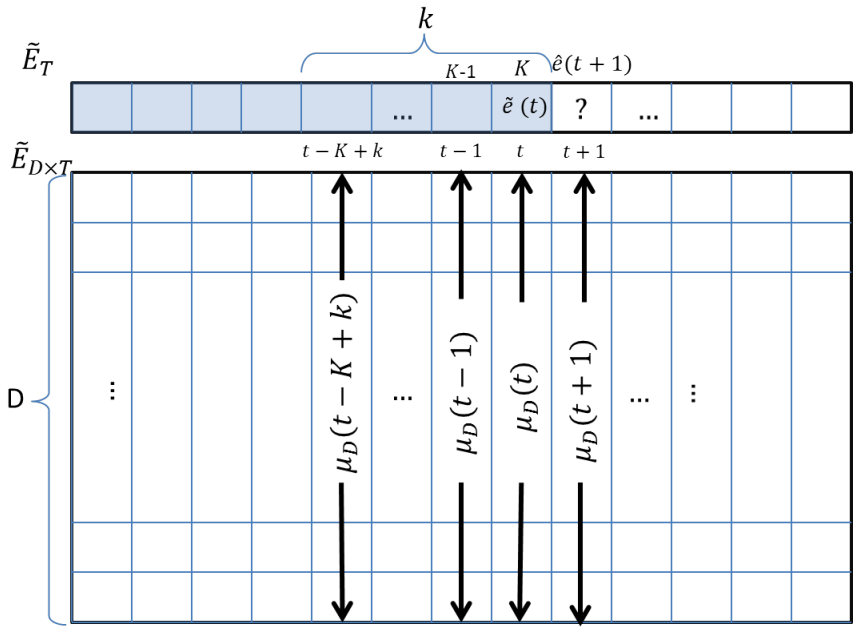

Figure 5.3: Prediction framework for solar-powered sensor nodes

The estimated value $\hat{e}(t)$ in following sections are denoted as $\mathcal{H}_t$. All measurements and estimations are in irradiance unit (W/m^2) which can be converted to the unit of energy unit Ah. The details are explained in the simulation section.

5.4 Problem Formulation

In this section, we explain the problem formulation for the task allocation in sensor networks equipped with energy harvesting devices. Task allocation problem which consists of task scheduling and mapping plays an essential role in parallel processing. Solving this problem results in execution sequence of tasks and assignment of tasks to the sensor nodes. The main objectives are to minimize the makespan and maximize the fairness (energy-balancing), while satisfying the task precedence constraints and energy harvesting causality constraints.

Decision variables:

The decision variable for this problem is defined as follows:

X: Valid mapping and scheduling of tasks $m \in \mathcal{M}$ to the sensor nodes $n \in \mathcal{N}$ at time slot $t \in \mathcal{T}$:

$$X_t^{m,n} = \begin{cases} 1, & \text{If task } m \in \mathcal{M} \text{ is assigned to sensor} \\ & \text{node } n \in \mathcal{N} \text{ at time slot } t \in \mathcal{T} \\ 0, & \text{Otherwise.} \end{cases} \tag{5.7}$$

Although, we have one decision variable, it is useful to define the following quantities, which depend upon X.

S^m: Start time slot of scheduled task $m \in \mathcal{M}$. It can be calculated as follows:

$$S_m = \underset{t}{\operatorname{argmax}} \left(\max_n X_t^{m,n} \right) \tag{5.8}$$

Y : An indicator function to show the busy time slot.

$$Y_t^{m,n} = \begin{cases} 1, & \text{If node } n \text{ is busy with task } m \\ & \text{at time slot } t \\ 0, & \text{Otherwise.} \end{cases} \tag{5.9}$$

This value can be calculated as a function of S_m and $X_t^{m,n}$ as follows:

$$Y_t^{m,n} = \begin{cases} 1, & t = S_m, S_m + 1, ..., (S_m + L_m); \\ & \forall\ n = \text{argmax}_m \max_t X_t^{m,n} \\ 0, & \text{Otherwise.} \end{cases} \tag{5.10}$$

5.4.1 Objective Function and Constraints

The following objective function and linear-integer constraints describe the optimization problem to be solved in order to compute an optimal task allocation.

$$\min_X \quad w_1 \left(\max_{m \in M} (S_m + L_m) \right) + w_2 \sum_{\substack{t \in \mathcal{T} \\ n \in \mathcal{N} \\ m \in \mathcal{M}}} g_t^{m,n} . X_t^{m,n} \tag{5.11}$$

Subject to:

$$S_k \geq S_j + L_j + T_c, \quad \forall (j,k) \in \mathcal{M},\ P_{j,k} > 0. \tag{5.12}$$

$$X_t^{m,n} \in \{0,1\} \quad \forall n \in \mathcal{N},\ \ \forall m \in \mathcal{M},\ \ \forall t \in \mathcal{T}. \tag{5.13}$$

$$\sum_{t \in T} \sum_{n \in N} X_t^{m,n} = 1, \quad \forall m \in \mathcal{M}. \tag{5.14}$$

$$\sum_{m \in M} Y_t^{m,n} \leq 1, \quad \forall n \in \mathcal{N} \;\; \forall t \in \mathcal{T}. \tag{5.15}$$

$$\mathcal{A}_{t+1}^n = [\mathcal{A}_t^n + \mathcal{H}_t^n - \eta_d . E_0 . Y_t^{m,n}]_0^B, \;\; \forall n \in \mathcal{N}, \forall t \in \mathcal{T}. \tag{5.16}$$

where T_c is the communication cost between immediate tasks precedence. $g_t^{m,n}$ is the cost associated with assigning task $m \in \mathcal{M}$ to sensor node $n \in \mathcal{N}$, at time slot $t \in \mathcal{T}$. This cost value is a linear function of $\mathcal{A}_t^n$ and task size (L_m). The cost function is defined as follows:

$$g_t^{m,n} = L_m \times (\mathcal{A}_t^n)^{-1}. \tag{5.17}$$

The objective function shows the tradeoff between the two task allocation objectives with weights w_1 and w_2. The first part corresponds to minimizing the scheduling length by minimizing the maximum finish time of all the tasks. The second part relates to minimizing the task mapping cost in order to achieve a balanced energy

availability through the network.

The constraint in (5.12) states the precedence constraint where a task cannot start until its predecessors are completed and data has been communicated to it if the preceding job were executed on different node, illustrated as a constant value T_c. As stated before, L_m is the size of task m, which refers to the number of time slots required to accomplish that task.

The constraint in (5.13) refers to boolean task mapping constraint. (5.14) and (5.15) show task allocation constraints. More precisely, (5.14) specifies that each task must be assigned once to exactly one node and (5.15) specifies that at most one task can be assigned to each sensor node at each time slot. The constraint shown in (5.16) indicates the energy harvesting causality constraint. This constraint keeps track of energy availability at each time. Moreover, this constraint avoids the energy harvesting overflow at each node by considering the capacity of the battery (B) as an upper bound for energy availability.

All together, the task allocation problem for wireless sensor networks equipped with energy harvesting systems is described in the above-mentioned objective function and constraints. This problem is NP-complete in general [56] and heuristic algorithms are applied to obtain the practical solution. Our proposed heuristic approach is presented in the next section.

5.5 Proposed Algorithm for Task Allocation in EH-WSNs

This section describes our solution approach for task allocation. The proposed scheme consists of a hybrid framework of static and dynamic stages. The static task allocation problem is divided into two phases. The first one is the task scheduling phase to determine the proper sequence of tasks. The main objective for the first phase is to minimize the scheduling length (shown in the first part of the objective function) and also satisfy the precedence constraint (5.12). This phase, which is explained in Section 5.5.1, results in the lower and upper bounds for the starting time of each task.

Given the bounds from the first phase, the second phase, explained in Section 5.5.2, runs the task mapping to the appropriate sensor nodes. The objective of the second phase is to maximize the energy-balancing among the nodes, considering the energy harvesting characteristics. It addresses the second part of the objective function as well as the constraints (5.13) to (5.16).

If the error margin, which is the difference between the energy predicted value and the actual harvested energy, is higher than some predefined thresholds, the dynamic adaptation stage (Section 5.5.3) is executed. Adaptation allows the system to cope with variation in renewable energy supply and maintain system's sustainability.

5.5.1 List Scheduling and Critical Nodes Path Tree (CNPT) Heuristic

This part presents the list scheduling algorithm. It uses to satisfy the first constraint (5.12) while optimizing the first part of the objective function. It computes a task sequence provided by a DAG to obtain the earliest start time (EST) and the latest start time (LST) of each task considering a Critical Path (CP). A CP of a task graph is defined as a path with the maximum sum of node and edge weights from an entry node to an exit node. Given these values, the tasks are queued into a list. The EST and LST for a task i can be computed recursively by traversing the DAG downward from the entry node and upward from the exit node respectively as follows:

$$EST_m = \max_{i \in pred(m)} EST_i + L_i \tag{5.18}$$

$$LST_m = \min_{i \in succ(m)} LST_i - L_i \tag{5.19}$$

where $pred(m)$ and $succ(m)$ are the set of immediate predecessors and successors of m respectively and L_i is the length of the task i. After the listing phase, the task graph is sequentialized into a queue and ready for the task assignment phase. The main objective of this part of the scheduling process is to determine the minimum scheduling length (makespan) while satisfying all precedence constraints. The tasks are queued for assignment to sensor nodes based on LST. This is because, it may give a sensor node the chance to harvest more energy before the task is assign to it.

5.5.2 Energy Harvesting aware Task Assignment Heuristic

In this phase, the proposed heuristic algorithm assigns the tasks to maximize the energy-balancing considering the energy harvesting characteristics. It satisfies the energy-neutral constraint and avoids the energy overflows.

The following steps describe the basic idea of our proposed energy harvesting aware task allocation heuristic:

STEP 1 Sort all the tasks based on LST from List Scheduling and CNPT in queue $\mathcal{Q}$;

STEP 2 Update the energy availability $\mathcal{A}_t^n$ of all nodes based on the predicted energy for the current slot;

STEP 3 For the task dequeued from queue $\mathcal{Q}$, calculate the cost associated with assigning the correspond task m to all sensor nodes $n \in \mathcal{N}$ at the current time slot t as, and find the minimum cost among them.

The cost is calculated as

$$C_t^{m,n} = g_t^{m,n} a_t^n$$

where $g_t^{m,n}$ can be calculated from 5.17. a_t^n is an indicator defined as

$$a_t^n = \begin{cases} 0, & \mathcal{A}_t^n \geq B \ \forall \text{ node } n \in \mathcal{N} \text{ at time slot } t \in \mathcal{T} \\ 1, & \text{Otherwise.} \end{cases} \tag{5.20}$$

This indicators shows that the cost is zero if the overflow occurs at the node. Hence, we immediately allocate the first task from the queue to that node.

As a result, since the listing in the queue is based on LST, it increases the chance

that the node can harvest enough energy and gains the failure tolerance. In other words, the task scheduling is *as late as possible* but within a boundary that results in the minimum schedule length. Since the task mapping is based on the available energy, in "STEP 2" the available energy for each slot is updated. "STEP 3" assigns the task based on the cost associated with each node for accomplishing the corresponding task and handles the overflow situation when the harvested energy may become greater than the maximum capacity. The proposed algorithm is shown in *Algorithm 1.*

Algorithm 1: Energy Harvesting Aware Task Allocation

Given: EST and LST of all the tasks $m \in \mathcal{M}$ from CNPT, $\mathcal{A}_t^n \ \forall \ n \in \mathcal{N}$ and $t \in \mathcal{T}$, $L_m \ \forall \ m \in \mathcal{M}$.

Sort all the tasks in respect to LST in queue $\mathcal{Q}$.

For all tasks m dequeued from $\mathcal{Q}$,

For all $n \in \mathcal{N}$,

For $EST_m < t < LST_m$,

If $\mathcal{A}_t^n \geq B$,

Assign task m to sensor node n,

$S_m = t$,

Else

$g_t^{n,m} = L_m \times (\mathcal{A}_t^n)^{-1}$

EndIf

EndFor

EndFor

$n^* = \text{argmin}_{t,n}(g_t^{n,m})$ (finding the best node)

$S_m = \text{argmin}_{n,t}(g_t^{n,m})$ (finding the best schedule)

EndFor

We briefly explain a potential extension of the current model to multi-hop scenario. In this case, a task i and its immediate predecessor task j might be allocated to nodes that are in one or more hops away of each other. Assume that j needs the data from i for execution. Hence, one needs to find the way to communicate this data through multi-hop. In WSNs, the communication is broadcast in nature. To represent the broadcast feature of wireless communication, the DAG representation of application is extended to Hyper-DAG. In which, the weight of edges between two computation tasks is represented as a separate communication task. Unlike in single-hop networks, there might be multiple simultaneous communications in multi-hop networks. In order to schedule the communication task, one models multi-hop channel as a virtual node on which only the communication task can be scheduled. To avoid the interference between simultaneous communication tasks, one may consider the penalty of infinity cost for the case of interference and zero otherwise. In case that the source and destination of a communication task are one or more hop away from each other, one can schedule based on the path generated by a low complexity routing algorithm [57].

Practical Example

In general, our task allocation algorithms can be applied for any WSNs' application, which can be represented by DAG. As a practical example, the collaborative target tracking can be named. The task allocation algorithms help to dynamically manage sensor resources and efficiently process distributed sensor measurements. One simple run of this application is shown in Figure 5.4. T_1, T_2 and T_3 are the sensing tasks, T_5 and T_6 are the computation tasks and T_4 is the storing task. In this example, once the target is detected by sensing task T_1, it searches for two other sensing data from its neighbors via tasks T_2 and T_3. These sensing data are required for running initialization (task T_5) and localizing the target (task T_6). The sensing data is stored via task T_4. Figure 5.4 also demonstrates our proposed task allocation algorithm for this simple example.

5.5.3 Online Dynamic Adaptation Stage

This stage is based on the real-time execution of these tasks allocated to the sensor nodes based on the actual energy harvesting data. At the beginning of each time slot, the corresponding energy budget is retrieved from memory and a corresponding baseline error margin is looked up. If the energy budget from the prediction does not match with actual harvested energy and the error margin is higher than predefined threshold, the dynamic adaptation phase is executed. Adaptation allows the system to cope with the variation in the renewable energy and maintain system sustainability. In addition, energy harvesting statistics with new updates are sent to the centralized

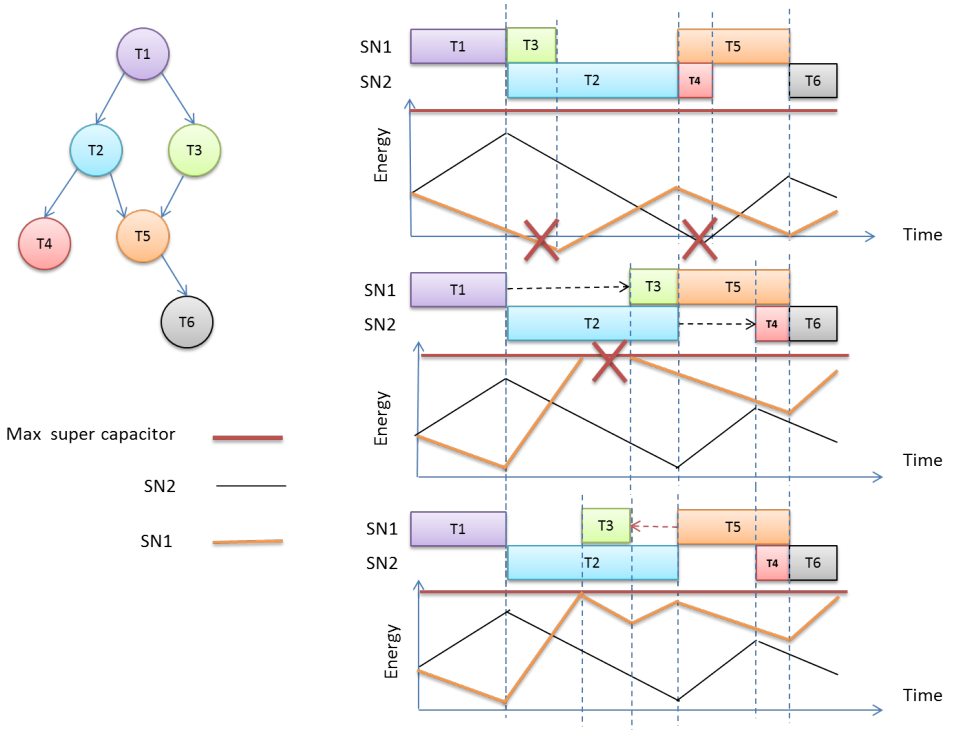

Figure 5.4: A simple example of the task allocation.

manager to update energy harvesting prediction of the next harvesting period.

The basic idea is that if a sensor node due to an environmental uncertainty does not have enough energy to execute the task, then it slows down the processor rate and stretches the execution time of that task. As a result, one may gain more time for the sensor node to harvest energy from environment at the price of operating at the lower processor power. This technique is called dynamic voltage and frequency scaling (DVFS) [36]. Based on the initial schedule, all tasks are executed at the full speed of the processor (P_{max}), which is not an energy-efficient scheme. We need to make use of the task slacks for the energy saving. DVFS is applied to stretch the execution time of each task and slow down the power of processor. Then, we shift all other potentially affected tasks accordingly. Assume the DVFS-enabled processor has K

discrete operating frequencies $f_k : \{f_k | 1 \leq k \leq K, f_{min} = f_1 < f_2 < ... < f_K = f_{max}\}$; and the power consumption with regards to f_k is denoted as P_k. We assume a linear relationship between the power P_k used for executing tasks and their execution time L. We can say: the higher the power P_k, the shorter the execution time L.

We define a decelerate factor ν_k as the normalized frequency of f_k with respect to the maximum frequency f_{max}, that is:

$$\nu_k = f_k / f_{max} \tag{5.21}$$

If task m is stretched by a slowdown factor ν_k, then its actual execution time at frequency f_k is L_m/ν_k.

Assume that initially the task m is assigned to the sensor node n considering the full speed of the processor. Let st_m and ft_m denote the starting time and finish time of the task m accordingly. The task m has enough energy to finish its execution if the following inequality holds:

$$\mathcal{A}(st_m) + \mathcal{H}(st_m, ft_m) \geq \mathcal{D}(st_m, ft_m) \tag{5.22}$$

where $\mathcal{C}(st_m)$ is the energy available at time instant st_m and $\mathcal{H}(st_m, ft_m)$ is the harvested energy during task execution and $\mathcal{D}(st_m, ft_m)$ is the energy demand of executing task. If this inequality does not hold, the decelerate factor is adjusted until

the following equality holds,

$$\mathcal{A}(st_m) + \mathcal{H}(st_m, st_m + \tfrac{ft_m - st_m}{\nu_n}) = \mathcal{D}(st_m, st_m + \tfrac{ft_m - st_m}{\nu_n}). \tag{5.23}$$

Subsequently, all of the tasks $\tau \in succ(m)$ need to be delayed dl_m which is the delay caused by stretching the task via DVFS. The result of this dynamic adaptation phase is to reserve time for the sensor node with lack of energy to harvest from the environment and execute with lower CPU frequency. Note that the schedule length in our formulation is not a hard constraint (or deadline). In the dynamic adaptation phase, the task is missed only if extending the task length to meet the energy neutral condition causes the frequency f_k to be below f_{min}. The sequence of the algorithm is shown in *Algorithm 2*.

Algorithm 2: Dynamic Adaptation Phase

Require: initial schedule, actual harvesting rate, actual energy available;

For task $m \in M'$ which M' is a set of tasks mapped to sensor node $n \in N$,

If $\mathcal{A}(st_m) + \mathcal{H}(st_m,\ ft_m) < \mathcal{D}(st_m,\ ft_m)$,

Calculate ν_n from (5.23);

For all the task $\tau \in succ(m)$,

$st_m \rightarrow st_m + dl_m$;

EndFor

EndIf

EndFor

5.5.4 Computational Complexity

In this part, the complexity of the proposed heuristics is calculated. Considering an application with m tasks, a network with n sensors and ε which is defined as $\varepsilon = \max_{m \in \mathcal{M}}(LST_m - EST_m)$ the complexity of the listing stage is $O(m)$ and the energy harvesting aware task assignment heuristic has the complexity of $O(n\ m\ \varepsilon)$ for the worst case. Hence, worst-case total complexity is $O(m) + O(n\ m\ \varepsilon) \simeq O(n\ m\ \varepsilon)$. The dynamic adaptation phase has a low complexity of $O(k\ l)$ where k is the number of tasks mapped to the sensor node which has the energy prediction error higher than predefined threshold and l is the number of those tasks' successors in the DAG.

5.6 Multi-Objective Genetic Algorithm for Task Allocation

The task scheduling and mapping into a parallel and distributed computing system is a well-defined NP-complete problem. It is considered as one of the most challenging problems in parallel computing [61]. The task allocation problem is included in this class of combinatorial optimization problems.

Genetic Algorithms (GAs) have been widely used as beneficial meta-heuristics for obtaining high quality solutions for a broad range of combinatorial optimization

problems including the task allocation problem [62]. Another distinct feature of the genetic search is that its inherent parallelism can be exploited to further reduce its running time. Hence, as a baseline, with which to compare our task allocation scheme, we implement a multi-objective genetic algorithm. This algorithm starts with an initial population of feasible solutions. Then, by applying some operators, the best solution can be found after some generations. The selection of the best solution is determined according to the value of the fitness function. In this section, the detailed implementation is presented.

Representation: The first step in designing a genetic algorithm for a particular problem is to develop a suitable representation scheme, i.e., a way to represent individuals in the GA population. A chromosome represents a mapping of tasks to sensor nodes. Figure 6.3(a) shows an example of such a representation of the chromosome. Tasks $2, 3, 6, 9$ will be scheduled on sensor node 1, tasks $5, 8$ on sensor node 2, and tasks $1, 4, 7$ on sensor node 3.

Fitness function: A fitness function attaches a value to each chromosome in the population, which indicates the quality of the schedule. The main objectives of the task allocation, which are minimizing scheduling length and maximizing energy-balancing considering the energy harvesting, are represented in the fitness function. In this case, the fitness function ($\mathfrak{F}$) needs to express two different objectives as follows:

$$\mathfrak{F} = w_1(\max_{m \in M}(S_m + L_m)) + w_2(\frac{1}{n}\sum_{i=1}^{n}(\mathcal{A}_i - \overline{\mathcal{A}})^2) \tag{5.24}$$

where $S_m + L_m$ is the finish time of task m and $\max_{m \in M}(S_m + L_m)$ is the schedule

length of a task graph. $\mathcal{A}_i$ is the available energy level of sensor node i considering the recharging with the energy harvester. $\overline{\mathcal{A}}$ is the mean value which is calculated as $\overline{\mathcal{A}} = \frac{1}{n}\sum_{i=1}^{n}\mathcal{A}_i$ where n is the number of sensor nodes. In order to show how balanced the energy levels are, the deviation from the mean of the remaining energy level of all the sensor nodes is evaluated. The lower this value is the more balanced available energy level among all the sensor nodes. Also, the lower scheduling length is better. So, our objective is to minimize the defined fitness function which is proportional to the schedule length and the energy variance. w_1 and w_2 are the weights to set the priority for the objectives.

Selection Operator: There are two selection phases used for the genetic algorithm. The first one is *parent selection*. This selection phase is used to select the parents for mutation and crossover based on the fitness. We have applied the fitness-proportional roulette wheel selection and tournament selection. The second selection phase is survival selection among the reproductive chromosome after crossover. For this phase, we use the Genitor selection, a.k.a. "delete worst" which means among parents and offsprings deleting the worst.

Crossover and Mutation Operator: Each chromosome in the population is subjected to crossover with probability P_c. Two chromosomes are selected from the population, and a random number $r \in [0, 1]$ is generated for each chromosome. If $r < P_c$, these chromosomes are subjected to the crossover operation using single point crossover as shown in Figure 6.3(b). For this work, the *non-uniform self-adaptation mutation*, which is a fitness-dependent mutation rate is utilized. The mutation rate initially set to be some high values then the lower value once it reaches to near to

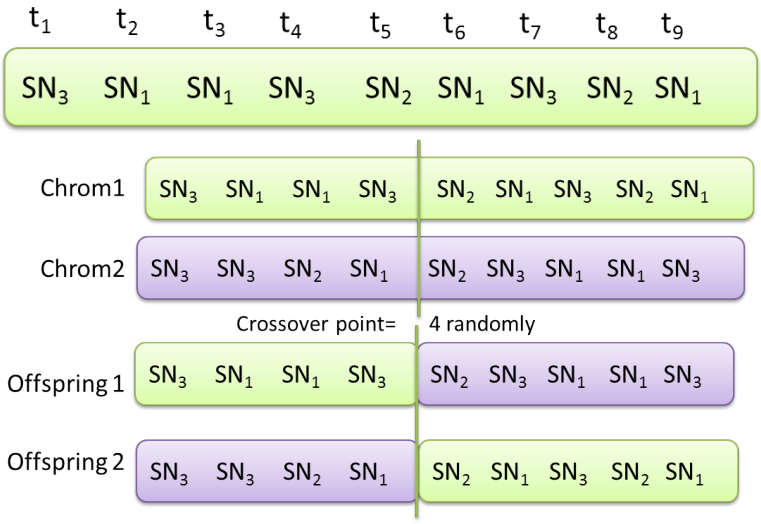

Figure 5.5: Representation of a chromosome and crossover operation.

optimal fitness.

5.7 Simulation Results

The performance of our proposed algorithms are evaluated through simulation. We have run several sets of simulations to investigate the following aspects:

- Performance of the energy harvesting prediction algorithm,
- Performance of the task allocation scheme in terms of energy-balancing and scheduling length objectives,
- Performance of the dynamic adaptation phase.

To the best of our knowledge, this is the first work that addresses an energy harvesting-aware task allocation at the network level. For small scale problems, we are able to solve MILP using the optimization toolbox in Matlab by calling the solver through the

Table 5.1: Simulation configuration.

Recombination	Single point crossover with probability $0.6 - 0.9$
Parent selection	a) roulette wheel b) Binary tournament
Survivor selection	GENITOR, a.k.a. "delete worst"
Population size	10 chromosomes
Number of task in the task graph	$7 - 30$
Number of sensor nodes	$2 - 50$
Maximum number of predecessors in task graph	2 or 3
Stopping criterion for genetic algorithm	10 unchanging generations.

syntax `intlinprog`. The results can be used as a baseline for our proposed heuristic. A multi-objective genetic algorithm based task allocation scheme (explained in details in Section 5.6) is also implemented. For large scale problems, the proposed scheme is validated by comparing the results of the genetic algorithm approach and some modified heuristics such as the critical node path tree (CNPT) algorithm [50] and extended CNPT (E-CNPT) algorithm [43]. The strategy for Extended CNPT (E-CNPT) algorithm in [43] is to assign the tasks along the most critical path first to the nodes with earliest execution start times. This algorithm operates by adjusting the number of sensors in each scheduling iteration and then choosing the schedule with the minimum energy consumption.

The energy harvesting profile is retrieved from the National Renewable Energy Lab website [58]. The data for the power consumption of a sensor node is extracted from the Mica-2 data sheet [59]. Some of the implementation specifications are shown in Table 5.2.

The example of a task graph and its corresponding task allocation to five sensor nodes are shown in Figure 5.7. The results from the convergence of a genetic algorithm based multi-objective fitness function for the minimum and average value after several

generations are shown in the Figure 5.7.

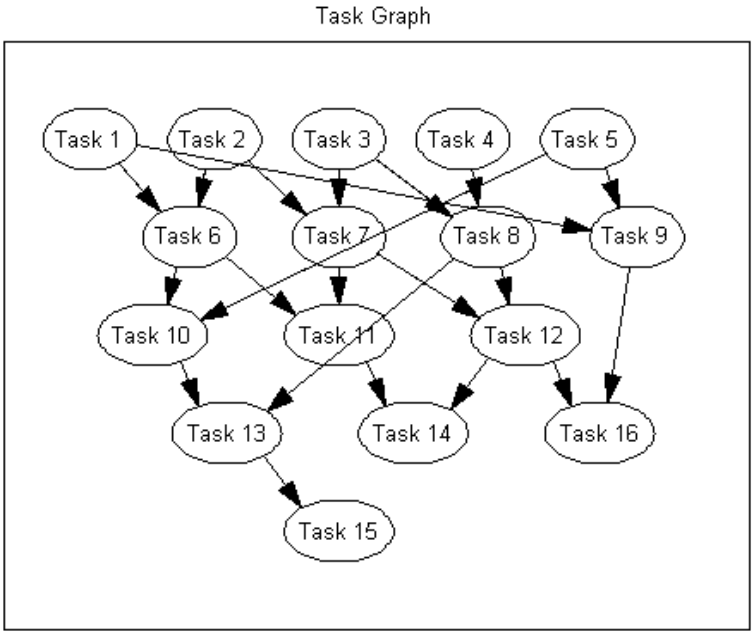

(a) Task graph

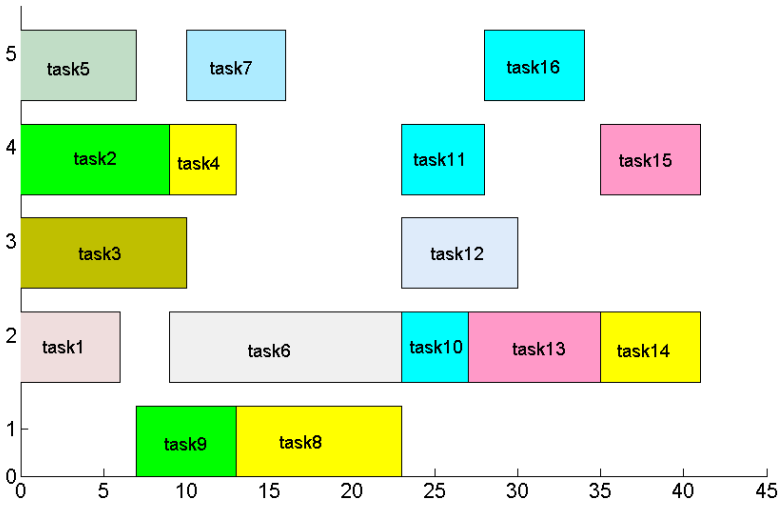

(b) Schedule for 5 sensor nodes

Figure 5.6: Task graph and corresponding task allocation based on our scheme.

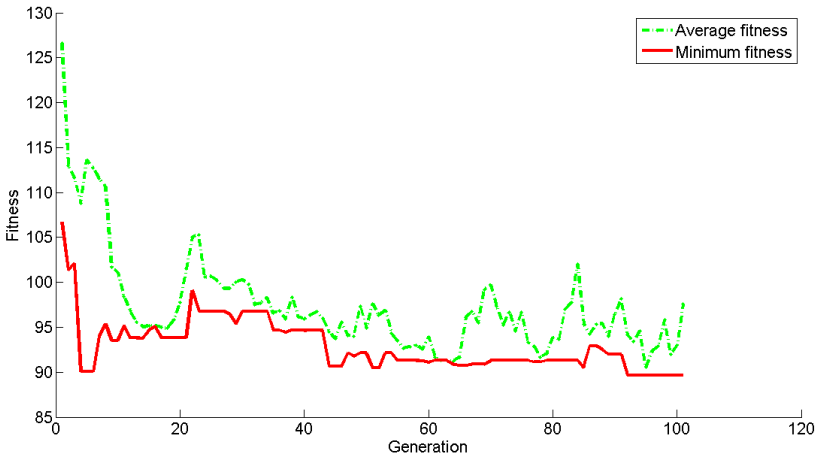

Figure 5.7: Convergence of multi-objective fitness function of genetic algorithm based task allocation.

5.7.1 Simulation Results for the Energy Harvesting Prediction Algorithm

To evaluate the performance of the proposed algorithm, simulations are carried out based on the available solar irradiance data from the solar energy received at different times of day and night. We consider the measurement trace of a solar panel in 4 consecutive days, with both the sunny and cloudy conditions from National Renewable Energy Lab [58]. The reported data is from California Solar Initiative (CSI) from 26 Oct. 2011 for 4 days. The unit of this data is an average solar irradiance (mW/m^2) and it is for every 1 hour. An irradiance unit is converted to an energy unit by linear conversion considering a solar panel size $9.6cm \times 6.4cm$, a solar cell efficiency 10% and a harvesting efficiency 80%. We use "Ah" as the unit of the energy quantity because the voltage is fixed at $1.2V$. To present the algorithm evaluation results, the following values used as algorithm parameters are: $T = 24$, $\alpha = 0.7$, $D = 4$ and $K = 4$. Recall that α, K and D denote weighing factor, number of previous slots and

number of previous days for each solar power data set. Figure 5.8 shows how closely our prediction algorithm can track the actual measured data. The evaluation metric used for this part is the average prediction error. It is computed as,

$$\epsilon = \frac{100}{n} \sum_{i=1}^{n} \frac{|e(i) - \tilde{e}(i)|}{e(i)}$$

where n is the time horizon of the predication which is $D \times T$. We compare the energy prediction accuracy of WCMA, ARMA and AR-WCMA. WCMA and AR-WCMA are addressed in the prediction algorithm part. ARMA refers to autoregressive moving average. This comparison can be seen in Figure 5.9 for the different weather conditions (i.e., sunny day and cloudy day).

ARMA only uses values from the previous day; hence, if the weather conditions change from one slot to another, this method has a large error in prediction (i.e., close to 30%). On the other hand, WCMA only takes into account the last few slots but not the useful information about the weather condition of the past few days. AR-WCMA produces much better results because it uses the values of the same slot over previous days and also the previous slots of the same day, which helps to calibrate against the actual weather condition. To conclude, WCMA, ARMA and AR-WCMA results in the average error of 23.6%, 28.6% and 8.7%, respectively.

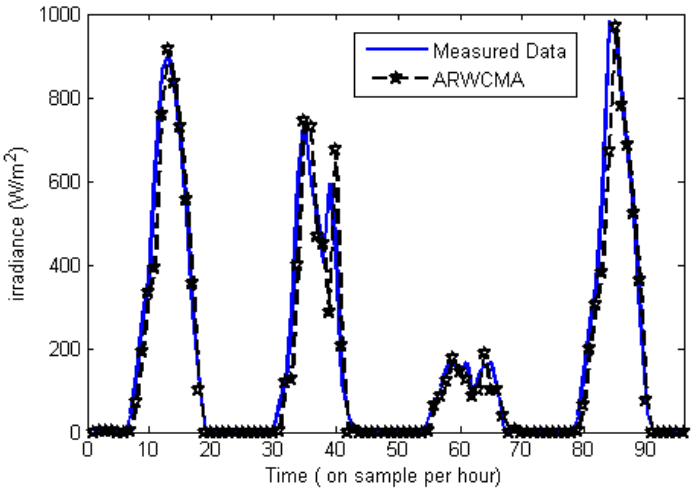

Figure 5.8: Predicted value for four consecutive days.

5.7.2 Discussion on Results for Energy-Balancing and Scheduling Length Objectives

In this section, the performance evaluation of our scheme in terms of our objectives which are minimizing the scheduling length and maximizing the energy-balancing considering energy harvesting characteristics are presented. The quantity used for energy balancing evaluation is the energy variance over all nodes which calculated as follows:

$$\nu = \frac{1}{n}\sum_{i=1}^{n}(\mathcal{A}_i - \overline{\mathcal{A}})^2$$

where $\mathcal{A}_i$ is the energy availability level of sensor node i after the allocation and $\overline{\mathcal{A}}$ is the mean value. We first conducted simulations for small scale problems, with $3-4$ sensor nodes and $7-10$ tasks with maximum 2 predecessors. The optimization toolbox in Matlab is used that calls the solver by syntax `intlinprog` to solve MILP for this small scale problem. The performance ratios of our proposed heuristic (ν_h) and genetic

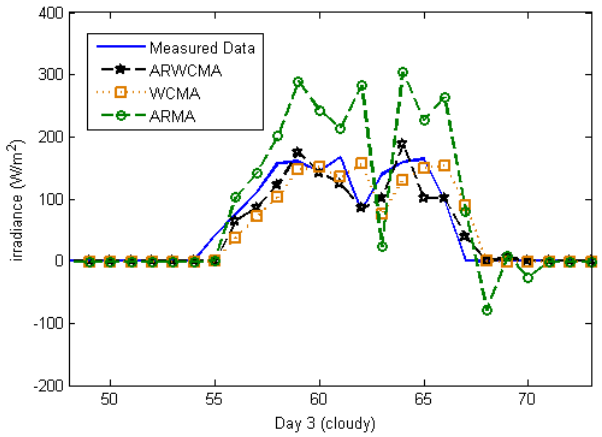

(a) Day 3 (Cloudy day)

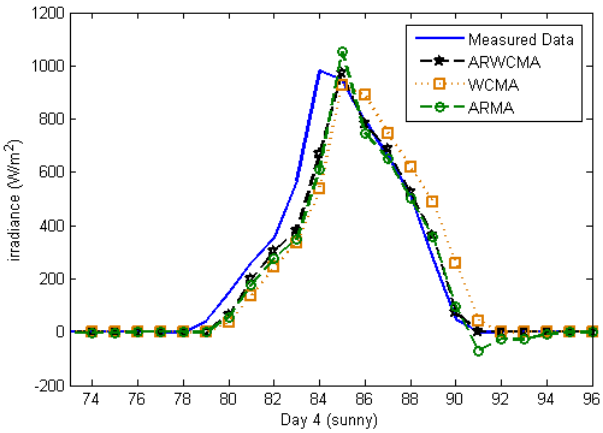

(b) Day 4 (Sunny day)

Figure 5.9: Comparison of prediction results.

algorithm (ν_g) over the optimum solution (ν_o) are shown in Figure 5.10. We can see that the heuristic achieved up to 70% of the solution obtained by the MILP-based approach for the conducted simulations. Moreover, the genetic algorithm results in the good enough performance (up to 82%) that can be later used as a baseline for the larger scale problem.

We then consider the simulations for larger scale problems. Task graph with 30 tasks and the maximum 3 predecessors are generated randomly. Similarly, the results shown in 5.11 are averaged over 100 instances where each point with a 95% confidence

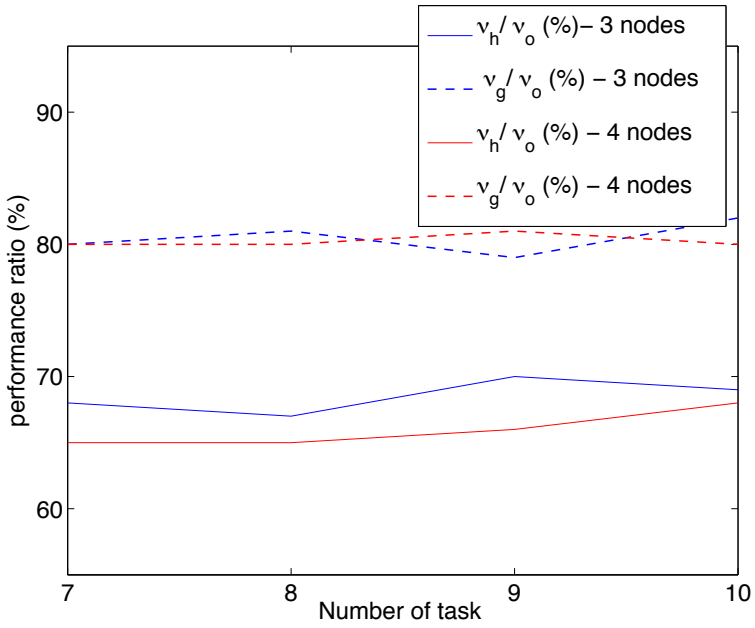

Figure 5.10: Performance comparison of optimum approach with genetic algorithm and the heuristic approach.

interval has a 10% (or better) precision. This result shows the variance of energy level over 2 to 16 nodes. The lower energy variance means achieving the more balanced energy level among the nodes. This result shows that the energy level of nodes using our scheme is more balanced than the E-CNPT algorithm in [43]. This is because although the E-CNPT is an energy efficient algorithm which schedules based on the the energy consumption of tasks, it considers constant energy profiles for nodes and it does not count for the energy variation of the harvested energy. The energy-balancing results from the GA-based scheme with optimum result and our heuristic are fairly close to each other.

In Figure 5.12, the scheduling length resulted from our scheme is compared with the CNPT algorithm proposed in [50], whose only objective is to minimize the scheduling length for each energy budget. Hence, in the best case, we can have the scheduling

length near to the optimum scheduling length over different energy budgets as can be seen in Figure 5.12. It is observed that for the different number of available sensor nodes, the results are fairly near to the CNPT and GA-based schemes.

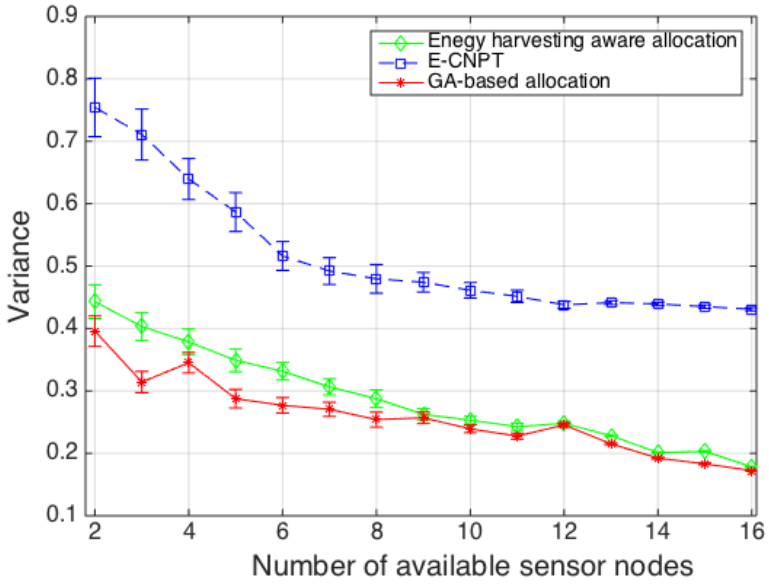

Figure 5.11: Energy variance level over different number of nodes.

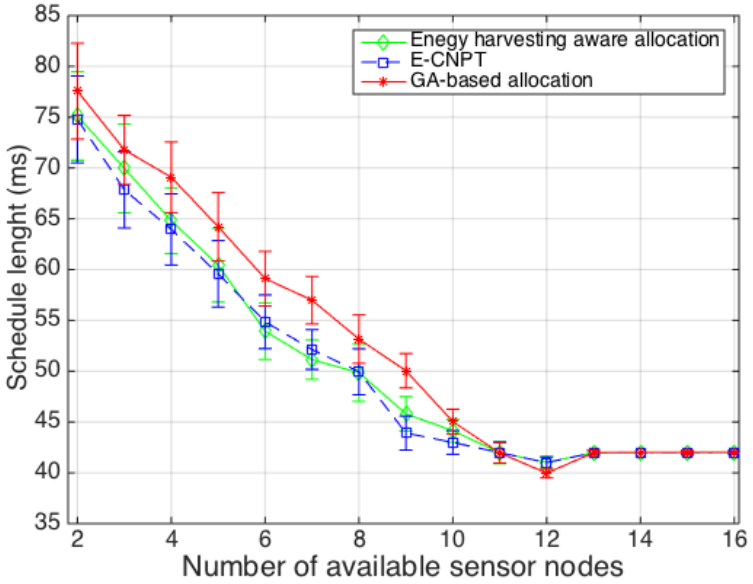

Figure 5.12: Scheduling length over different number of nodes.

In order to validate the performance of our approach, more complex system parameters such as the number of tasks and precedences in DAG and number of sensor nodes are considered. This result is shown in Table 2. Our method attains more balanced residual energy level while achieving a near optimum scheduling lengths, for different system parameter settings.

Table 5.2: Results from different system parameters.

	Sensor nodes	Tasks	Precedence	Schedule length (ms)	Variance
Our approach	30	15	2	29	0.23
GA	30	15	2	29	0.19
E-CNPT	30	15	2	29	0.37
Our approach	40	22	3	36	0.27
GA	40	22	3	35	0.24
E-CNPT	40	22	3	35	0.48
Our approach	50	30	3	48	0.32
GA	50	30	3	47	0.28
E-CNPT	50	30	3	46	0.55

5.7.3 Discussion on Results for Dynamic Adaptation Stage

In this section, the performance of our proposed dynamic adaptation algorithm in the presence of the variable solar-based energy harvesting is evaluated. For this evaluation, we consider 8 different prediction error ratios between 0 and 40 percentage points. For each error ratio point, 100 runs of the task allocation simulation with the random initial available energy of all the nodes are executed. Then, the percentage of the allocation failure, called *missing ratio*, is measured for the "static allocation" and "static allocation with the dynamic phase". An allocation failure occurs once tasks and their precedences are missed due to unavailability of resources. In the dynamic adaptation phase, the task is missed only if stretching the task length to

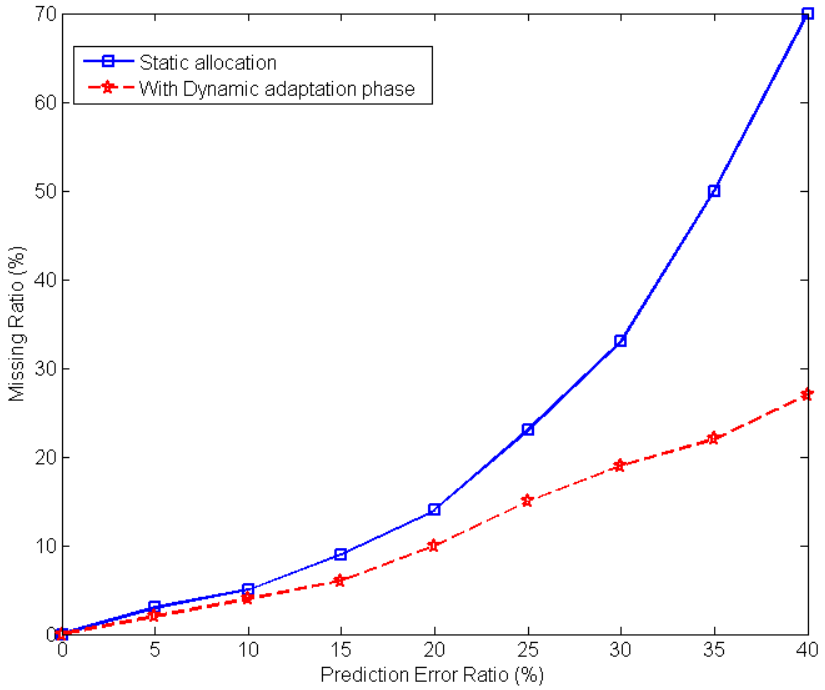

Figure 5.13: Allocation missing ratio with different prediction error ratio.

meet the energy neutral condition, causes the frequency f_k to be below f_{min}. Figure 5.13 shows the significant improvement in terms of the missing ratio by implementing the dynamic adaptation phase.

5.8 Conclusions

In this chapter, the task allocation problem for a sensor network powered by harvesting natural environmental phenomenon is considered. The goals are to minimize the makespan and maximize the fairness in energy-driven task mapping (i.e., energy-balancing), while satisfying the task precedence constraints and energy harvesting causality constraints. The problem is accurately formulated as a mixed integer linear programming problem. The proposed framework for this problem has a hybrid frame-

work of static and dynamic adaptation stages. Heuristic algorithms are proposed to solve the static problem in two phases: scheduling of the task graph and mapping to the appropriate solar powered sensor nodes. The performance of our proposed algorithms, in terms of energy-balancing and scheduling length, is evaluated through simulation and compared with other approaches, including a genetic algorithm as a baseline. We achieve more balanced residual energy levels across the network while attaining a near-optimum scheduling length. The results also show the significant improvement in terms of allocation failure ratio due to implementing the dynamic adaptation stage.

Chapter 6

Toward Integration of Energy Storage for Smart Grids that Enable Renewables

6.1 Introduction

Uncertainties associated with renewable sources, which are intermittent and essentially variable, create a challenge for their integration in to the current power grids [84]. Energy storage can play an important role in integrating renewable energy sources. Variable demand and prices are other sources of uncertainty in the operation of energy systems that can be mitigated by energy storage devices. These devices allow users to exploit the price variations without having to shift their demand to the low-cost periods with dynamic pricing [85]- [88].

Classically the energy storage for solar panels is mostly designed for stand-alone

applications. This means that an amount of energy must be stored to fill at least the production gap of several cloudy weather days. If a location, such as a dwelling, is grid-connected, an energy storage system should not necessarily have to cope with long periods of low solar panel production, as the grid is available as a back-up. Hence, the storage and solar panel sizing criteria can be different from autonomous systems.

In this work, we focus on grid-connected houses equipped with a solar panel and a battery. The battery is useful for the following:

- Regulating the demand from the grid: reducing the variability of the demand from the grid. This variability is undesirable for the utility company that may impose a tariff where peak demands are penalized by a higher price.

- Time-of-day pricing: to account for the time-dependent pricing of electricity. In this situation, the storage should be used to buy electricity only when it is cheap, if possible.

In this chapter, we show the advantages of using energy storage for these reasons. The analysis of suitable policies for storing, buying, selling and using energy in the presence of many sources of uncertainty is complex.

6.1.1 Contributions of This Chapter

First, we develop a methodology for selecting a good parametric policy (PP) for storing, buying, selling and using energy and the corresponding optimum size of the battery and solar panel. This approach uses a small test panel to measure the

local availability of solar energy as a function of time and the house smart meter readings to track the actual load. These measurements are made for some time prior to making the investment decisions. An algorithm then simulates the system for different values of policy parameters and sizes of the battery and panel and evaluates the corresponding operating and capital costs. The outcome of these measurement-driven simulations is a choice of policy parameters and size of the battery and solar panel. Note that after the solar activity has been collected, the measurements can be combined with the smart meter readings of other houses in a similar location to select their appropriate system.

We also analyze how well the PP performs by comparing them to the solution of a Markov decision problem that assumes a genie who reveals hidden state information.

The goal of the proposed policies is to minimize the long-term average cost while fully meeting the variable demand. The cost includes the capital cost of solar panels and batteries, as well as the operating cost of buying energy from the grid.

This chapter is structured as follows. We introduce the system model and problem formulation in Sections 6.2 and 6.3. In Section 6.4, we present the proposed parametric policies for the problem formulation with two cost functions. Numerical results for parametric policies and dynamic programing are provided in Section 6.5. Section 6.6 concludes and summarizes this chapter.

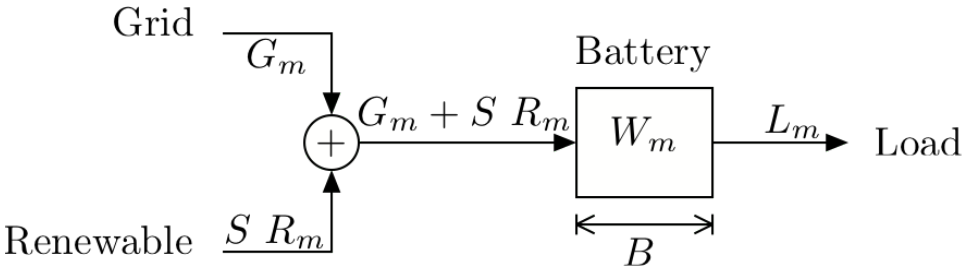

Figure 6.1: System model.

6.2 System Model

We consider a grid-connected system with a renewable source and a battery. The discrete time system model is sketched in Figure 6.1. The time unit of this model is one hour and a time slot is denoted by $n \in \{1, 2, \ldots\}$. In this model, solar energy is used as a renewable energy source. S denotes the size of the solar panel and R_n is the energy that a unit-size solar panel produces. Hence, $R_n S$ is the total amount of energy produced in time slot n. The energy bought from the grid at time n is G_n. The energy consumed at time n is denoted as L_n. The methodology does not assume that a model is known for the random sequences $\{R_n, n \geq 1\}$ and $\{L_n, n \geq 1\}$. We evaluate the performance of the methodology when these sequences are functions of irreducible time-homogeneous Markov chains X and Y on some finite state space $\mathcal{X}$ and $\mathcal{Y}$, respectively. This evaluation tells us by how much one could further reduce the cost if one had a more precise stochastic model of the weather, demand, and prices. It turns out that this additional reduction is small, so that our oblivious methodology is effective.

At time, $n \geq 1$, the battery with capacity B has accumulated an amount of energy denoted as $W_n \in \{0, 1, \ldots, B\}$.

At time slot n, the difference between the available energy $G_n + R_nS$ and the demand L_n is stored in the battery. Thus,

$$W_{n+1} = [W_n + G_n + R_nS - L_n]_0^B$$

where $[x]_0^B := \max\{0, \min\{x, B\}\}$.

The main objective is to explore approaches for choosing G_n, the size of the battery B and the size of the renewable source S such that the overall cost is minimized. The cost contains the capital cost of solar panel and energy storage devices as well as the operating cost of buying energy from the grid.

6.3 Problem Formulation

Considering this model, one can precisely formulate the advantage of using the battery for grid-connected systems equipped with solar panels. Assuming that we want to meet the load L_n all the time, the problem is to minimize the overall average capital and operating costs. This leads to the problem statement described below.

$$\begin{aligned} &\text{Minimize } \gamma S + \beta B + \lim_{N\to\infty} \frac{1}{N} \sum_{n=1}^{N} E(c_n(G_n)) \\ &\text{over } S, B, G_n \\ &\text{subject to } \; G_n + R_nS + W_n \geq L_n, \forall n \geq 1 \end{aligned} \tag{6.1}$$

where $c_n(.)$ denotes the cost of buying energy from the grid and it is strictly monotonic increasing on the amount of energy and periodic as a function of time n. Here, γ and β are the amortized costs per time slot of a unit-size solar panel and battery, respectively. The control policy is of the form $G_n = f_n(R^n, W^n, L^n), \forall n \geq 1$. In this expression, $R^n = \{R_1, R_2, \ldots, R_n\}$ and similarly for W^n and L^n.

We study the effect of using energy storage in the different scenarios:

Scenario 1: In this scenario, the amount of the energy that one buys is independent of the time-of-day pricing. The goal is to regulate the demand from the grid. In order to motivate the user to smooth out the demand, one uses a convex increasing cost of energy such as $c_n(G_n) = G_n^2$.

Scenario 2: In this scenario, the cost function accounts for the time-of-day pricing of electricity. The goal is to adjust for time-of-day variation of the price, renewable source and load. In this case, the cost of energy is a linear function of the amount of the energy that one buys that depends periodically on time n, such as $c_n(G_n) = a_n G_n$ where a_n is periodic.

Scenario 3: In this scenario, one includes the possibility of selling back electricity to the grid. We assume that the selling price is $\kappa E(n)$ during time slot n, where $E(n)$ is the buying price and $\kappa \in [0, 1]$.

6.4 Approximation

One might formate the problem as a Markov decision problem with incomplete observations that would then give the optimal control policy G_n. This approach is not

satisfactory for a number of reasons:

- The optimal policy is complicated and depends on unknown parameters. Since, the control policy G_n at each time is a function of (R^n, W^n, L^n), solving the DP equations requires discretizing these distributions, which results is a very large state space.

- Lack of guidelines and insight. This approach is brute-force and provides numerical results with no insight into how they depend on various aspects of the system.

For these various reasons, our goal is to develop a more insightful and scalable methodology that may suggest practical learning mechanisms.

6.4.1 Parametric Policies (PP)

In this section, we discuss a measurement-based approach to optimize the design and control of the system. First, we collect measurement traces for the specific dwelling, or we use measurements previously made in the same neighborhood that we recalibrate. We describe the former case. One first installs a small test solar panel on the roof of the house to record a time series of the solar power that such a panel produces. In parallel, one uses the smart meter readings to record the electrical consumption of the house over time. This monitoring produces two time series: R^n and L^n.

Given the traces (R^n, L^n) $\forall n \geq 1$, one performs parallel trace-driven simulations for different solar panel and battery sizes and parameters of control policies. These

simulations track the operating costs of these different systems and allow to identify the values that result in the smallest cost.

To implement this methodology, one must define parametric control policies. For the first scenario (as described in Section 6.3), the strategy for different values of α, S and B is as follows: we buy electricity at constant rate $G_n = \alpha$, $\forall n \geq 1$ except that we stop buying when the battery is full and we buy $L_n - R_n S$ when the battery is empty. We assume that the cost of buying electricity from the grid is a non-linear function of the amount of energy. These simulations keep track of the average cost of buying electricity for different values of B and S. From these simulations, one can determine the best values of those parameters. This strategy corresponds to a simple policy for buying energy from the grid.

For the second scenario, the PP is slightly different. Essentially, the policy buys electricity at rate λ_1 and λ_2 during the night (off-peak) and day (on-peak), respectively. However, this policy is adjusted to meet the load and not overflow the battery.

More precisely, the policy is defined as follows. Let W_n be the charge of the battery at time n and B the capacity of the battery. Assume that a solar panel of size S would produce the power $R_n S$, where R_n is the power that the test (unit-size) panel produces. Finally, recall that the load is L_n. Let $\lambda(n) = \lambda_1$ if electricity is cheap during time slot n and let $\lambda(n) = \lambda_2$ otherwise. The policy buys G_n from the grid.

Define

$$A_n = W_n + R_n S - L_n.$$

Then, if $A_n < 0$,

$$G_n = \max\{\lambda(n), -A_n\}, W_{n+1} = \max\{0, \lambda(n) - A_n\}.$$

Also, if $A_n > 0$,

$$G_n = \min\{\lambda(n), \max\{B - A_n, 0\}\}, B_{n+1} = \min\{B, A_n + \lambda(n)\}.$$

For instance, if $A_n > 0$, then the renewable energy plus the energy in the battery suffice to serve the load. In that case, the battery charge reaches the value $\max\{B, A_n\}$ without the grid. One then buys $\max\{\lambda(n), B - \max\{B, A_n\}\}$ to further recharge the battery. The other cases are similar.

The cost of the system at time n is then

$$C_n = E(n)G_n + \gamma S + \beta B$$

recall that $E(n)$ is the unit price of the electricity during time slot n, γ is the amortized cost of a unit-size solar panel and β that of unit-size battery per time slot. We assume for simplicity that the costs are linear in the size, but that assumption can be relaxed easily to conform to actual prices.

For the third scenario, we include the possibility of selling back electricity to the grid. We assume that the selling price is $\kappa E(n)$ during time slot n, where $E(n)$ is the buying price and $\kappa \in [0, 1]$. If $\kappa = 0$, then the optimal policy will not sell electricity. The policy sells electricity if the battery would overflow otherwise and also if there is

some available energy and if $\lambda(n) < 0$. The policy buys $G(n)$ from the grid.

$$G_n = \begin{cases} \min\{B - A_n, \lambda(n)\}, & \text{if } A_n > B \text{ or} \\ & 0 < A_n < B \text{ and } \lambda(n) > 0; \\ \max\{-A_n, \lambda(n)\}, & \text{if } 0 < A_n < B \text{ and} \\ & \lambda(n) < 0; \\ -A_n, & \text{if } A_n < 0. \end{cases}$$

Also,

$$W_{n+1} = A_n + G_n$$

and the cost of operating the system during time slot n is C_n where

$$C_n = E_n G_n 1\{G_n > 0\} + \kappa E_n G_n 1\{G_n < 0\} + \gamma S + \beta B.$$

From the trace-driven simulation, one can then compute an average cost per hour $C(S, B, \lambda_1, \lambda_2)$ as follows:

$$C(S, B, \lambda_1, \lambda_2) = \frac{1}{N} \sum_{n=0}^{N-1} C_n.$$

Using these results, one can determine the values of $(B, S, \lambda_1, \lambda_2)$ that minimize the capital and operating costs of the system.

Item	Cost	Units	Typical Values
Electricity, night	κ_1	¢/kWh	20
Electricity, daytime	κ_2	¢/kWh	30
Battery	β	¢/kWh	7
Average Solar Panel	γ	¢/kWh	15
Average Load	l	kWh/day	30

Table 6.1: Parameters of the system.

6.5 Numerical Results

We now compare numerical results for both the PP and DP. The traces (R^n, L^n) are generated as follows. There are K solar power and K load profiles, which indicate the solar power and load, resp., during the 24 hours of the day.. The k_{th} solar power profile and load profile are $(R(k,1),\ldots,R(k,24))$ and $(L(k,1),\ldots,L(k,24))$, resp. The solar power profile and load profile for day d is $X(d)$ and $Y(d)$, resp. The sequences $X(d)$ and $Y(d)$ are independent Markov chains with given transition matrices. Recall that these models are used to evaluate the policies, but that the policies are oblivious to these models.

Figure 6.2 shows the model (in which $K = 3$) used for the simulation. This model is used to generate traces that have certain features. For instance, there is typically a time offset between the peak solar power and peak load. Similarly, there is a time offset between cheap electricity prices electricity and peak consumption. Note that these profiles are used to generate traces, but they are fairly arbitrary. The representative traces for the renewable energy and load are shown in Figure 6.3.

The key parameters of the system are the various costs, shown in Table 6.1. The typical values are obtained as follows. κ_1 and κ_2 are from [80]. For the battery cost,

we consulted catalogs and found that 12 Volt, 100 Ah battery costs about \$150. This means \$150 for 1.2 kWh, or \$120 per kWh. We assume that this battery will last 1800 days, which gives a cost of 7 cents per kWh per day. Let's consider a simple example with a battery and no solar panel to clarify this cost. With a small battery capacity of 1 kWh, one may buy 1 kWh electricity during a night and use it later during a day. Then, $\kappa_1 - \kappa_2 - \beta$ cents can be saved per day. For solar panels, we use [82] that quotes a net cost of $\$10,000$ for a system that produces about $4,000$ kWh per year. We assume that the system is paid at the rate of \$600 per year, over 25 years, which gives an amortized cost equal to 15 cents per kWh per day, including rebates. For the average load, we used [83] that quotes an average household use of 903 kWh per month, or 30 kWh per day. For the sake of performance evaluation, different ranges of these values might be used.

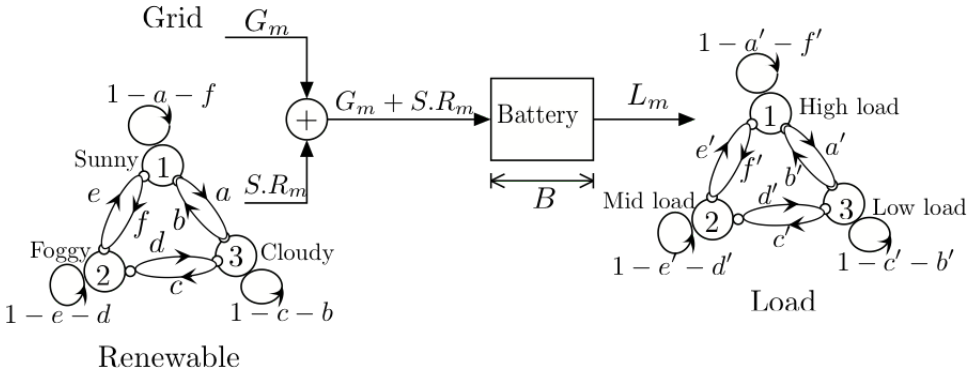

Figure 6.2: The model used for the simulation.

6.5.1 Dynamic Programing

To verify the effectiveness of the simple PP, we compare them to more complex policies derived using DP. These complex policies assume complete knowledge of the states

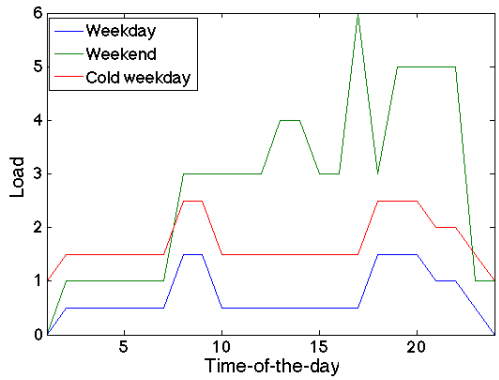

(a) Daily load.

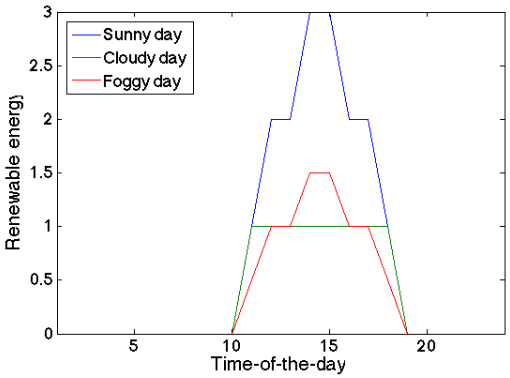

(b) Daily renewable energy.

Figure 6.3: Measurement traces.

$X(d)$ and $Y(d)$, and the transition matrices and sequences $R(d,n)$ and $L(d,n)$. Thus, these complex policies represent the best that one could do will full information. If our policies perform well compared to these ideal policies, we can be reassured that not much is lost because of the simplicity.

Bellman's equation for the long-term average cost is [?]:

$$c^* + \mathcal{H}(x) = \max_{u \in \mathcal{U}} [\mathrm{c}(x,u) + \sum_{x'} P(x,x';u)\mathcal{H}(x')]. \tag{6.2}$$

In this expression, c^* is the optimum cost, $\mathcal{H}(x)$ is the differential cost starting from

state x and $c(x, u)$ is the cost for taking action u in state x. We use value iteration for average cost to compute the optimal policy.

The system states for the first scenario introduced in Section 6.3 are $(W_n,\ R_n,\ L_n)$. At each time slot n, the action is made based on the states at that time. The action denoted as U_n indicates units of the energy drained from the battery and the one dispatched from the grid to satisfy the load. This simulation runs for different values of B and S. Then, the optimum action, B^* and S^* are calculated based on the minimum average total cost $C^*_{DP_1}$.

The system states are slightly different for the second and third scenarios in Section 6.3. The periodic time is also a part of states as $(T_n,\ W_n,\ R_n,\ L_n)$ where $T_n = n\ mod\ 24$. This is due to the time-of-day pricing in the model. The action is the same as before. The average total costs for these scenarios are denoted as C_{DP_2} and C_{DP_3}, respectively. The parameters of the system are from Table I. We initially consider the transition probability as $a = b = c = d = e = f = 0.3$, $a' = b' = c' = d' = e' = f' = 0.4$.

For the first scenario, Figure 6.4 shows the effect of the battery size B on the different costs when $S = 3$. By increasing B, the cost of buying from the grid decreases and the battery cost increases. The optimum value is the battery size that results in minimum total cost. Figure 6.5 shows the effect of S and B on the average total cost (in *cent*/kWh). It can be seen that by increasing the battery size, the optimum value of the solar panel size S^* slightly increases. In other words, by harvesting more energy, larger battery sizes may result in lower costs.

Considering the first scenario, it is observed in Table 6.2 that if the probability of

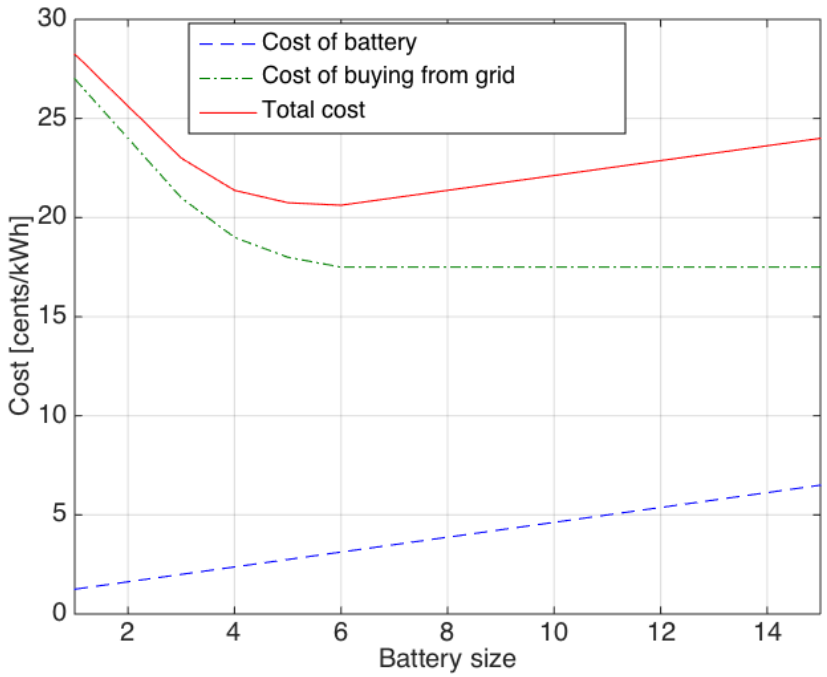

Figure 6.4: Example of different costs (cents/kWh) over B when $S = 3$.

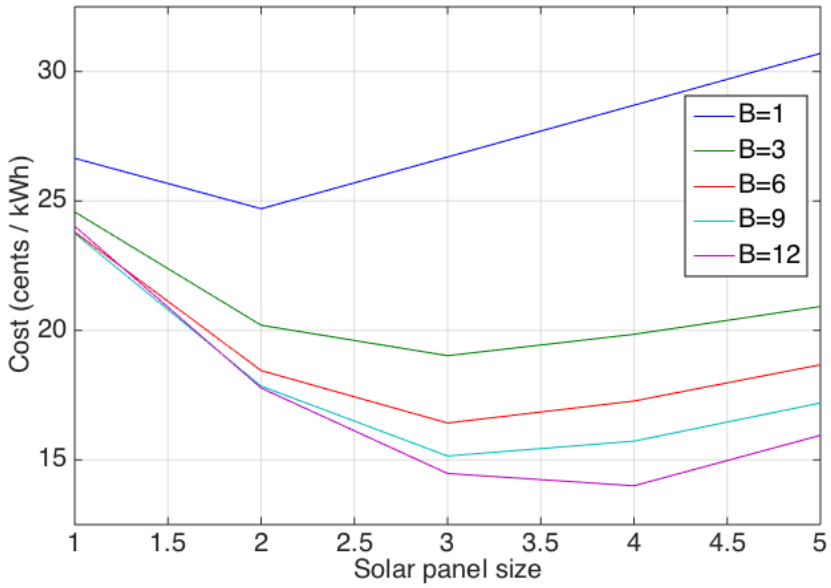

Figure 6.5: Example of the average total cost (cents/kWh) over S and B.

a	d	B^*	$C^*_{DP_1}$ $(cent/\text{kWh})$
0.3	0.3	8	19.1
0.5	0.6	10	20.2
0.6	0.7	12	22.4
0.6	0.8	12	23.6

Table 6.2: Different weather conditions.

going to the cloudy state increases (by increasing a and d), the optimum battery size and average total cost ($C^*_{DP_1}$) increase. This is because there is a higher chance for larger battery sizes to store more during the sunny state and save it for the cloudy state. However, by increasing a and d, B^* may not increase from the certain level, because there is insufficient renewable energy to fill up the battery. Hence, one may not gain by using larger battery sizes.

Using the first and second scenarios, the average total costs from DP ($C^*_{DP_1}$ and $C^*_{DP_2}$) are compared with the no battery and no solar panel case ($C^*_{NO_1}$ and $C^*_{NO_2}$) (in Figure 6.6). This shows how much one can earn by using solar panels and batteries with different costs. The reason for the convergence of the average total cost is that by increasing β, the battery size approaches zero. Considering the effect of solar panel, the costs from DP are always lower than the costs from the no battery and no solar panel case.

6.5.2 Results for Parametric Policies

We now present results for the the PP. The decision variables for the scenario 1 are α, S and B. Table 6.3 shows these values and the average total cost versus β (¢/kWh). C^*_1 denotes the optimum cost for this problem. Not surprisingly, by increasing β, the

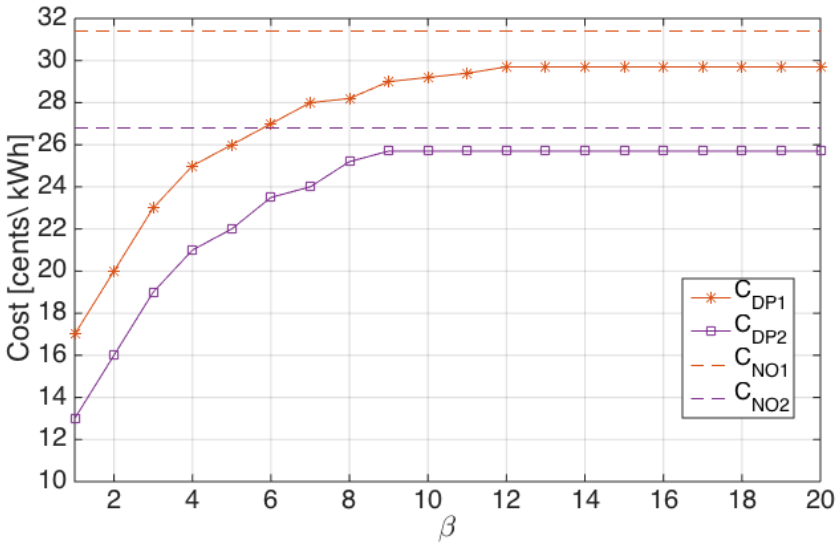

Figure 6.6: Comparison between different costs over β.

	B^*	S^*	α^*	C_1^* $(cent/\text{kWh})$
$\beta = 5$	8	1	4	26.1
$\beta = 7$	7	2	3	28.5
$\beta = 9$	5	2	2	30.4
$\beta = 12$	4	2	2	31.7

Table 6.3: Decision variables vs. β $(cent/\text{kWh})$ for Scenario 1

battery size decreases and the size of the solar panel is almost the same. Moreover, α decreases and the average cost increases as β increases. This is because, the smaller battery can store a lower value of the constant electricity rate α.

The result for scenario 2 is presented in Table 6.4. The decision variables for this problem are λ_1, λ_2, S and B. C_2^* denotes the optimum cost for this scenario. We set $\kappa_1 = 20$ and evaluate the performance for varying $(\kappa_2 - \kappa_1)$. Increasing $(\kappa_2 - \kappa_1)$ leads to larger battery sizes. This is because one may be able to store more energy during the night when electricity is comparably cheaper. Similarly, the value for λ_1 increases (and λ_2 decreases) as $(\kappa_2 - \kappa_1)$ increases.

	B^*	S^*	λ_1^*	λ_2^*	C_2^* ($cent$/kWh)
$(\kappa_2 - \kappa_1)$=5	8	2	3	2	17.1
$(\kappa_2 - \kappa_1)$=8	10	3	4	1	19.3
$(\kappa_2 - \kappa_1)$=10	12	3	4	0	20.4
$(\kappa_2 - \kappa_1)$=12	13	3	5	0	23.6

Table 6.4: Decision variables vs. $(\kappa_2 - \kappa_1)$ for scenario 2.

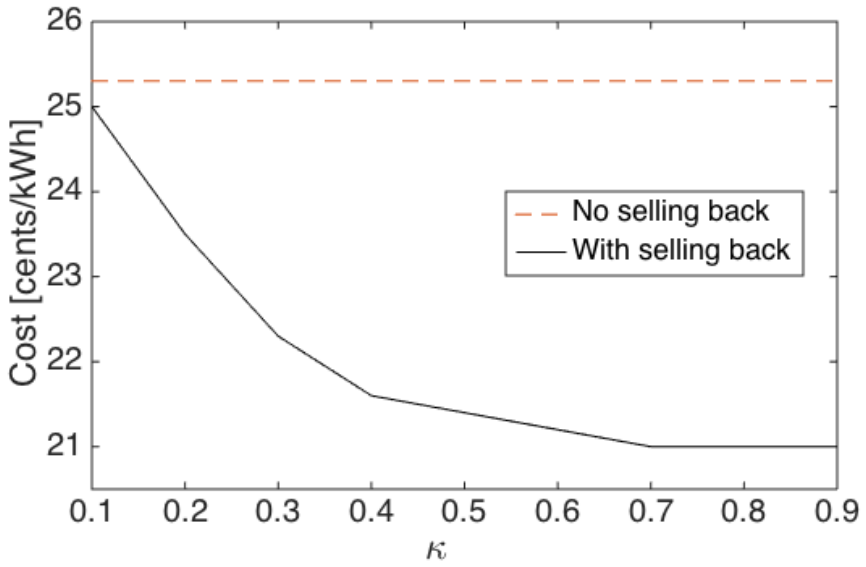

Figure 6.7: Cost reduction by selling back to the grid.

Figure 6.7 shows the amount that one can save by having the opportunity to sell back to the grid. Recall that one may sell back at the cost $\kappa E(n)$, where $E(n)$ is the rate for buying electricity at time n. For simplicity, $E(n)$ is κ_1 and κ_2 for the electricity price at night and day, respectively. The costs are defined in Table I. The total cost decreases as κ increases, because the selling back rate increases. Hence, one may use larger batteries to store more than the daily load to sell it back to the grid. Given these parameters of the system, the battery cannot be larger than a certain value.

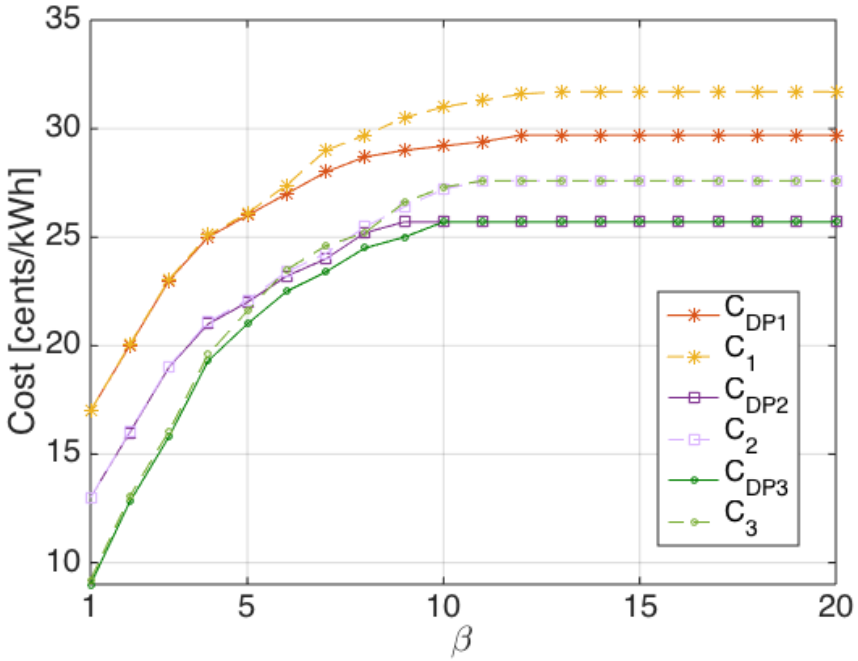

Figure 6.8: Comparison of the costs from PP and DP vs. β.

Figure 6.8 shows that, as β varies, the costs of the PP are very near to the optimum costs from DP. However, the gap between these costs increases as the cost of the battery increases. This shows that the PP may not be good for smaller battery sizes where more accurate battery energy management is required. Moreover, it can be seen that with lower battery cost one can save more by selling electricity back to the grid. Hence, the cost gap between scenarios 2 and 3 decreases as β increases.

6.6 Conclusions

In this chapter, we developed a methodology for selecting a good parametric policy for storing, buying, and using energy and the corresponding optimum size of the battery and solar panel for grid-connected households. The main goal is to minimize the

overall long-term average cost. The problem is a complex Markov decision problem. The simple parametric policies are provided to address the solutions. The outcome is a choice of policy parameters and size of the battery and solar panel. The numerical results show that the parametric policies are good enough in comparison to the results from dynamic programing.

Chapter 7

Reflections and Future Works

In this thesis, several challenges in the design of control policies for systems that completely or partially operate with renewable energy sources are studied. This chapter concludes the thesis with the summary of the main contributions and provides possible future research directions.

7.1 Reflections

In this thesis, we have made progress to address the following questions:

- How to control the systems that store renewable energy to serve the varied demands and how to reduce the state space of such a complex Markov decision problem?
- How to jointly control the energy usage and data sampling rate in energy harvesting wireless sensor networks?

- What is the best performance level that can be achieved through allocating tasks to the resources of wireless sensor networks with renewable energy?

- What is the role of renewable energy sources and energy storage devices in reducing the cost of smart grid's operation and how to control such systems?

7.1.1 A Methodology for Designing the Control of Systems That Store Renewable Energy

A methodology for addressing the variability of renewable energy and the electric load in the control of systems with energy storage devices was explored in Chapter 3. The problem is to maximize the long-term utility of the energy by controlling how it is used. One may formulate the problem as a Markov decision problem. The main idea of this part is to replace this Markov decision problem by an optimization problem with probabilistic constraints based on the theory of large deviations. We compared three methods for evaluating the small probability that the battery goes empty for a given control policy. These methods use the fact that the battery discharge increments are functions of a Markov chain. The three methods are: 1) a direct method based on Chernoff's inequality and the first step equations of a Markov chain; 2) a method based on the analysis of the occupation measure and contraction principle; 3) Gaussian approximation.

Our examples indicate that the direct method and the occupation measure yields essentially the same estimates, but that the first approach is numerically simpler. The examples confirm that the Gaussian approximation usually yields poor estimates

that are not satisfactory to address the optimization problems. Using the occupation measure approach, we could derive properties of the large deviations. We showed a decomposition result when the source and load are function of independent Markov chains. We demonstrated the use of the approach for random walk process and two-state Markov chain. The methodology applies to much more complex situations. The benefit is that the resulting control law is simple, as it does not depend on the instantaneous charge of the battery.

7.1.2 Jointly Control of the Energy Usage and Data Sampling Rate

A methodology with the technique for state space dimension reduction for solving optimal control of systems with coupled data buffer and energy storage was presented in Chapter 4. The technique consists of relaxing the underflow constraint on the energy level in the battery and overflow constraint on the data backlogs in data buffer by replacing them with a bound on the probability of energy underflow and data overflow as derived via large deviation theory. The considered policies do not depend on the state of the battery and data buffer. We demonstrated the use of the approach for the control of a wireless sensor node equipped with a solar panel and compared the results with the solution of the Markov decision problem with dynamic programing. This approach works for even more complex and large state space models.

7.1.3 Task Allocation Problem

In Chapter 5, we studied the task allocation problem for a sensor network powered by harvesting energy from natural environmental phenomeno. The goals are to minimize the makespan and maximize the fairness in energy-driven task mapping (i.e., energy-balancing), while satisfying the task precedence constraints and energy harvesting causality constraints. The problem is precisely formulated as a mixed integer linear problem. The proposed framework for this problem has a hybrid framework of static and dynamic adaptation stages. Heuristic algorithms are proposed to solve the static problem in two phases: scheduling of the task graph and mapping to the appropriate solar powered sensor nodes. The performance of our proposed algorithms, in terms of energy-balancing and scheduling length, is evaluated through simulation and compared with the optimum results for the small scale and with other approaches, including a genetic algorithm for the larger scale problem. We achieve more balanced residual energy levels across the network while attaining a near-optimum scheduling length. The results also show the significant improvement in terms of allocation failure ratio due to implementing the dynamic adaptation stage.

7.1.4 Integrating Renewable Energy and Energy Storage into Smart Grids

In Chapter 6, we developed a methodology for selecting a good parametric policy for storing, buying, and using energy and the corresponding optimum size of the battery and solar panel for grid-connected households. The main goal is to minimize

the overall long-term average cost while the variable demand is completely served. The cost contains the capital cost of the solar panel and energy storages as well as the operating cost of buying energy from the grid. The problem is a complex Markov decision problem. The simple parametric policies are provided to address the solutions. One may use this outcome for making the investment decisions. The numerical results show that parametric policies are good enough in comparison to the results from dynamic programing.

7.2 Suggestions for Future Research

In this thesis, we investigate various resource management problems and propose solutions using different techniques. In this part, we discuss the limitations and possible extensions of these models and approaches.

7.2.1 Extending to Multi-hop Energy Harvesting Wireless Sensor Network

One may extend our single hop scenario used in Chapter 4 to a multi-hop setting for data transmission. In the multi-hop case, the problem under study is the joint optimal energy allocation for data-sampling rate, scheduling for transmissions and routing policy. The sensor nodes sense the field and transmit data to a fusion node. In each time slot, the sensor node can harvest energy from the environment and store it in a rechargeable battery for future use. Considering the sleep/awake cycling for each sensor node, it is in either sleep mode or active mode in any time slot. In the

sleep mode, the sensor nodes can only harvest energy, but cannot sense or transmit data. In the active mode, the sensor nodes can harvest energy, sense, process, and transmit data. Each node may need to transmit data to any other nodes in this network. For this model, one may aim to develop a scheduling policy that ensures a fair utilization of the network resources. One may also consider the fact that the energy harvesting process is stochastic in nature, and develop adaptive routing and scheduling algorithms that are able to dynamically adapt to timely changes in the energy harvesting process and network environments.

7.2.2 Extending the Proposed Methodology for Systems with Renewable Energy

The analysis of the proposed methodologies in Chapter 3 and 4 assumes that the statistics of the renewable source and the environment are known. It might be interesting to explore the methodology that suggests adaptive schemes that do not require such knowledge and to analysis these schemes.

Moreover, in Chapter 4, we studied the methodology for a system where we have resource and data queues. The resources are used to provide rate to support the data flows. Therefore, the resource queue and data queue are highly coupled. It is interesting to see how this framework can be applied to other similar applications that have a resource buffer. Also, one may investigate whether the performance gap can be improved in the order of buffer sizes.

7.2.3 Extending the Energy Prediction Analysis

Given the precise information about the future energy generation, the method used in Chapter 5 achieves a near optimal system performance. We pointed out that overly precise optimization of the application parameters turns out to be useless if major prediction errors occur. However, it may be useful to explore that how the prediction errors actually degrade the performance of the system.

Moreover, the energy prediction studied in Chapter 5 can be extended in many directions. One may consider reducing the computational load of the energy prediction algorithm. If the environmental phenomenon being harvested is spatially correlated, one can apply the idea of dynamic clustering, where the prediction algorithm only runs once for all the sensor nodes in each cluster. The clusters may also dynamically alter their topology depending on the changing environmental characteristics, e.g., different sun radiation angles and shadows of objects such as buildings and trees.

7.2.4 Interplay Between Energy Storage and the Energy Market in Smart Grid Systems

It might be interesting to explore what will happen to the energy market when a significant fraction of users adopt the energy storage. A possible consequence is that the resulting steady demand process will cause convergence of the energy market resulting in the smaller price variance. This might be beneficial for both energy producers and users without energy storage, a less volatile price process will decrease the possibilities for exploiting price fluctuations for users with storage capacities.

Consequently, the cost savings obtained from energy storage may decrease beyond the break-even point. The relationship between energy storage and the energy market is an interesting topic for the future research.

Bibliography

[1] Basagni, Stefano, M. Yousof Naderi, Chiara Petrioli, and Dora Spenza. "Wireless sensor networks with energy harvesting," *In Proceedings of Mobile Ad Hoc Networking: The Cutting Edge Directions*, 2013.

[2] O. Vermesan, P. Friess, P. Guillemin, S. Gusmeroli, H. Sundmaeker. "Internet of things strategic research roadmap," *In Proceedings of Internet of Things-Global Technological and Societal Trends*, 2011.

[3] X. Fang, S. Misra, G. Xue, and D. Yang. "Smart grid The new and improved power grid: A survey," *IEEE Communications Surveys and Tutorials,* vol. 14, no. 4, pp. 944-980, 2012.

[4] J. Abouei, D. Brown, K. N. Plataniotis, and S. Pasupathy. "Energy efficiency and reliability in wireless biomedical implant systems," *IEEE Transactions on Information Technology in Biomedicine*, vol. 15, no. 3, pp. 456-466, 2011.

[5] Sudevalayam, Sujesha, and Purushottam Kulkarni. "Energy harvesting sensor nodes: Survey and implications," *IEEE Communications Surveys and Tutorials*, vol. 13, no. 3, pp. 443-461 2011.

[6] A. Kansal, J. Hsu, S. Zahedi, M. B. Srivastava, "Power management in energy harvesting sensor networks," *ACM Transactions on Embedded Computing Systems (TECS)*, vol. 6, no. 4, 2007.

[7] P. Sitka, P. Corke, L. Overs, P. Valencia, and T. Wark. "Fleck A platform for real-world outdoor sensor networks," *In Proceedings of ISSNIP*, pages 709-714, Dec. 2007.

[8] V. Kyriatzis, N. S. Samaras, P. Stavroulakis, H. Takruri Rizk, and S. Tzortzios. Enviromote: "A new solar-harvesting platform prototype for wireless sensor networks," *In Proceedings of IEEE PIMRC*, pages 1-5, September 2007.

[9] P. Dutta, J. Hui, J. Jeong, S. Kim, C. Sharp, J. Taneja, G. Tolle, K. Whitehouse, and D. Culler, "Trio: Enabling sustainable and scalable outdoor wireless sensor network deployments," *In Proceedings of ACM IEEE IPSN*, pages 407-415, Nashville, TN, April 19-21 2006.

[10] F. Simjee and P. H. Chou. "Everlast: Long-life, supercapacitor-operated wireless sensor node," *In Proceedings of ISLPED*, pages 197-202, Tagernsee, 2006.

[11] Z. Zhong, T. Zhu, T. He, and Z. Zhang, "Demo Abstract: Leakage-Aware Energy Synchronization on Twin-Star Nodes," *ACM conference on Embedded network sensor systems*, 2008.

[12] M. Minami, T. Morito, H. Morikawa, and T. Aoyama. "Solar Biscuit: A battery-less wireless sensor network system for environmental monitoring applications," *In Proceedings of INSS*, pages 1-6, June 2005.

[13] A. Bari, J. Jiang, W. Saad, and A. Jaekel. "Challenges in the smart grid applications: an overview," *International Journal of Distributed Sensor Networks*, 2014.

[14] A. Kansal, D. Potter, and M. B. Srivastava, "Performance aware tasking for environmentally powered sensor networks," *In Proceedings SIGMETRICS,* 2004.

[15] X. Jiang, J. Polastre, D. Culler, "Perpetual environmentally powered sensor networks," *In Proceedings IEEE IPSN*, 463-468, 2005.

[16] T. Zhu, Z. Zhong, Y. Gu, T. He and Z. Zhang,"Leakage-Aware Energy Synchronization for Wireless Sensor Networks," *In Proceedings of the ACM 7th international conference on Mobile systems, applications, and services,* pp. 319-332, 2009.

[17] M.E. Hellman, J. Raviv, "Probability of error, equivocation, and the Chernoff bound," *IEEE Transactions on Information Theory*, 1970.

[18] D. P. Bertsekas "Dynamic programming and optimal control," *Athena Scientific*, vol. 1, no. 2, 1995.

[19] T. H. Cormen, C. E. Leiserson, R. L. Rivest, C. Stein, " Introduction to algorithms," *Cambridge: MIT press*, vol. 2, pp. 531-549, 2001.

[20] B. V. Roy, and D. F. Daniela "Approximate linear programming for average-cost dynamic programming," *Advances in neural information processing systems,* 2002.

[21] J. Yang and S. Ulukus, "Optimal Packet Scheduling in an Energy Harvesting Communication System," IEEE Trans. on Communications, 60(1):220-230, Jan. 2012.

[22] O. Ozel, K. Tutuncuoglu, J. Yang, S. Ulukus, and A. Yener, "Transmission with energy harvesting nodes in fading wireless channels: Optimal policies," *IEEE Journal on Selected Areas in Communications,* vol. 29, no. 8, 2011.

[23] K. Tutuncuoglu and A. Yener, "Optimum transmission policies for battery limited energy harvesting nodes," *IEEE Transactions on Wireless Communications*, vol. 11, no. 3, 2012.

[24] J. Yang and S. Ulukus, "Optimal packet scheduling in a multiple access channel with rechargeable nodes," *in Proc. IEEE ICC*, Kyoto, Japan, June 2011.

[25] J. Yang, O. Ozel, and S. Ulukus, "Broadcasting with an energy harvesting rechargeable transmitter," *IEEE Transactions on Wireless Communication*, vol. 11, no. 2, pp. 571-583, Feb. 2012.

[26] S. Chen, P. Sinha, N. Shroff and C. Joo, "Finite-Horizon Energy Allocation and Routing Scheme in Rechargeable Sensor Networks," *IEEE INFOCOM*, pp. 2273-2281, April 2011.

[27] R.-S. Liu, K.-W. Fan, Z. Zheng, and P. Sinha, "Perpetual and fair data collection for environmental energy harvesting sensor networks," *IEEE/ACM Transactions on Networking*, vol. 19, no. 4, 2011.

[28] Z. Mao, C. E. Koksal, and N. B. Shroff, "Near optimal power and rate control of multi-hop sensor networks with energy replenishment: Basic limitations with finite energy and data storage," *IEEE Transactions on Automatic Control*, vol. 57, no. 4, 2012.

[29] M. Gatzianas, L. Georgiadis, and L. Tassiulas, "Control of wireless networks with rechargeable batteries," *IEEE Transactions on Wireless Communications*, vol. 9, no. 2, 2010.

[30] V. Sharma, U. Mukherji, V. Joseph, and S. Gupta, "Optimal energy management policies for energy harvesting sensor nodes," *IEEE Transactions on Wireless Communications*, vol. 9, no. 4, 2010.

[31] O. Ozel and S. Ulukus, "Achieving AWGN Capacity Under Stochastic Energy Harvesting," *IEEE Trans. on Information Theory*, vol. 58, no. 10, pp. 6471-6483, Oct. 2012.

[32] A. Cammarano, D. Spenza, and C. Petrioli. "Energy-harvesting WSNs for structural health monitoring of underground train tunnels," *IEEE Conference on. Computer Communications Workshops (INFOCOM WKSHPS)*, 2013.

[33] M. Gorlatova, P. Kinget, I. Kymissis, D. Rubenstein, X. Wang, "Challenge: ultra low power energy-harvesting active networked tags (EnHANTs)," *In proceedings of the ACM 15th annual international conference on Mobile computing and networking*, 2009.

[34] G. Virone, A. Wood, L. Selavo, Q. Cao, L. Fang, T. Doan, "An advanced wireless sensor network for health monitoring," *Transdisciplinary Conference on Distributed Diagnosis and Home Healthcare (D2H2)*. 2006.

[35] S. Sudevalayam, P. Kulkarni,"Energy Harvesting Sensor Nodes: Survey and Implications," *IEEE Communications Surveys and Tutorials*, vol. 13 , no. 3, pp 443 - 461, 2011.

[36] J. Zhuo, C. Chakrabarti, "Energy-Efficient Dynamic Task Scheduling Algorithms for DVS Systems," *ACM Transactions on Embedded Computing Systems (TECS)*, vol. 7, no. 2, 2008.

[37] W. Li, F. C. Delicato, A. Y. Zomaya, "Adaptive energy-efficient scheduling for hierarchical wireless sensor networks," *ACM Transactions on Sensor Networks (TOSN)*, vol. 9, no. 3, May 2013.

[38] H. S. AbdelSalam, S. Olariu, "Toward Efficient Task Management in Wireless Sensor Networks," *IEEE Transactions on Computers*, vol. 60, no. 11, 2011.

[39] N. Edalat, X. Wendong, T. Chen-Khong, E. Keikha, O. Lee-Ling, "A price-based adaptive task allocation for Wireless Sensor Network," *In Proceedings of IEEE 6th International Conference on Mobile Adhoc and Sensor Systems*, pp.888-893, 2009.

[40] T. Zhu, A. Mohaisen,Y. Ping, and D. Towsley, "DEOS: Dynamic energy-oriented scheduling for sustainable wireless sensor networks," *In Proceedings of INFOCOM*, 2012.

[41] T. La Porta, C. Petrioli, and D. Spenza, "Sensor-mission assignment in wireless sensor networks with energy harvesting", *In Proceedings of SECON*, 2011.

[42] A. Pathak, V.K. Prasanna, "Energy-efficient task mapping for data-driven sensor network macroprogramming", *IEEE Transactions on Computers*, vol. 59, no. 7, pp 955 - 968, 2010.

[43] Y. Tian, J. Boangoat and E. Ekici and F. Ozguner, "Real-time task mapping and scheduling for collaborative in-network processing in DVS-enabled wireless sensor networks", *In Proceedings of 20th International Parallel and Distributed Processing Symposium* , 2006.

[44] Y. Tian, Y. Gu and E. Ekici and F. Ozguner, "Dynamic Critical-Path Task Mapping and Scheduling for Collaborative In-Network Processing in Multi-Hop Wireless Sensor Networks," *In Proceedings of International Conference on Parallel Processing*, 2006.

[45] S. Liu, Q. Qiu, and Q. WU, "Energy Aware Dynamic Voltage and Frequency Selection for Real-Time Systems with Energy Harvesting," *In Proceedings of Design, Automation, and Test in Europe*, Mar. 2008.

[46] S. Liu, Q. WU and Q. Qiu, "An Adaptive Scheduling and VoltagelFrequency Selection Algorithm for Real-time Energy Harvesting Systems," *In Proceedings of Design Automation Conference*, Jul. 2009.

[47] A. Allavena, and D. Mosse, "Scheduling of FrameÂBased Embedded Systems with Rechargeable Batteries," *In Proceedings of Workshop on Power Management for Real-time and Embedded Systems*, May 2001.

[48] C. Moser, D. Brunelli and L. Thiele and L. Benini, "Lazy Scheduling for Energy Harvesting Sensor Nodes", *In Proceedings of Conference on Distributed and Parallel Embedded Systems*, Oct. 2006.

[49] C. Moser and D. Brunelli and L. Thiele and L. Benini, "Real-Time Scheduling for Energy Harvesting Sensor Nodes", *Real-Time System Journal*, vol. 37, no. 3, pp 233-260, 2007.

[50] T. Hagres and J. Janecek, "A high performance, low complexity algorithm for compile-time job scheduling in homogeneous computing environments", *In Proceedings of International Conference on Parallel Processing Workshops*, 2003.

[51] J. Recas, C. Bergonzini, D. Atienza, and T. S. Rosing, "Prediction and management in energy harvested wireless sensor nodes", *In Proceedings of VITAE'09*, May 2009.

[52] C. Renner. "Solar harvest prediction supported by cloud cover forecasts," *In Proceedings of ENSSys*, 2013.

[53] A. Cammarano, C. Petrioli, and D. Spenza. "Pro-Energy: A novel energy prediction model for solar and wind energy-harvesting wireless sensor networks," *In Proceedings of IEEE 9th International Conference on Mobile Adhoc and Sensor Systems (MASS)*, 2012.

[54] R.H. Shumway and D.S. Stoffer, "Time Series Analysis and Its Applications", *Springer-Verlag,* 2000.

[55] D. C. Montgomery, L. A. Johnson, J. S Gardiner, "Forecasting and Time Series Analysis", *McGraw-Hill*, 1990.

[56] Michael, R Garey and David, S Johnson, "Computers and intractability: a guide to the theory of NP-completeness", WH Freeman & Co., San Francisco, 1979.

[57] Al-Karaki, Jamal N and Kamal, Ahmed E, " Routing techniques in wireless sensor networks: a survey," *IEEE Wireless communications*, vol. 11, no. 6, pp 6-28, 2004.

[58] National Renewable Energy Lab website. http://www.nrel.gov/midc/

[59] Crossbow Technology INC. Mica-2 Data Sheet. [Online] Crossbow, http://www.xbow.com.

[60] Dong Kun. Noh, Lili. Wang, Yong. Yang, Hieu Khac. Le, Tarek. Abdelzaher, "Minimum variance energy allocation for a solar-powered sensor system," *In Proceedings of 5th IEEE International Conference on Distributed Computing in Sensor Systems*, DCOSS 2009.

[61] H. El-Rewini, T.G. Lewis, H.H. Ali, "Task Scheduling in Parallel and Distributed Systems", *Prentice-Hall International Editions*, 1994.

[62] A.S. Wu, H. Yu, S. Jin, K.-C. Lin, G. Schiavone, "An incremental genetic algorithm approach to multiprocessor scheduling", *IEEE Transactions on Parallel and Distributed Systems*, vol. 15, no. 9, pp 824 - 834, 2004.

[63] H Bevrani, A Ghosh, G Ledwich "Renewable energy sources and frequency regulation: survey and new perspectives," *Renewable Power Generation,* vol. 4, no. 5, pp. 438-457, 2010.

[64] Walrand, Jean, and Pravin Pratap Varaiya. High-performance communication networks. Morgan Kaufmann, 2000.

[65] S.R.S. Varadhan. " Large Deviations," *The Annals of Probability*, vol. 36, no. 2, 397-419, 2008.

[66] S.R.S. Varadhan, "Asymptotic probability and differential equations," Comm. Pure Appl. Math. no. 19, pp. 261-286, 1966.

[67] R. R. Bahadur. " Some Limit Theorems in Statistics," *SIAM*, Philadelphia, 1971.

[68] S.R.S. Varadhan. " Large Deviations and Applications," *CBMS86*, SIAM, 1986.

[69] A. Dembo, O. Zeitouni. " Large Deviations Techniques and Applications," *Springer*, 1998.

[70] J. D. Deuschel, and D. W. Stroock . " Large Deviations," *Academic Press*, Inc., Boston, MA 1989.

[71] G. Kesidis, J. Walrand, C. S. Chang, " Effective bandwidths for multiclass Markov fluids and other ATM sources," *IEEE/ACM Transactions on Networking*, vol. 1, no. 4, pp. 424-428, 1993.

[72] G. D. Veciana, J. Walrand, "Effective bandwidths: Call admission, traffic policing and filtering for ATM networks," *Queueing Systems* 20, no. 1, pp. 37-59, 1995.

[73] R. S. Ellis. " Large Deviations for the Empirical Measure of a Markov Chain with an Application to the Multivariate Empirical Measure," *The Annals of Probability*, vol. 16, no. 4, Oct., 1988.

[74] I. H. Dinwoodie, P. Ney. " Occupation measures for Markov chains," *Journal of Theoretical Probability*, vol. 8, no. 3, pp 679-691, July 1995.

[75] S. Halfin, W. Whitt. " Heavy-Traffic Limits for Queues with Many Exponential Servers," *Operations Research*, 1981.

[76] R. Guerin, H. Ahmadi, M. Naghshineh, "Equivalent capacity and its application to bandwidth allocation in high-speed networks," *IEEE Journal on Selected Areas in Communications*, vol. 9, no. 7, pp 968-981, 1991.

[77] D. P. Bertsekas "Dynamic Programming and Optimal Control," *Athena Scientific*, vol. 2, 3rd Edition, 2007.

[78] P. Whittle "Optimization over time," *John Wiley and Sons Inc.*, vol. 2, 1982.

[79] `http://platformx.sourceforge.net/home.html`

[80] PG&E *Residential Time of Use Pricing.* `http://www.pge.com/nots/rates/tariffs/ResElecCurrent.xls`

[81] Wikipedia *Electric Vehicle battery.* `http://en.wikipedia.org/wiki/Electric_vehicle_battery`

[82] Energy Informative *How Much Solar Panels Cost.* `http://energyinformative.org/solar-panels-cost/`

[83] U.S. Energy Information Administration *How Much Electricity Does an American Home Use?* `http://www.eia.gov/tools/faqs/faq.cfm?id=97&t=3`

[84] Ye Yan, Yi Qian, Hamid Sharif, and David Tipper, "A survey on smart grid communication infrastructures: Motivations, requirements and challenges," *IEEE Communications Surveys and Tutorials*, vol. 15, no. 1 pp. 5-20, 2013.

[85] M.d H. Albadi and E. F. El-Saadany, "'A summary of demand response in electricity markets," *Electric Power Systems Research*, vol. 78, no. 11, pp. 1989-1996, 2008.

[86] G. Barbose and C. Goldman, "A survey of utility experience with real time pricing,"Berkeley National Laboratory, Tech. Rep. LBNL-54238, 2004.

[87] H. Allcott, "Rethinking real-time electricity pricing," *Resource and Energy Economics*, vol. 33, no. 4, pp 820-842, 2011.

[88] A-H. Mohsenian-Rad, V. WS Wong, J. Jatskevich, R. Schober, and A. Leon-Garcia. "Autonomous demand-side management based on game-theoretic energy

consumption scheduling for the future smart grid," *IEEE Transactions on Smart Grid*, vol. 1, no. 3, pp. 320-331, 2010.

[89] W. Ketter, J. Collins, P. P. Reddy, and M. D. Weerdt, "The 2013 Power Trading Agent Competition," ERIM Report Series Reference No. ERS-2013-006-LIS, 2013.

[90] H. I. Su and A. El Gamal, "Modeling and Analysis of the Role of Energy Storage for Renewable Integration: Power Balancing," *IEEE Transactions on Power Systems*, vol. 28, no. 4, pp. 4109-4117, 2013.

[91] D. Gayme and U. Topcu, "Optimal power flow with distributed energy storage dynamics," *IEEE American Control Conference (ACC)*, pp. 1536-1542, 2011.

[92] M. van de Ven, N. Hegde, L. Massoulie and T. Salonidis. "Optimal control of end-user energy storage," *IEEE Transactions on Smart Grid*, vol. 4, no. 2, pp. 789-797, 2013.

[93] I. Koutsopoulos, V. Hatzi, and L. Tassiulas, "Optimal energy storage control policies for the smart power grid," *In IEEE International Conference on Smart Grid Communications (SmartGridComm)*, pp. 475-480. 2011.

[94] A. Mishra, D. Irwin, P. Shenoy, J. Kurose, and T. Zhu, "SmartCharge: cutting the electricity bill in smart homes with energy storage." *In Proceedings of ACM 3rd International Conference on Future Energy Systems: Where Energy, Computing and Communication Meet*, 2012.

[95] B. Urgaonkar, M. J. Neely, and A. Sivasubramaniam, "Optimal Power Cost Management Using Stored Energy in Data Centers," *In ACM SIGMETRICS* , pages 221-232, 2011.

[96] L. Huang, J. Walrand, and K. Ramchandran, "Optimal Demand Response with Energy Storage Management," *IEEE Third International Conference on In Smart Grid Communications (SmartGridComm)*, pages 61-66, 2012.

[97] H. Sasle and O. S. Grande, "Demand response from household customers: experiences from a pilot study in Norway," *IEEE Transactions on Smart Grid*, vol. 2, no. 1, pp. 102-109, 2011.

[98] K. Ahlert and C. Van Dinther, "Sensitivity analysis of the economic benefits from electricity storage at the end consumer level," *IEEE Bucharest PowerTech* , pp. 1-8, 2009.

[99] J. Rajasekharan, and V. Koivunen, "Optimal Energy Consumption Model for Smart Grid Households with Energy Storage," arXiv preprint arXiv:1310.3424 (2013).

List of Publications

- **N. Edalat**, M. Motani, J. Walrand, and L. Huang. "A Methodology for Designing the Control of Energy Harvesting Sensor Nodes." *IEEE Journal on Selected Areas in Communications (JSAC)* vol. 33, no. 3, pp. 1-10, 2015.

- **N. Edalat**, M. Motani, J. Walrand. "Optimum Control for End-User of Smart Grid with Renewable Energy and Storage." (To be submitted to) *IEEE Transactions on Sustainable Energy.*

- **N. Edalat**, M. Motani. "Energy Aware Task Allocation for Energy Harvesting Sensor Networks." (Second-round review) *EURASIP Journal on Wireless Communications and Networking (Springer).*

- **N. Edalat**, M. Motani, J. Walrand, and L. Huang. "Control of systems that store renewable energy." *In Proceedings of E-energy, ACM-SIGCOMM*, pp. 15-25, 2014.

- **N. Edalat**, W. Xiao, M. Motani, N. Roy, and Sajal K. Das. "Auction-based task allocation with trust management for shared sensor networks." *Security and Communication Networks* vol. 5, no. 11, pp. 1223-1234, 2012.

- **N. Edalat**, W. Xiao, M. Motani, N. Roy, and Sajal K. Das. "Combinatorial auction-based task allocation in multi-application wireless sensor networks." *In Proceedings of IEEE International Conference on Embedded and Ubiquitous Computing (EUC)*, pp. 174-181, 2011.

Appendix A

Statement in Direct Method (support documents for Chapter 3)

This is to show:

$$s_{n+1}(y) = E[\exp\{\theta Z_1\}|Y_1 = y] \sum_{y'} P(y, y') s_n y', \forall y \in \mathcal{Y}.$$

Starting from LHS, we have,

$$\begin{aligned}
s_{n+1}(y) &= E[\exp\{\theta(Z_1 + \cdots + Z_{n+1})\}|Y_1 = y], \\
&= E[\exp\{\theta Z_1\}.\exp\{\theta(Z_2 + \cdots + Z_{n+1})\}|Y_1 = y], \\
E[\exp\{\theta(Z_2 + \cdots + Z_{n+1})\}|Y_1 = y] & \\
&= \sum_{y' \in \mathcal{Y}} E[\exp\{\theta(Z_2 + \cdots + Z_{n+1})\}\mathbf{1}\{Y_2 = y'\}|Y_1 = y], \\
&= \sum_{y' \in \mathcal{Y}} E[\exp\{\theta(Z_2 + \cdots + Z_{n+1})\}|Y_2 = y'] \\
&\times P[Y_2 = y'|Y_1 = y], \forall y \in \mathcal{Y}.
\end{aligned}$$

Appendix B

Gaussian Approximation for Markov Chain (support documents for Chapter 3)

Let $\{X_n\}$ be a $\{0,1\}$-Markov chain with $P(0,1) = a$ and $P(1,0) = b$. We want to show that

$$\text{var}(X_1 + \cdots + X_n) \approx n\sigma^2$$

where

$$\sigma^2 := cd(\frac{2}{a+b} - 1)$$

where $c := a/(a+b)$ and $d := 1 - c$.

We have (see Figure B.1)

$$E((\sum_{m=1}^{n} X_m)^2) = 2T - D$$

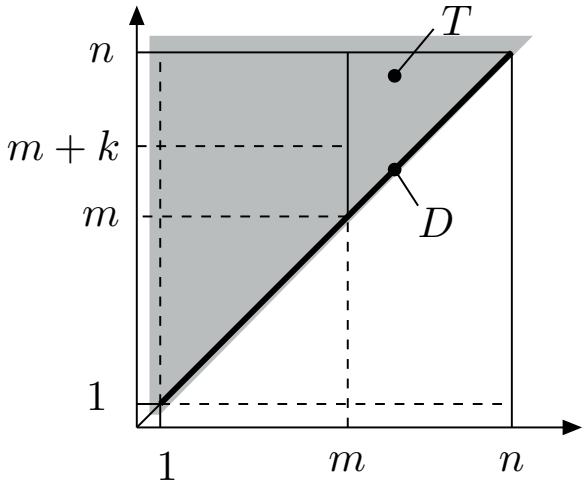

Figure B.1: The sum over $(m, n) \in \{1, \ldots, n\}^2$ is decomposed into twice the sum over T minus the sum over D because the terms are symmetric in (m, n).

where

$$T := \sum_{m=1}^{n} \sum_{k=0}^{n-m} E(X_m X_{m+k})$$

and

$$D := \sum_{m=1}^{n} E(X_m^2) = \sum_{m=1}^{n} E(X_m) = nc.$$

One can verify that

$$P^k(1, 1) = c + d\lambda^k, \text{ with } \lambda = 1 - a - b.$$

Now,

$$\begin{aligned}
T &= \sum_{m=1}^{n}\sum_{k=0}^{n-m} P(X_m = 1)P[X_{m+k} = 1|X_m = 1] \\
&= \sum_{m=1}^{n}\sum_{k=0}^{n-m} cP^k(1,1) \\
&= \sum_{m=1}^{n}\sum_{k=0}^{n-m} c(c + d\lambda^k) \\
&= \sum_{m=1}^{n}\sum_{k=0}^{n-m} c^2 + cd\sum_{m=1}^{n}\sum_{k=0}^{n-m}\lambda^k \\
&= c^2\frac{n^2+n}{2} + cd\sum_{m=1}^{n}(1 + \lambda + \cdot + \lambda^{n-m}).
\end{aligned}$$

Also,

$$\begin{aligned}
\sum_{m=1}^{n}(1 + \lambda + \cdots + \lambda^{n-m}) &= \sum_{m=1}^{n}\frac{1-\lambda^{n-m+1}}{1-\lambda} \\
&= \frac{n}{1-\lambda} - \frac{1}{1-\lambda}\sum_{m=1}^{n}\lambda^{n-m+1} \\
&= \frac{n}{1-\lambda} - \frac{\lambda(1-\lambda^n)}{(1-\lambda)^2}.
\end{aligned}$$

Hence,

$$\begin{aligned}
T &= c^2\frac{n^2+n}{2} + \frac{ncd}{1-\lambda} - \frac{cd\lambda(1-\lambda^n)}{(1-\lambda)^2} \\
&\approx c^2\frac{n^2+n}{2} + \frac{ncd}{1-\lambda}.
\end{aligned}$$

Finally, we get

$$E((\sum_{m=1}^{n} X_m)^2) \approx c^2(n^2+n) + \frac{2cdn}{1-\lambda} - nc.$$

Thus,

$$\begin{aligned}\operatorname{var}(X_1 + \cdots + X_n) &\approx c^2(n^2 + n) + \frac{2cdn}{1-\lambda} - nc - n^2c^2 \\ &= n[c^2 + \frac{2cd}{1-\lambda} - c] = ncd\frac{1+\lambda}{1-\lambda} \\ &= ncd\frac{2-a-b}{a+b},\end{aligned}$$

as we wanted to show.

Appendix C

Calculate ψ (support documents for Chapter 4)

To determine ψ, one argues as follows. Consider the backlog process $\{Z_n, n \geq 0\}$ and fix $Q \gg 1$. Define a cycle as a time interval between two successive times when $Z_n = Q$. Since the arrival rate into the queue is larger than the service rate, the backlog does not reach the value 0 during most cycles.

Consider a cycle of such that Z_m reaches the value 0 in n steps. During these n steps, the departures occur at some rate

$$d = \frac{D_0 + \cdots + D_{n-1}}{n},$$

and the arrivals occur at some rate

$$a = \frac{A_0 + \cdots + A_{n-1}}{n}.$$

Thus, one has

$$Q = n(d - a).$$

Indeed, say that the cycle starts at time 0 with $Z_0 = Q$ and is such that $Z_n = 0$ and $0 < Z_m < Q$ for $m = \{1, 2, \ldots, n-1\}$. Then, since Z_m does not hit the boundaries 0 or Q during the cycle,

$$Z_{m+1} = Z_m + A_m - D_m, m = 0, \ldots, n-1.$$

In particular,

$$Z_n = Z_0 + (A_0 + \cdots + A_{n-1}) - (D_0 + \cdots + D_{n-1}),$$

so that

$$0 = Q + (A_0 + \cdots + A_{n-1}) - (D_0 + \cdots + D_{n-1}) = Q + n(a - d),$$

which implies that $Q = n(d - a)$.

Thus, the probability that a cycle hits 0 is the probability that, for some $d > a$, and $n = Q/(d - a)$, the arrivals occur with average rate a and the departures with average rate d during n steps.

It is shown in [65] that, if $a > E(A_m)$, then

$$\lim_{n\to\infty} \frac{1}{n} \log\{P(A_1 + \cdots + A_n \geq na)\} = -\inf_{\theta>0}\{\theta a - \log(\lambda_A(\theta, p)\} \tag{C.1}$$

where $\lambda_A(\theta, p)$ is the largest eigenvalue of the matrix $G^A_{\theta,p}$ defined by

$$G^A_{\theta,p}(y^1, \tilde{y}^1) = [\sum_u e^{\theta u} p(y^1, u)] P_1(y_1, \tilde{y}^1)$$

where $p_1(y^1, \tilde{y}^1) = P[Y^1_n = \tilde{y}^1 | Y^1_{n-1} = y^1]$.

We need a similar result for the probability that the empirical rate is less than some value a smaller than the average rate.

Applying the previous result directly, we conclude that, if $a < E(A_m)$,

$$\begin{aligned}
&\lim_{n\to\infty} \frac{1}{n} \log\{P(A_1 + \cdots + A_n \le na)\} \\
&\quad = \lim_{n\to\infty} \frac{1}{n} \log\{P(-A_1 - \cdots - A_n \ge -na)\} \\
&\quad = -\inf_{\theta>0}\{\theta(-a) - \log(\rho_{-A}(\theta, p))\}.
\end{aligned}$$

Since

$$G^{-A}_{\theta,p}(y^1, \tilde{y}^1) = [\sum_u e^{-\theta u} p(y^1, u)] P_1(y_1, \tilde{y}^1) = G^A_{-\theta,p}(y^1, \tilde{y}^1),$$

we find that

$$\begin{aligned}
&\lim_{n\to\infty} \frac{1}{n} \log\{P(A_1 + \cdots + A_n \le na)\} = -\inf_{\theta>0}\{\theta(-a) - \log(\lambda_A(-\theta, p)\} \\
&\quad = -\inf_{\theta<0}\{\theta a - \log(\lambda_A(\theta, p)\} =: \phi_A(a, p)
\end{aligned}$$

Similarly, one has

$$\lim_{n\to\infty} \frac{1}{n} \log\{P(D_1 + \cdots + D_n \ge nd)\} = -\phi_D(d, q)$$

with

$$\phi_D(d,q) = \sup_{\theta>0}[\theta d - \log(\lambda_D(\theta,q))],$$

where $\lambda_D(\theta,q)$ is the largest eigenvalue of the matrix

$$G^D_{\theta,q}(y,y') = E[\exp\{\theta(D_1)\}|Y_1^2 = y]P_2(y,y').$$

Note the asymmetry between the definitions of $\phi_A(a,p)$ and $\phi_D(d,q)$: in the former, the supremum is over $\theta < 0$ whereas in the latter, it is over $\theta > 0$.

Accordingly, for any $a > 0, d > 0$, one has

$$\lim_{n\to\infty} \frac{1}{n} \log\{P(A_1 + \cdots + A_n \le na \text{ and } D_1 + \cdots + D_n \ge nd)\} = -\phi_A(a,p) - \phi_D(d,q)).$$

As stated earlier, the probability that a cycle hits 0 is the probability that, for some $d > a$, and $n = Q/(d-a)$, the arrivals occur with average rate a and the departures with average rate d during n steps.

For $Q \gg 1$, one sees that, with $n = Q/(d-a)$,

$$\lim_{Q\to\infty} \frac{1}{Q} \log P(A_1 + \cdots + A_n \le na \text{ and } D_1 + \cdots + D_n \ge nd) = -\frac{\phi_A(a,p) + \phi_D(d,q)}{d-a}.$$

Consider the event $\mathcal{E}$ that a busy cycle reaches the value 0 when

$$A_1 + \cdots + A_n \le na \text{ and } D_1 + \cdots + D_n \ge nd$$

for *some* a, d, n where $d > a$ and $n = Q/(d-a)$. The probability of that event is the sum over $d > a$ of the probabilities that the event occurs for given values of a and d. Since each of these probabilities is approximately $\exp\{-Qh(a,d)\}$ for some $h(a,d) > 0$, the sum of these terms, when $Q \gg 1$, is dominated by the term with the smallest value of $h(a,d)$. For instance, $\exp\{-3Q\} + \exp\{-2Q\} + \exp\{-4Q\} \approx \exp\{-2Q\}$ for $Q \gg 1$. The precise justification of this result is the *contraction principle* for large deviations (see Theorem 2.4 in [65]).

Thus, one expects the probability of the event $\mathcal{E}$ to be such that

$$\lim_{Q\to\infty} \frac{1}{Q} \log\{P(\mathcal{E}))\} = -\inf_{d>a} h(a,d) = -\inf_{d>a} \frac{\phi_A(a,p) + \phi_D(d,q)}{d-a}, \tag{C.2}$$

So, as claimed

$$\psi(p,q) = \inf_{d>a} \frac{\phi_A(a,p) + \phi_D(d,q)}{d-a}.$$

Now, let p be the probability that a cycle hits 0, α the average duration of a cycle that hits 0, and γ the average number of steps that the queue is 0 in a cycle that hits 0. Let also δ be the average duration of a cycle that does not hit 0 (see Figure C.1). Thus, during $n \gg 1$ cycles, there are approximately np cycles that hit 0 and the queue is empty during approximately $np\gamma$ steps. These n cycles take approximately $np\alpha + n(1-p)\delta$. Accordingly, the fraction of time π that the queue is

empty is approximately given by

$$\pi(Q) = \frac{np\gamma}{np\alpha + n(1-p)\delta} = \frac{p\gamma}{p\alpha + (1-p)\delta}.$$

One can expect that $\alpha = O(Q), \gamma = O(1), \delta = O(1)$. Indeed, the time to hit 0, given

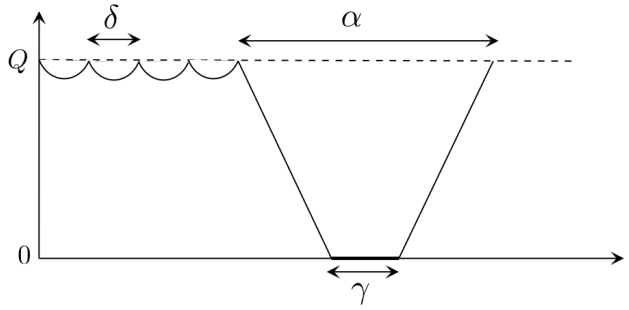

Figure C.1: This figure clarifies the notations used for cycles in this appendix.

that the cycle hits 0 is $Q/(d-a)$ where a and d achieve the minimum in (C.2) and the average time from empty to Q is $Q/(E(A_1) - E(D_1))$.

Since $p = O(\exp\{-\lambda Q\})$ with $\lambda = \psi(p, q)$, one sees that

$$\pi(Q) \approx \frac{\gamma \exp\{-\lambda Q\}}{C_1\ Q\ \exp\{-\lambda Q\} + (1 - \exp\{-\lambda Q\})\delta} \approx C_2 \exp\{-\lambda Q\},$$

so that

$$\lim_{Q\to\infty} \frac{1}{Q} \log\{\pi(Q)\} \to -\lambda = -\psi(p, q).$$

Thus, the steady state probability that $Z_n = 0$ is such that

$$\lim_{Q\to\infty} \frac{1}{Q} \log\{P(Z_n = 0)\} \to -\psi(p, q),$$

as we wanted to show.